TESTING RECENT CHRONOLOGICAL TECHNIQUES FOR PEAT SITES WITH CONTRASTING ANTHROPOGENIC INFLUENCES

CAROLINE MARGARET DONNELLY

Thesis presented for the degree of Master of Science
College of Science and Engineering

University of Glasgow

Scottish Universities Environmental Research Centre
East Kilbride

ABSTRACT

This thesis presents the results of a study of recent radionuclide chronological techniques applied to two contrasting locations in an ombrotrophic peat bog in West Central Scotland. The locations differed in that one was undisturbed but the other had been previously forested. The study demonstrated that with a limit of detection of 5 Bq kg^{-1} or better, rigorous sampling technique and high resolution (2 cm) sampling increments, ^{210}Pb dating using either the CIC method or the CRS method and ^{241}Am dating method all gave consistent chronologies. Use of a low resolution field sampling technique gave consistent CIC but not CRS chronologies. The study indicated that neither ^{137}Cs nor ^{32}Si could be used to derive reliable chronologies for peat. Implied temporal variations in deposition of anthropogenic species (ash, Pb and Pb isotopes) were consistent with known historical variations and other studies of archived materials, lake sediments and peat deposits. Metal inventories were observed to be consistently higher for the unforested site than for the previously forested site, but comparison with chronologies implied that this was a long term feature of the two sites rather than an influence of the relatively short term presence of the forest. This observation highlights the limitations of extrapolating from a single core to derive information on larger scale regional deposition of contaminants.

TABLE OF CONTENTS

LIST OF TABLES

LIST OF FIGURES

ACKNOWLEDGEMENTS

I would like to thank everyone who gave me advice, support and encouragement throughout this project.

At SUERC, my supervisor Professor Gus MacKenzie for constant support, advice, encouragement and never ending patience without which I would never have made it to the end.
At Glasgow University, my supervisor Dr Ian Pulford for advice, encouragement and an insight into soil science.

Also at SUERC, colleagues past and present for encouraging words and advice when needed, in particular Phil and the radiocarbon laboratory staff, Susie & Anne. Also Valerie for ICP-MS analysis and information and Gill & Helen for help with sampling.

At South Lanarkshire Council, John Hawell and Louisa Maddison for valuable advice and information about Langlands Moss as well as Maureen Potter of The Friends of Langlands Moss for her informed knowledge of the sample site.

I would also like to thank my Mum and Dad for always being there and my friend Susanne for encouragement and a regular supply of meal deals.

Finally, I would like to thank Darren & Lynne, Ross, Debi & Shona, Michelle & Steve and Stacey for constant encouragement and that special card which got me through the bad days.

DECLARATION

The material presented in this thesis is the result of independent research carried out by me at the Scottish Universities Environmental Research Centre and it has not been submitted in any previous application for a Higher Degree. Any published or unpublished results of other workers have been given full acknowledgement in the text.

Caroline Margaret Donnelly

1 Introduction

1.1 Overview

This project involved a study of two sites within an ombrotrophic peat deposit at Langlands Moss, East Kilbride. The sites differed in that one was undisturbed, whilst the other had previously been forested from the mid-1950s until 1995.

The aim of the research was to evaluate the applicability of conventional radionuclide recent chronologies and to establish inventories and temporal variations in atmospheric depositional fluxes of selected metals at each site. The secondary aim was to attempt to quantify the concentration of biogenic silica (BSi) at each site in order to evaluate the potential of ^{32}Si dating for peat deposits.

Specific objectives were to establish:

- Inventories and concentration profiles for ^{210}Pb, ^{137}Cs and ^{241}Am.
- Metal inventories and concentration profiles.
- ^{210}Pb chronologies using high and low resolution vertical increment sampling.
- Stable lead isotope ratios as an aid to Pb source apportionment.
- The suitability or otherwise of a method developed for analysis of lake sediment for extraction of BSi from peat.

1.2 Peat deposits as archives of environmental data

Concentration profiles of anthropogenic contaminants in accumulating natural systems such as lake sediments, glaciers and ombrotrophic peat deposits can provide a means of reconstructing temporal and spatial trends of atmospheric deposition when used in conjunction with a reliable chronology. The concentrations of contaminants, such as heavy metals and persistent organic pollutants, deposited on the earth's surface will vary in response to variations in atmospheric deposition. Once deposited onto an accumulating system such as a peat deposit the contaminant will gradually be buried as the system accumulates. Assuming no mixing or post depositional movement, this then allows a historical record of contaminant depositional trends to be derived from the vertical profile if a suitable chronology can be established. It is also possible to establish inventories of contaminants in accumulating deposits, enabling spatial variations in deposition to be established. The observed trends are influenced by both natural and anthropogenic inputs, with the human impact arising from sources such as industrial operations, combustion of fossil fuels, mining and smelting of metal ores, vehicle exhaust emissions and agricultural land use. As discussed below, studies of contaminant lead can be extended by the use of stable Pb isotope ratios to provide information as to the origin of the Pb.

Peat bogs comprise predominately organic soils, typically containing less than 25% mineral material, which form from partially decomposed plant material and other organic remains in cold, waterlogged, acidic conditions (Zaccone et al., 2008). New organic matter is continuously added through production at the surface. CO_2 and DOC (dissolved organic carbon) are released in the near surface peat from rapid aerobic decay. CH_4 production, as well as DOC production, takes place by slower anaerobic decay in layers a few cm below the water table and evidence suggests CO_2 and CH_4 production continues much deeper into the peat deposit (Clymo and Bryant, 2008). The two main layers in a peat system are the upper unsaturated, aerobic acrotelm, which can be up to 50 cm deep and has a high organic matter decay rate, and the deeper, permanently saturated, anaerobic catotelm with a lower organic matter decay rate (Ingram, 1978; Clymo, 1984). The boundary layer between these two zones is the mesotelm

where water table fluctuations generate complex, varying conditions which were simulated by Clymo and Bryant (2008) to account for dissolved gas age profile offsets (Figure 1-1).

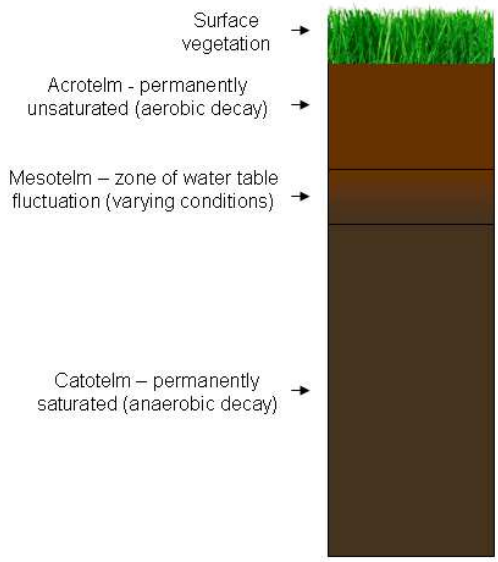

Figure 1-1 Main vertical sub division categories in peat (Clymo and Bryant, 2008)

The characteristic dark colour of peats comes from humic substances. Humic substances are the biggest contributor of natural organic matter (NOM) in soils and are found in three forms: humic acids (HA), fulvic acids (FA) and humin. HA and FA are weak acids which dissociate and dissolve under alkaline conditions. The operational distinction between the two is that HA re-precipitates if the pH is readjusted to 1 whereas FA remains in solution. Humin is not extractable by either strong acids or strong alkalis (Website - IHSS). Humic acids are natural polymers formed by chemical and microbial action and environmental influences on decaying plant and animal material (Savel'eva et al., 2010).

Peat deposits can be defined as either minerotrophic or ombrotrophic, depending on the source from which they receive nutrient input, with the former receiving input from various hydrological sources such as surface, flood

or groundwaters (Lähteenoja et al. 2009). Ombrotrophic peat deposits receive all of their input from the atmosphere by way of precipitation and dry deposition and are not influenced by groundwater or river inputs. This gives rise to low intrinsic metal and nutrient concentrations in ombrotrophic peat deposits which act as accumulating sinks for carbon, metals and radionuclides. Peat deposits are therefore highly sensitive systems in which to study temporal and spatial trends of contaminant metal deposition, but have the drawback of very low accumulation rates, giving relatively poor temporal resolution. Since the start of the Holocene approximately 10,000 years ago, peat deposits have played an important role in carbon sequestration by uptake of carbon dioxide, and the total quantity of C sequestered has been significant relative to the global carbon cycle. One of the most comprehensive estimates of the quantity of C currently stored in peat is that of Gorham (1991) who calculated a total inventory of 455 Pg (petagrams) of C for Northern Hemisphere peat deposits. This represents approximately one third of the world's soil carbon stock, while peat deposits only cover approximately 3% of the land surface. It is therefore important to be able to derive accurate chronologies for peat in order to quantify carbon deposition rates. Studies of the exchange processes of carbon in peat deposits show an uncertainty in the current sink, neutral or source status of peatlands with respect to C cycling. Factors such as topography and other sequestered elements have been studied along with production and movement mechanisms (diffusion and mass flow) of dissolved gasses with a view to establishing the net effect on carbon budgets and accumulation rates (eg Waddington and Roulet, 1996; Gunnarsson et al. 2008; Clymo and Bryant, 2008). Moreover, there is considerable uncertainty over the potential effects of climate change, in particular global warming, on the stability of existing peat bogs and on future rates of C sequestration (Gorham, 1991).

1.3 The Natural Radioactive Decay Series and Secular Equilibrium

There are three naturally occurring radioactive decay series, each one beginning with a primordial radionuclide and ending with a stable lead isotope; ^{238}U (uranium or radium series), ^{235}U (actinium series) and ^{232}Th (thorium series) (Figure 1-2). Uranium and thorium are found in mg kg^{-1} levels in most rocks,

sediments and soils, so natural decay series radionuclides are a ubiquitous feature of the environment.

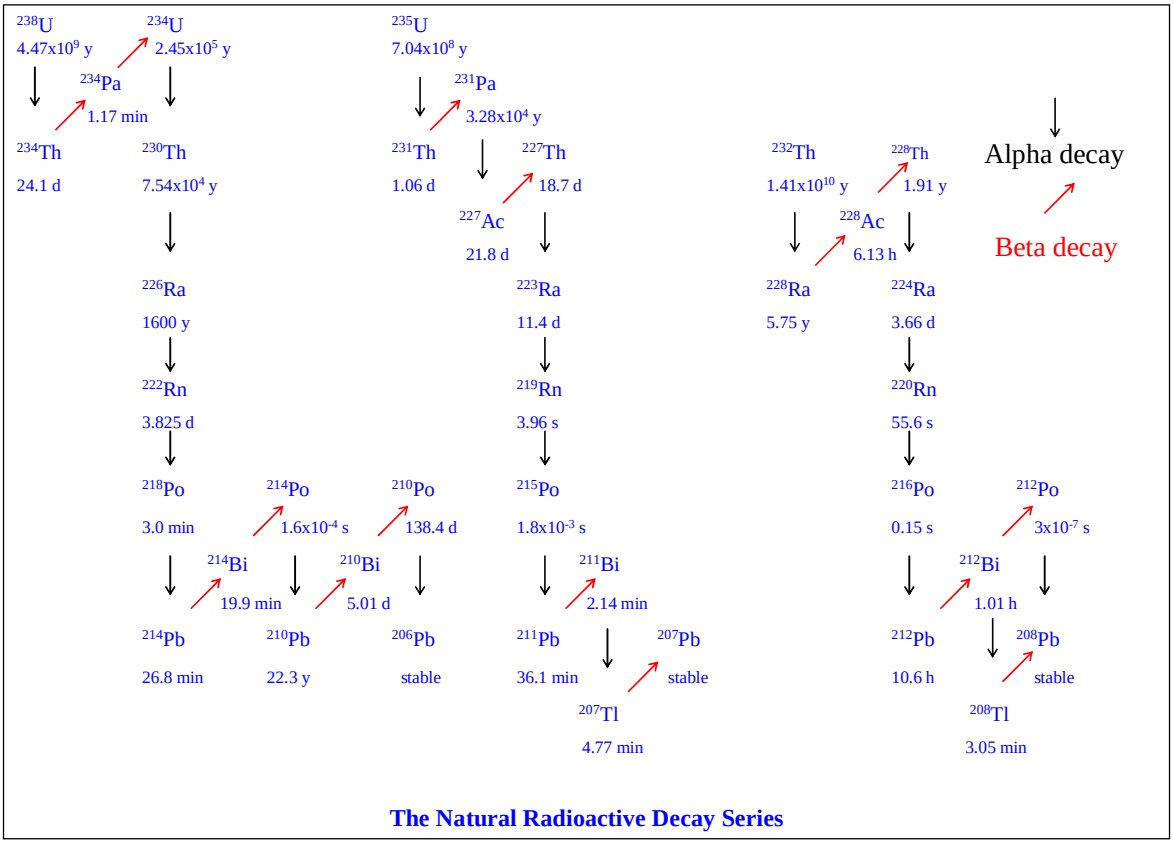

Figure 1-2 The Natural Radioactive Decay Series

In sequential radioactive decay, as in the natural decay series, if a parent radionuclide, A, decays to produce a daughter radionuclide B:

$A \rightarrow B \rightarrow$

and $(t_{1/2})_A >> (t_{1/2})_B$, so $\lambda_A << \lambda_B$

then the activity of B will grow in towards equilibrium with an initially pure sample of A according to:

$$\left(A_B\right)_t = A_A\left(1-e^{-\lambda_B t}\right) \qquad (1.1)$$

Where (A_A) = activity of A which is assumed to be constant; $(A_B)_t$ = activity of B at time t and λ = decay constant of B.

When t becomes large relative to the half-life of B:

$$e^{-\lambda_B t} \approx 0 \qquad (1.2)$$

giving a situation where $(A_B)_t = A_A$ This state of radioactive equilibrium is known as Secular Equilibrium. Graphically (Figure 1-3), ingrowth of the activity of B towards secular equilibrium with A is of the form:

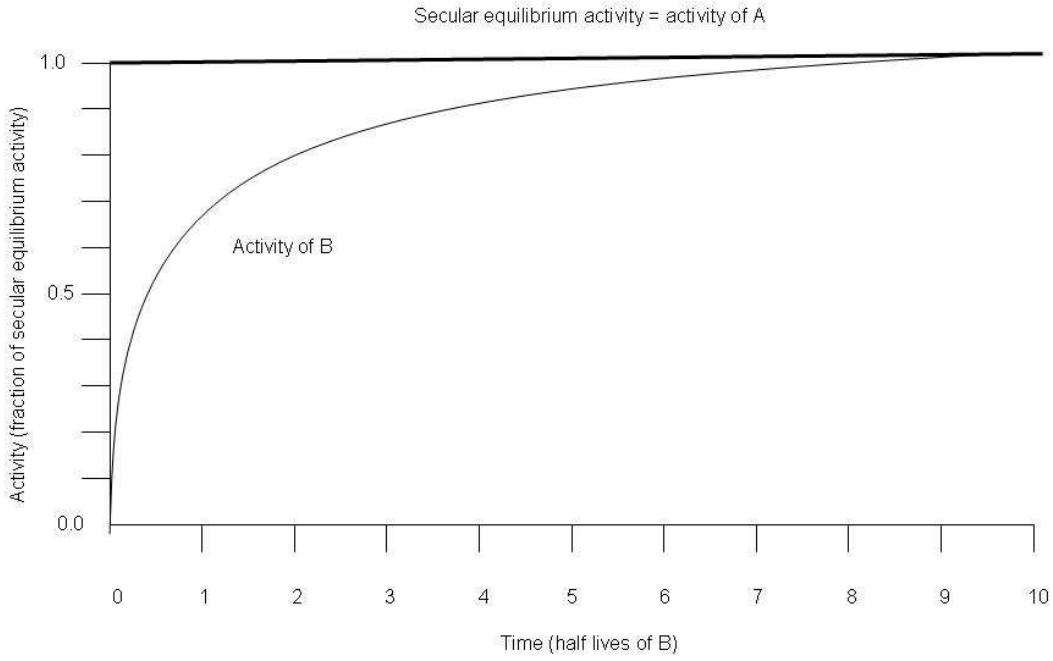

Figure 1-3 Ingrowth of activity of daughter B towards secular equilibrium with parent A

In minerals which have been closed systems for geological timescales, there will be a state of secular equilibrium throughout each of the three natural decay series.

1.4 ^{210}Pb dating

^{210}Pb, which is a member of the ^{238}U natural decay series, has a half-life of 22.3 years and decays through a series of radioactive daughters to produce stable ^{206}Pb. Goldberg (1963) first developed ^{210}Pb dating and applied the technique to the dating of glacial ice sheets In Greenland. In a geological system (eg a mineral in a rock) that has been closed for a time that is long relative to the half life of the longest lived decay chain member (^{234}U; $t_{1/2}$ = 2.45x10^5 y) the ^{238}U decay series will be in a state of secular equilibrium throughout. Secular equilibrium is therefore attained after a time of about 2 million years and in most rocks and minerals, the ^{238}U decay series approximates to a state of secular equilibrium. However, a small proportion of the inert gas ^{222}Rn escapes to the atmosphere, where it decays through a series of short half-life daughter products to ^{210}Pb (Figure 1-4). The ^{210}Pb is then deposited on the earth's surface or on the sea or in lakes by dry deposition via dust particles or wet deposition via precipitation. ^{210}Pb deposited in aquatic systems is rapidly transported to the underlying sediment while in peat it binds to organic material at the peat surface. Decay then occurs post deposition, giving a depth distribution which, in an accumulating deposit with suitable conditions, allows determination of chronologies using the vertical distribution of ^{210}Pb. In the case of lake or marine sediments there is an additional smaller contribution to the total ^{210}Pb activity from in situ decay of soluble ^{226}Ra and/or ^{222}Rn in the water column. This input, combined with that from wet and dry atmospheric deposition, constitutes what is defined as the unsupported or excess component of the total ^{210}Pb activity. There is also an input to the total ^{210}Pb activity from detrital minerals in which the ^{238}U decay series is at, or close to, secular equilibrium. This is known as the supported component of ^{210}Pb. In the case of ombrotrophic peat, where the mineral content is very low, this supported component is usually negligible.

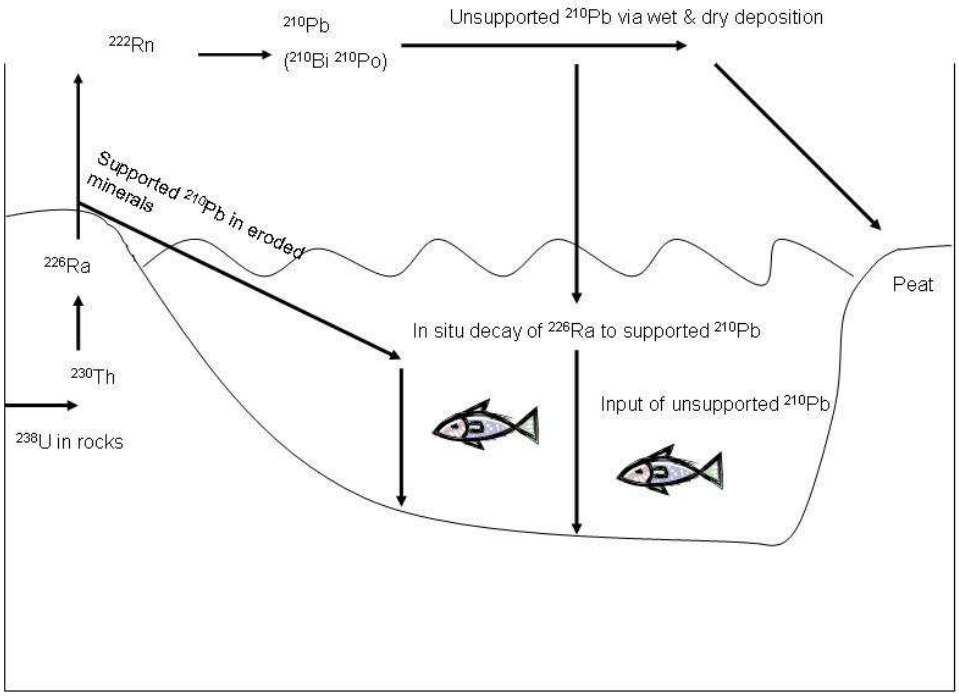

Figure 1-4 Schematic diagram of supply of ^{210}Pb to peat and lake sediment

In practical terms ^{210}Pb dating is normally performed by gamma spectroscopy, with total ^{210}Pb being determined using its own 46.5 keV gamma emission while the supported activity is quantified using the gamma emissions of ^{214}Pb and ^{214}Bi (with the assumption of radioactive equilibrium between these radionuclides and ^{226}Ra).

Figure 1-5 shows linear and logarithmic plots for the specific activity of unsupported ^{210}Pb in a system with a constant rate of supply of ^{210}Pb and a constant accumulation rate. In a system which is accumulating uniformly the unsupported ^{210}Pb activity will decrease exponentially with depth as shown in Figure 1-5 (b). Under these conditions the accumulation rate can be calculated on the basis of the first order radioactive decay equation:

$$A_t = A_o e^{-\lambda t} \qquad (1.3)$$

Where A_t is activity at time t, A_0 is activity at time 0 and λ is the decay constant.

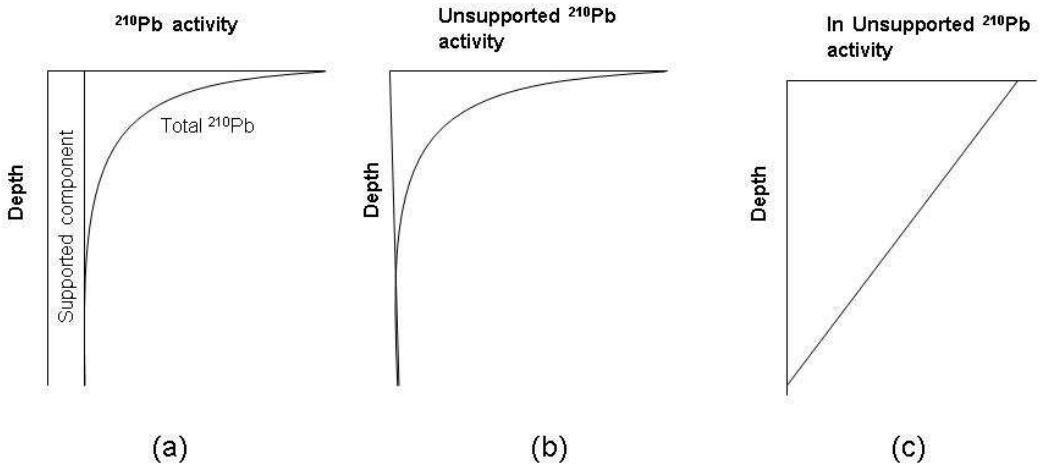

Figure 1-5 Vertical profiles for (a) Total ^{210}Pb (b) Unsupported ^{210}Pb (c) ln Unsupported ^{210}Pb

Two different models are commonly used to derive ^{210}Pb chronologies. The first is the Constant Initial Concentration (CIC) model, which makes the assumption that both the accumulation rate of the system and the rate of supply of unsupported ^{210}Pb are constant. It also assumes that there is no mixing in the system and that the ^{210}Pb is immobile after deposition. Thus, application of the CIC model is limited to systems where ^{210}Pb in the receiving layer can be assumed to be deposited at a constant rate (Goldberg, 1963; Robbins, 1978).

Under these conditions, the plot of the natural logarithm of the unsupported ^{210}Pb activity against depth is a straight line from which the accumulation rate can be calculated using the equation:

$$g = -\frac{S}{\lambda} \qquad (1.4)$$

where g = gradient, S = accumulation rate and λ = ^{210}Pb decay constant.

The second method, the Constant Rate of Supply (CRS) model, is used when the accumulation rate is variable; however it also assumes a constant rate of supply

of ^{210}Pb and no post depositional mobility or mixing. This method is based on inventories (ie Bq m^{-2}) and the age of any given layer in a deposit can be calculated using the equation:

$$t_i = \frac{1}{\lambda} \ln \frac{I_T}{I_i} \qquad (1.5)$$

where t_i = age of ith layer, λ = ^{210}Pb decay constant, I_T = total unsupported ^{210}Pb inventory and I_i = unsupported ^{210}Pb inventory below the ith layer.

Compaction and degradation of organic matter result in a marked increase in density with increased depth in peat so that there is not a linear relationship between depth and age. To overcome this complication, cumulative mass (g cm $^{-2}$) is often used rather than depth, and accumulation rates are expressed in g cm $^{-2}$ y $^{-1}$.

As highlighted by Smith (2001) ^{210}Pb chronologies, where practicable, should be corroborated by an independent method and a common approach to achieve this involves comparison with chronologies derived from the distribution of anthropogenic radionuclides such as ^{137}Cs and ^{241}Am (Appleby, 2001, 2008).

In systems subject to biological and/or physical mixing processes or complex transport processes resulting in particle redistribution (e.g. sediment focussing) it may be difficult to apply either model confidently. However, such complex processes are generally insignificant in peat. Robbins and Herche (1993) emphasised the need for accurate models which take account of all of the complicated factors (e.g. biological, chemical, transport and mixing processes) which contribute to establishing the vertical distribution of ^{210}Pb from which chronologies are derived. They also noted that ironically the timespan over which the ^{210}Pb dating method is most effective is also the timespan over which anthropogenic activities have complicated the analysis of chronologies. Binford (1990) stressed the need for correct application of the CIC and CRS models and the importance of accounting for all sources of error, whether measurable or otherwise. He noted that models presuming negligible movement and mixing of ^{210}Pb after deposition could be erroneous and even an apparently small (1 cm) underestimation of the depth to which mixing occurs can give up to 30% error in

calculated dates. Accumulating systems can be subject to different types of mixing, eg total mixing or diffusive mixing. Total mixing results in homogenisation of ^{210}Pb activity in the mixed zone. This is commonly observed in nearshore marine sediments (MacKenzie et al. 2006), but is not generally recognised as being of importance in peat. Diffusive mixing is primarily a biological process which usually occurs in systems such as deep sea sediments in which the accumulation rate is very slow relative to the ^{210}Pb half-life. In such systems, biodiffusive mixing occurs at a slow, constant rate and generally results in an exponential decrease in unsupported ^{210}Pb activity with increasing depth (Dellapenna et al., 1998).

Factors such as sampling methods play a vital role when calculating ^{210}Pb chronologies using the CRS method. For example it is crucial to collect the entire profile, including surface vegetation as failure to do so will generate erroneous chronologies. Farmer et al. (2006) reached this conclusion in a study of peat cores from an ombrotrophic peat bog at Flanders Moss, Scotland. In this study Pb isotopic ratios (^{206}Pb/^{207}Pb) were used to correct for an estimated loss of 25±7 years of material from one core. This could have arisen from natural topographical variations, removal of peat sections for fuel or inconsistent core collection methods. Olid et al. (2008) also identified a similar discrepancy when calculating ^{210}Pb chronologies, pointing out that the surface layer is the initial receiving zone for atmospheric deposition and estimating a 12% undervaluation in total Pb and 39-49% undervaluation in ^{210}Pb inventories if surface vegetation is not included. A more accurate validation of ^{210}Pb dates with man made radionuclides was achieved when surface vegetation was included.

MacKenzie et al. (2011) highlighted the importance of core length to ensure that material was collected to a depth where the unsupported ^{210}Pb had reached the detection limit. Failure to do so could result in inaccurate inventories thereby giving inaccurate dates. There is also an inherent problem in attempting to define accurate values for the terms in the CRS equation. This specific problem was originally highlighted by Robbins (1978) and further discussed by Binford (1990) and Robbins and Herche (1993). The use of measured core inventories as approximations for the CRS equation terms I_T and I_i will result in underestimation of these terms and the overall effect on derived ages is to give erroneously older values for the deeper sections of cores. This problem can be

exacerbated by poor ^{210}Pb detection limits. Therefore, an important factor in measuring ^{210}Pb is the use of a detection system with a suitably low background. A detection system with a high peak to Compton ratio will facilitate measurements with a lower limit of detection and minimise the unquantifiable contribution of atmospheric ^{210}Pb at depths below the level at which the limit of detection is reached (MacKenzie et al., 2011).

^{210}Pb dating chronologies have an important role in the interpretation of the information stored in recent sediments and peats and give valuable information to help understand processes such as peat bog growth, erosion rates where landscapes have been modified or disturbed, monitoring of inorganic, organic and radioactive pollutants, and investigation of processes in glacier formation (Appleby, 2001; MacKenzie et al., 2011).

Peatlands form under specific climatic and environmental conditions and are potentially vulnerable to both natural and anthropogenic variations in these conditions (Gorham, 1991). For example peatland stability could be affected by natural or human induced climate change and human activities such as extraction for fuel, afforestation, deforestation and the installation of wind farms. It is therefore vital to have accurate methods to define peat accumulate rates in order to quantify natural processes, to detect the effects of changing conditions and to monitor restoration after human interventions. ^{210}Pb dating is of basic importance in this context and is a valuable tool in the management of peatland resources (Bao et al., 2010; Grover et al., 2012).

^{210}Pb dating of peat soils has been widely used to characterise peat chronologies internationally (e.g. Shotyk et al., 1996, 2002; Vile et al., 2000; Novák et al., 2003; Turetsky et al., 2004; Le Roux et al., 2005) and numerous studies of this type have also been carried out in Scotland (MacKenzie et al., 1998(a); Cloy et al., 2008). One of the most widely used application of ^{210}Pb dating has been in the assessment of historical trends in atmospheric deposition of metals by combining chronologies with metal concentration profiles in peat cores. This approach has been extensively used in studies of Pb, the most significant heavy metal pollutant, but has also been used for other metals.

The study of Pb in the environment has been extended by the use of stable Pb isotope measurements. There are four stable Pb isotopes: primordial ^{204}Pb (~1% natural abundance) and ^{206}Pb (~24%), ^{207}Pb (~23%) and ^{208}Pb (~52%) which have both primordial and radiogenic components, since they are the end members of the three natural radioactive decay series (Komárek et al., 2008). Stable Pb isotope ratios vary between Pb from different sources dependent on their age and U and Th content. The most commonly used isotope ratio in such studies is ^{206}Pb/^{207}Pb, but use of the ^{208}Pb/^{207}Pb ratio and the relationship between the two ratios can provide valuable information on the source of atmospheric deposition. Typical ^{206}Pb/^{207}Pb ratios from sources influencing Scottish peatlands are ~1.16-1.18 from indigenous geological materials, including the historical smelting of native lead ores, ~1.17-1.19 from coal combustion and ~1.06-1.09 for UK petrol lead, which was strongly influenced by imported lead ores mainly of Australian origin with a ^{206}Pb/^{207}Pb ratio of ~1.04 (Sugden et al., 1993; Farmer et al., 1996, 1999, 2000, 2005, 2006; MacKenzie et al., 1997, 1998(a); MacKenzie and Pulford, 2002; Cloy et al.,2008) .

A useful way of presenting Pb isotope data is in a graph of the ^{206}Pb/^{207}Pb ratio against the ^{208}Pb/^{207}Pb ratio and Figure 1-6 shows the positions in such a graph of some of the major Pb sources influencing Scottish peat deposits.

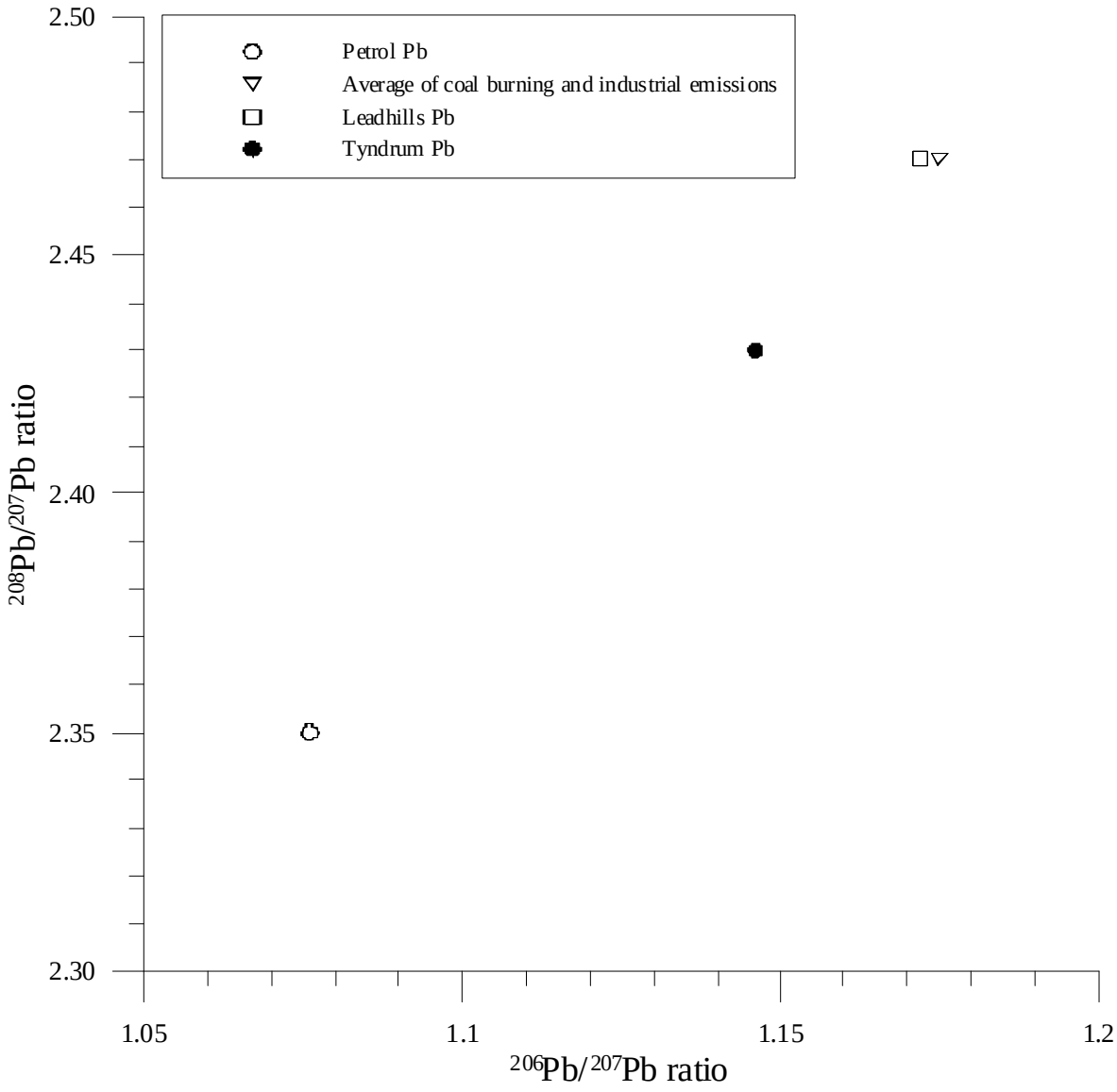

Figure 1-6 Plot of $^{208}Pb/^{207}Pb$ ratio against $^{206}Pb/^{207}Pb$ ratio for major sources of Pb to the environment in Scotland (Sugden et al., 1993; Farmer et al., 1996, 1999, 2000, 2005, 2006; MacKenzie et al., 1997, 1998(a); MacKenzie and Pulford, 2002; Cloy et al.,2008)

In cases where the Pb composition is derived from two dominant sources, isotopic data for samples lie on a tie line between the two end members and the fractional contribution of each source can be calculated using a simple binary mixing model (MacKenzie et al. l997). The trends observed in $^{206}Pb/^{207}Pb$ ratio as a function of time derived from dated cores from Scotland are illustrated by the work of Farmer et al. (2002) who observed a $^{206}Pb/^{207}Pb$ ratio of ~1.17 for peat deposited in the 19th century and this value was in excellent agreement with that for archived Scottish moss for this period. The peat data indicated that the $^{206}Pb/^{207}Pb$ ratio gradually fell to values of 1.127±0.010 in the 1970s and 1.120±0.018 in the 1980s due to the influence of petrol Pb. With the phasing out of leaded petrol the $^{206}Pb/^{207}Pb$ ratio started to rise again and reached a value of 1.137±0.010 in peat deposited in the 1990s. After the ban on sale of leaded petrol in 2000 the ratio again rose to a value of 1.151±0.009 (Farmer et al., 2002).

Peatlands are also subject to atmospheric deposition of organic contaminants such as PCBs (polychlorinated biphenyls) and PAHs (polycyclic aromatic hydrocarbons), which originated from sources such as burning of fossil fuels and widespread industrial activities since the start of the industrial revolution. PCBs are potentially toxic and carcinogenic while PAHs are potentially carcinogenic and mutagenic and are widespread in the environment particularly in areas subject to human impact (Berset et al., 2001). PCBs and PAHs are adsorbed and bound on organic rich peat soils. The weakly acidic, anoxic environment in peatlands is low in microbial activity therefore little post depositional diagenesis or degradation occurs. This gives an ideal accumulating system from which to study historical trends and fluxes of anthropogenic organic contaminants and ^{210}Pb chronologies are again of fundamental importance in this context. A study over the 150 year period from 1850-2000 (the timescale ideally suited to the ^{210}Pb half-life of 22.3 years) demonstrated geographical variations and trends attributable to a post industrial revolution increase in deposition of organic pollutants from fuel burning, vehicular exhausts and industrial activities, with a subsequent decrease as alternative fuel sources (e.g. hydroelectric, natural gas, nuclear power) were found and heavy industry diminished (Berset et al.,2001; Dreyer et al., 2005).

Peatlands are a natural reservoir for carbon and contain approximately one third of the global soil carbon stock (Gorham, 1991). It is therefore important to understand factors affecting accumulation rates of peatlands and in turn their corresponding short and long term carbon sequestration ability. Such factors include age, latitude, vegetation types, hydrological, geochemical and climatic conditions, land use and other anthropogenic influences. ^{210}Pb dated peat cores have been widely used in establishing accumulation rates to improve understanding of the current and future carbon sequestration status (source, sink or neutral) of global peat and to facilitate planning of measures required to deal with climate change and global warming. (Wieder et al., 1994; Wieder, 2001; Asada and Warner, 2005; Novak et al., 2008; Bao et al., 2010; Grover et al., 2012).

^{210}Pb dating is therefore very widely used to develop chronologies for peat but in publications dealing with ^{210}Pb negligible details are generally given of how the chronologies are established. In particular with the use of the CRS model, no indication is generally given of how inaccuracies in evaluating I_T and I_i were addressed.

1.5 Anthropogenic Radionuclide Chronologies

Man-made radionuclides, released into the atmosphere from a variety of planned or accidental origins, can, under suitable circumstances, be used to establish chronologies. Observed peaks from periods of known maximum releases can give characteristic trends in radionuclide concentration profiles which enable accurate dating of accumulating systems.

The largest source of man-made radionuclides to the UK environment was fallout from atmospheric nuclear weapons testing, in which the main radionuclides are the products of nuclear fission and neutron capture reactions. UNSCEAR (2000) estimated that there were a total of 543 atmospheric nuclear weapons tests, with a yield of 440 Mt. This is an increase of 23 tests and a decrease of 102 Mt relative to the previous estimate (UNSCEAR, 1993). The updated data come from the compilation of published figures from the nations involved i.e. the USA, the USSR, the UK and France.

Nuclear weapons tests were initiated by the USA in July 1945 in New Mexico with the Trinity test, which had an approximate fission yield of 19 kt (Carter and Moghissi, 1977). This was closely followed by the detonation of a nuclear weapon over each of the cities of Hiroshima and Nagasaki, Japan, in August of the same year. The number of tests then followed a gradual increase in the 1950s until November 1958, when there was a moratorium imposed, involving the USA, the UK and the USSR. When the moratorium ended in September 1961 there was a sharp rise in testing until October 1963 when a Limited Test Ban Treaty for atmospheric tests was signed by the USSR, the USA and the UK. There have been very few atmospheric tests since the introduction of the Test Ban Treaty, with the last having been carried out by China in October 1980. The peak deposition of fallout radionuclides in 1963 provides a characteristic horizon of maximum activity in sediment profiles that can be used to establish chronologies. In principle, the horizon marking the onset of testing in 1952 could also be used in this way, but mixing and diffusion processes often prevent this.

Reported underground testing of nuclear weapons carried on until 1998 (MacKenzie, 2000; UNSCEAR, 2000) and a proposal from most countries involved to ban all nuclear weapons testing resulted in The Comprehensive Test Ban Treaty, which opened for signatories on 24th September 1996. The Comprehensive Test Ban Treaty Organisation (Website - CTBTO) report that to date, 183 countries have signed and 157 have ratified the Treaty, but 8 of the 44 countries with nuclear testing capability required to ratify in order to enforce the treaty have yet to do so. There have been no reported atmospheric tests since the opening of the treaty and limited underground tests. The effects of underground testing are limited to the vicinity of the test and they have therefore had no detectable influence on the UK environment.

The long lived radionuclides still present in the environment from atmospheric nuclear weapons testing include ^{137}Cs, ^{90}Sr, ^{14}C, ^{238}Pu, ^{239}Pu, ^{240}Pu and ^{241}Pu. The alpha energies of ^{239}Pu (5.1478 MeV, 15.1%; 5.1555 MeV, 73.2 %) and ^{240}Pu (5.1237 MeV, 26.38 %; 5.1682, 73.5%) are too close to be resolved by alpha spectroscopy, so the combined peak is usually measured and activities are reported as a combined ^{239,240}Pu value. ^{90}Sr, being a pure beta emitter, is difficult to analyse, as are the alpha emitting Pu isotopes and analysis of these radionuclides can be costly and time consuming. Gamma emitters in general are

most useful for generating chronologies due to the non destructive ease of analysis, the most widely used being ^{137}Cs. ^{137}Cs binds tightly to clay minerals in sediments in marine and lake environments and therefore can be useful in establishing chronologies in these systems. Various studies of this type have been carried out in Scotland (e.g. McKinley et al., 1981; Swan et al., 1982; Eades et al., 1998). ^{137}Cs is, however, mobile in organic soils as the presence of humic materials inhibits its adsorption to this type of soil, so it is less widely used for chronological applications in peat (Maguire et al.,1992; Shand et al., 1994).

^{241}Am, which is also a gamma emitter, although not directly produced in large quantities in fallout, has grown in from decay of fallout ^{241}Pu:

^{241}Pu ($t_{1/2}$ = 14.4 y) $\rightarrow$ ^{241}Am ($t_{1/2}$ = 433 y) $\rightarrow$

^{241}Am is present in the environment in very low activities, so it has been less widely used to develop chronologies, but is potentially a useful tracer in peat due to its immobility.

The other main source of anthropogenic radionuclides to peatlands in the UK is from the accident at the Chernobyl nuclear power plant in the Ukraine in April 1986. The accident involved an explosion, followed by a fire and meltdown of the reactor core, resulting in releases to the atmosphere of substantial quantities of radionuclides which were then transported and deposited as fallout over a wide area. Most of the USSR, Western Europe and Scandinavia were contaminated by considerable quantities of fission and neutron capture products from Chernobyl, the most significant and enduring being ^{137}Cs ($t_{1/2}$ = 30.0 y), ^{134}Cs ($t_{1/2}$ = 2.06 y) and ^{90}Sr ($t_{1/2}$ = 28.5 y). The 134 mass chain produced in nuclear fission stops at stable ^{134}Xe, so ^{134}Cs is not present in nuclear weapons testing fallout. However, ^{134}Cs is produced in nuclear reactors from neutron capture by ^{133}Cs and it was highly useful in identifying Chernobyl fallout which had a charcteristic $^{134}Cs/^{137}Cs$ activity ratio of ~0.50-0.55. The $^{134}Cs/^{137}Cs$ activity ratio was therefore a useful diagnostic tool when interpreting ^{137}Cs source in sediment profiles (Mitchell et al., 1992). However, with a half life of only 2.06 y, Chernobyl derived ^{134}Cs has now decayed to undetectable levels in the UK environment. While Chernobyl fallout radiocaesium was widely used in

establishing lake sediment chronologies it is not generally used in peat studies due, as noted above, to its mobility.

Examples of other nuclear power station accidents include those at Three Mile Island, USA (1979), which released ~370 PBq of noble gases (mainly ^{133}Xe) and 550 GBq of ^{131}I (MacKenzie, 2000) and more recently at the Fukushima Dai-ichi nuclear power plant in Japan (2011), which resulted in the atmospheric release of a range of radionuclides including ^{131}I and ^{137}Cs . Studies to determine the total activity of material released from Fukushima are ongoing, but an estimated release rate of $>10^{15}$ Bq h^{-1} for ^{131}I at the peak of the accident was calculated from environmental data combined with computer based atmospheric dispersion models (Katata et al., 2012). Although locally of major importance, these nuclear power station accidents resulted in little or no deposition of radionuclides in the UK.

There was a significant input to the UK environment from an accident involving failure of a US rocket to achieve orbit in 1964. The rocket burned up in the atmosphere over the Indian Ocean resulting in release to the atmosphere of 630 TBq of ^{238}Pu from a SNAP (System for Nuclear Auxiliary Power) device. This increased the $^{238}Pu/^{239,240}Pu$ activity ratio in the UK environment from the fallout value of approximately 0.02 in 1963 to approximately 0.045 in 1964 after the SNAP input (UNSCEAR, 2008)

The Sellafield nuclear fuel reprocessing plant in Cumbria, NW England, has been a major source of anthropogenic radionuclide contamination, especially in the mid 1970s, via low level liquid radioactive waste discharges to the Irish Sea. While there has been significant contamination of the marine system and local onshore transfer of radionuclides around the Irish Sea, the Sellafield discharge has not affected peatlands away from the coast (MacKenzie and Scott, 1993; Gleizon and McDonald, 2010).

There are numerous other minor sources of man-made radionuclides e.g. hospitals, universities, nuclear and non-nuclear industries and military activities which give rise to localised, point source contamination, but these are not significant for the peatland in this study.

1.6 ^{14}C Chronologies

^{14}C, which is formed in the atmosphere by interaction of cosmic rays with nuclei of N atoms, is widely used for the determination of archaeological dates, but is also one of the primary methods for establishing sediment chronologies on the 10^2 – 10^3 y timescale and has various other applications in geology, hydrology and oceanography. The foundation for this method was established by Libby's prediction in 1946 of the presence of ^{14}C in living organisms (Burleigh, 1981).The underlying assumption in the method is that the rates of production and decay of ^{14}C in the atmosphere are in equilibrium, giving a constant ^{14}C specific activity in atmospheric CO_2. Uptake of CO_2 by plants results in an equilibrium between ^{14}C in the atmosphere and living organisms on earth (Libby, 1946), but once an organism dies it no longer absorbs ^{14}C. The ^{14}C absorbed until the time of death then decays allowing age calculation from the first order decay equation:

$$t = \frac{1}{\lambda} \ln \frac{A_0}{A_t} \qquad (1.6)$$

where A_t is activity at time t, A_0 is activity at time 0 and λ is the decay constant.

Since the technique was first introduced, it has been recognised that the production rate of ^{14}C is not in fact constant but shows small variations due to natural factors, such as variations in cosmic ray intensity. Therefore a correction must be applied by use of calibrations curves based on the analysis of materials of known age. One such calibration method, the Bristlecone Pine programme, is described by Libby (1970), whereby dendrochronology is used to provide tree rings of known age as the basis for the calibration. Bard et al. (2004) used a stratigraphic method of calibration by measuring planktonic foraminifera in a deep sea core. In studies of this type where marine organisms are used, account must be taken of reservoir effects i.e. a variance in ^{14}C age of land based organisms compared with those mainly or completely marine based where dilution of the ^{14}C occurs (Bard et al., 2004; Ascough et al., 2005).

Models have been developed to facilitate the calibration of ^{14}C ages in both archaeological (e.g. OxCal) and modern (e.g.CALIB) applications (Bronk Ramsay

2001, 2008; Molto et al., 1997; Reimer and Reimer, 2001). As new data sets become available, ongoing programmes (e.g. INTCAL09 and MARINE09) continue to update calibration curves to improve the accuracy of ^{14}C derived ages (Reimer et al., 2009).

Human activities since the end of the 19th century have resulted in changes in the specific activity of ^{14}C in atmospheric CO_2 and this must be taken into account in ^{14}C analysis of recent materials. Anthropogenic effects that must be considered when using ^{14}C dating are the "Suess" effect and "bomb" effect. The former involves a dilution of atmospheric ^{14}C by carbon from the burning of fossil fuel containing no ^{14}C. The latter effect involves the input of anthropogenic ^{14}C from weapons testing mainly in the 1950s and 1960s and with peak input in 1963. To minimise these effects proxies used to validate ^{14}C dates should be of an appropriate age where these influences are negligible (Ascough et al., 2005). The presence of the large peak in atmospheric ^{14}C in 1963 (the bomb peak) and subsequent decline in activity has allowed recent chronologies to be derived through the application of "wiggle matching" i.e. matching observed ^{14}C vertical distributions in peat with the known record of atmospheric input from nuclear weapons (e.g. Goslar et al., 2005; van der Linden et al., 2008 (a); van der Linden et al., 2008 (b)).

^{14}C dating has been widely used for sediments and peats to derive chronologies dating back from a few hundred years up to tens of thousands of years (e.g. Thomson et al., 1995; Cloy et al., 2005). An excellent example of the combined use of ^{210}Pb and ^{14}C dating of peat is provided by studies carried out by Cloy et al. (2008) on cores from four ombrotrophic peat bogs in geographically diverse regions of Scotland. The study utilised $^{206}Pb/^{207}Pb$ isotopic ratios for Pb source apportionment and chronologies were derived to establish trends in atmospheric Pb deposition from pre-Roman times through the Middle Ages and industrial revolution until the present day. Evidence of the mining and smelting of British and European lead ores was seen at all sites relating to pre-Roman times through to the Middle Ages. At the northerly and central sites the dominant source of anthropogenic Pb input for the timescale covering the period from the start of the industrial revolution through to the early 20th century was from the mining and smelting of native Scottish Pb ores. However, there was also an observed influence in the north-easterly site from industrial sources in Spain. At the

southerly site the influence of imported Australian ores as well as native British ores was observed. The effect of the use of imported Australian lead as a petrol additive from the mid 20th century was perceptible at all sites as well as a major contribution from coal burning. The overall trend from the study agreed with Pb archive data and showed an increase in anthropogenic Pb deposition from the start of the industrial revolution, peaking between the late 19th and mid 20th centuries with a gradual decline into the start of the 21st century. There was also a noted decrease in atmospheric Pb deposition the further north the site was. Some regional variations were observed pointing to localised isotopic influences from indigenous sources (Cloy et al., 2008). The general observation from studies of this type is that Pb depositional fluxes in Scotland increased from values of the order of 1 mg m^{-2} y^{-1} before the industrial revolution to values of 40 – 50 mg m^{-2} y^{-1} in the mid-late 20th century after which they showed a decrease in response to decreased Pb emissions.

Extending the work of Cloy et al. (2008), Farmer et al (2009) examined contaminant mercury (Hg) deposition in peat and found an average deposition rate of 4.1 µg m^{-2} y^{-1} relating to pre-industrial times up to 1800 A.D. This rose to an average maximum value of 68.5 µg m^{-2} y^{-1} across the four sites covering the approximate time period 1900 to 1970 before falling away to an average of 27 ± 15 µg m^{-2} y^{-1}, corresponding to the late 1990s/early 2000s. These trends were compared with data for Pb and arsenic (As) in the cores and with known UK emission data since 1970 and it was proposed that there was an input of atmospheric Hg via long range deposition from activities beyond the UK during this timescale. The validity of the chronology was enforced by the excellent agreement between the $^{206}Pb/^{207}Pb$ isotopic ratio data from one of the cores with those for archived Scottish Sphagnum moss samples of known age. This again gives confidence in the use of accurately determined ^{210}Pb chronologies for determination of atmospheric metal depositional trends and also the need to include overlying vegetation in any analysis was reinforced (Farmer et al., 2009). Numerous studies using ^{210}Pb chronologies have been carried out internationally investigating deposition of various other contaminants such as arsenic and antimony, with ^{14}C chronologies being used in conjunction when longer timescales (> 150 years) are being studied (e.g. Shotyk et al., 1996; Cloy et al., 2005).

Combined ^{210}Pb and ^{14}C chronologies thus permit both recent and long term studies of peat. It would have been beneficial to use ^{14}C analysis in the study however funding restrictions prevented its use so the current research therefore concentrated on recent chronologies.

1.7 ^{32}Si Chronologies

The usefulness of ^{210}Pb for establishing chronologies on timescales of up to about 150 years and of ^{14}C for chronologies from a few hundred years up to tens of thousands of years is well established. There is, however, a gap between the times that can be covered accurately by these methods and it has been apparent since its discovery that the cosmic ray produced radionuclide ^{32}Si could potentially provide chronologies to fill that gap. The existence of ^{32}Si had been predicted in the early 1950s and it was first detected, as an artificially produced spallation product by Lindner (1953). Natural ^{32}Si was first detected in the marine environment by Lal et al. (1960) and it is now well established that ^{32}Si is a cosmogenic radionuclide produced in the atmosphere. The atmosphere comprises 0.93% by volume argon (Ar), which gives rise to spallation products via a range of nuclear reactions induced by cosmic rays (Marquez and Costa, 1955). Spallation, is a nuclear process whereby high energy particles bombard nuclei causing ejection of many lighter particles. One of the spallation products of Ar is ^{32}Si for which the production mechanism is believed to be ^{40}Ar(p,p2α)^{32}Si (Nijampurkar et al., 1998). ^{32}Si decays by ß$^{-}$ emission to its daughter product ^{32}P which is also a ß$^{-}$ emitter with a half life of 14.3 days.

Production rates for ^{32}Si are very low and have been calculated by various methods. One method, using observed fallout of cosmogenic ^{32}P and applying a production probability ratio for ^{32}Si/^{32}P of 0.2±0.02, gave a ^{32}Si production rate of 2.2 x10^{-4} atom cm^{-2} s^{-1}, which was in agreement with other early estimations (Lal et al., 1960). A more recent estimate is 0.95 x 10^{-4} atom cm^{-2} s^{-1} (Fifield and Morgenstern, 2009). Production rates are dependent on both the cosmic ray flux and on magnetic latitude and can vary by a factor of four between the equator and the poles (Simpson, 1951(a), 1951(b), 1951(c); Suess , 1958).

Determination of ^{32}Si in the environment is carried out by extraction of BSi, followed by purification and subsequent milking of the daughter ^{32}P. Low background counting techniques are required for this analysis and during the early development of the method, analysis was by a gas flow beta counter (Lal et al.,1960). In a study of groundwater in limestone aquifers, Morgenstern et al. (1995) used a semiconductor surface barrier PIPS (Passivated Implanted Planar Silicon) detection system. However limitations of these systems when measuring close to the limit of detection required a method of higher detection efficiency to be explored. Morgenstern et al. (2001) used liquid scintillation spectrometers in an attempt to achieve this, but the observed count rates were still close to the limit of detection even using a high efficiency liquid scintillation spectrometer. The possibility of using AMS (accelerator mass spectrometry) has been explored and, while useful in the study of ice cores where the ratio of ^{32}Si to stable silica is high enough to allow detection (Fifield and Morgenstern, 2009), it is not applicable in sediments where concentrations of stable Si are much higher. However in peat the low intrinsic stable silica content may allow this method to be feasible. Ongoing attempts are being made at SUERC to develop a low background silicon diode detection system for analysis of ^{32}Si, but a working detector is not yet available (Sanderson, Pers Comm.). Attention in this study was therefore focussed upon the development of the chemical pretreatment method for potential application of ^{32}Si dating in peat.

Lal et al. (1960) realised the potential of ^{32}Si for studying the mixing processes of water masses as well as other applications involving tracing accumulating systems containing biogenic silica, but acknowledged that the low abundance in terrestrial environments coupled with dilution with stable Si would make this problematic. He analysed three siliceous sponges from the Gulf of California, by milking the ^{32}P after allowing time for its ingrowth from ^{32}Si, and found an average specific activity for ^{32}Si of 19.6 ± 1.3 dpm kg^{-1} (0.327 ± 0.022 Bq kg^{-1}) SiO_2. A much wider study by Lal et al. (1976), covering the world's major oceans, found specific activities in the range 4-80 dpm (0.067-1.333 Bq) of ^{32}Si kg^{-1} SiO_2 with highest values in the Atlantic Ocean (35-76 dpm kg^{-1}, 0.583-1.267 Bq kg^{-1}) compared to the Antarctic Ocean which had the lowest values (4-7 dpm kg^{-1}, 0.067-0.117 Bq kg^{-1}). Morgenstern et al. (2001) applied ^{32}Si dating to marine sediments from Bangladesh, enabling the study of anthropogenic environmental

impacts over a thousand year timespan covering important historical events. He derived an initial specific activity for ^{32}Si of 5.9 dpm kg^{-1} (0.098 Bq kg^{-1}) SiO_2 which agreed with results by DeMaster (1980) for a varved sediment core in the Gulf of California.

Despite these limited demonstrations of the value of ^{32}Si dating, the technique has not been widely adopted, partially because of the difficulty of analysis, but also because of previous uncertainty over the half life value. Early estimates of the half life varied widely from less than 100 y up to 710 y (Lindner, 1953). However, recent AMS measurements, supported by determinations made from stratigraphic studies, direct decay measurement and equilibrium measurement, have provided confidence in a value of 144±11 y (Fifield and Morgenstern, 2009).

After wet deposition as silicic acid or dry deposition on particulate matter, ^{32}Si is taken up by organisms such as diatoms and integrated into their skeletal structures and also by plant materials which, on decay, form silica rich phytoliths. The ^{32}Si integrated within this biogenic silica can then accumulate in systems such as sediments and soils. The separation of biogenic silica from these environments is carried out by alkaline extraction by well-established methods which have been compared and summarised by Conley (1998) and Sauer et al. (2006). A problem associated with the extraction method is the possible dissolution of mineral silica along with the biogenic component. A technique which addresses this issue involves the concurrent determination of aluminium which is derived almost exclusively from the mineral fraction (Koning et al., 2002). There are however no reported applications of ^{32}Si dating of peat, so the aim of this part of the study was to evaluate if an existing method for extraction of biogenic Si from lake sediments is applicable to analysis of peat.

1.8 Study site

The study site was Langlands Moss, which is a raised peat bog located in West Central Scotland to the South of the town of East Kilbride (Nat. grid ref. NS 6343 5136) (Figures 1-7, 1-8 & 1-9).

Figure 1-7 Location of Langlands Moss study site (Grid reference NS 6343 5136)

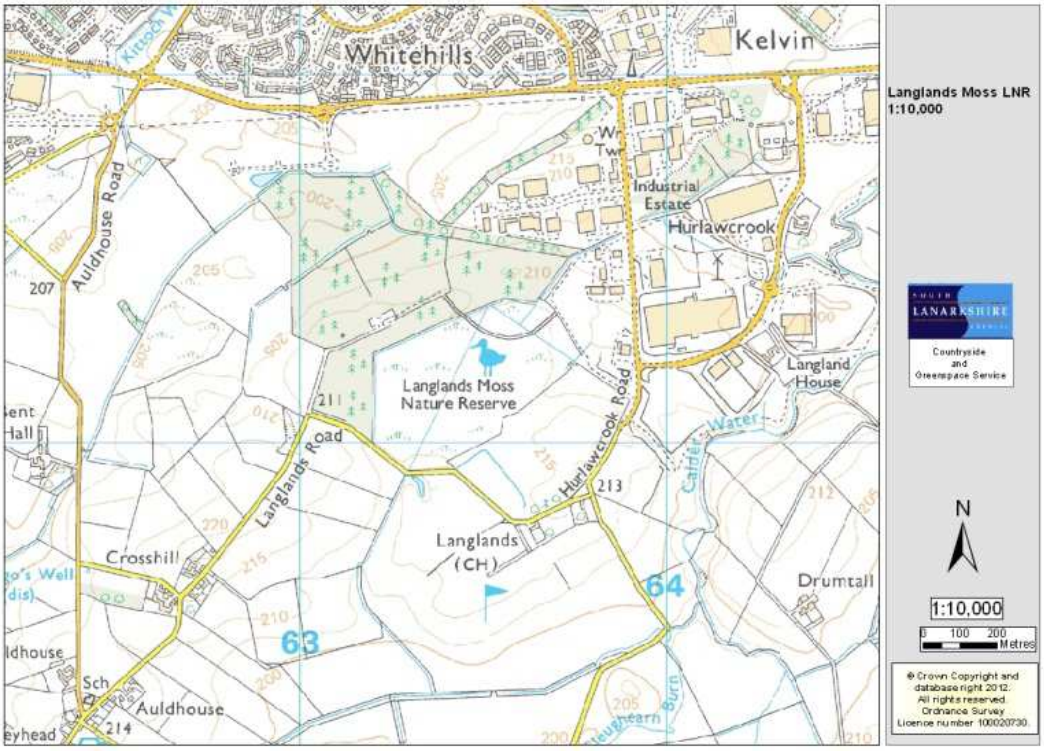

Figure 1-8 Detailed map of Langlands Moss

Figure 1-9 Aerial view of Langlands Moss

In 1996, Langlands Moss was established as South Lanarkshire's first formally designated Local Nature Reserve. The bog has developed during the Holocene in a "kettle hole", which is a depression formed by fragmenting ice towards the end of the last ice age around 10,000 years ago (Website- Friends of Langlands Moss). The bog has an area of 25 hectares, with a total depth of peat of more than 8 m at the centre and a gradual decrease in depth towards the edges. It is located at an altitude of 214 m, has a mean annual air temperature of 7.3^{o}C and receives an approximate annual precipitation of 971mm. The vegetation is dominated by heather, cotton grass and mosses (Figure 1-10) (Langdon and Barber, 2005).

Figure 1-10 Vegetation on Langlands Moss

Langlands Moss was chosen as the sampling site for this study as it is ombrotrophically fed, with no streams or rivers draining the bog. However it is bounded to the south by the River Calder and a large drainage ditch, with dams to prevent water flow, divides the western and eastern sides of the bog (Figure 1-11).

Figure 1-11 Dam system on Langlands Moss

The western part of the bog has been subject to anthropogenic influence by way of afforestation and subsequent deforestation after a period of about 40 years. A commercial conifer plantation was planted in the mid 1950s, but was felled in March 1995 before reaching full economic viability when the importance of conserving the peat bog became paramount. In the deforestation process, the trunks of the trees were cut through near the base and the trees were carefully removed by helicopter, leaving the stumps in place to minimise disturbance of the bog. The tree stumps and roots are still evident on the western section of the site at present (Figure 1-12).

Figure 1-12 Tree stumps on Langlands Moss

This method of removal of the trees means that material incorporated in the peat during the period when it was forested was left in place. The site therefore offers a useful situation in which to study differences between the peat in the forested location and that in the other sections of the bog which were left in their natural state. A large part of the bog was also subject to a fire in June 2000. (Maureen Potter, Friends of Langlands Moss; John Hawell, SLC, pers. comm.).

2 Methods

2.1 Sampling procedure

Five cores were collected from the study site over two visits as summarised in Table 2-1.

Core ID	Collection date	Site co-ordinates and characteristics	Sample collection method
FH	05/10/10	N55°44'09.1" W004°10'34.7" Elevation 218m Forested	7.5 cm I.D. core tube; vertical sampling resolution 2 cm
FL	05/10/10	N55°44'09.1" W004°10'34.7" Elevation 218m Forested	Excavated section, 10x10 area x5 cm depth sections
UH	05/10/10	N55°44'03.5" W004°10'36.0" Elevation 221m Unforested	10 cm I.D. core tube; vertical sampling resolution 2 cm
UL1	05/10/10	N55°44'03.5" W004°10'36.0" Elevation 221m Unforested	Excavated section, 10x10 area x5 cm depth sections
UL2	16/06/11	N55°44'03.5" W004°10'36.0" Elevation 221m Unforested	Excavated section 20x20 area x5cm sections

Table 2-1 Sample codes and site characteristics

Samples FH and UH were collected using plastic coring tubes with diameters as indicated in Table 2-1. The tube was carefully placed in position, ensuring overlying vegetation was included, and gently hammered into the peat as shown in Figure 2-1(a). The area around the tube was then excavated as shown in Figure 2-1(b), to allow a spade to be placed under the base and the core was extracted by simultaneously levering with the spade and pulling on a handle inserted through the top of the tube. Samples FL, UL1 and UL2 were collected by excavating a pit to expose a clean vertical face in the peat, as shown in Figure 2-1 (c), allowing the required depth increments to be measured and removed by trowel, again ensuring overlying vegetation was included. The cores from the previously forested site were deliberately collected from a location several metres from the nearest tree stumps to avoid the influence of roots. All samples were bagged, labelled and sealed for further processing in the laboratory. The cores collected in tubes were extruded using a plunger to push the core upwards and where possible the peat was sectioned in 2 cm vertical increments. However the vegetation at the surface of core FH made this impossible and as a result, a 3 cm increment was used for the first sample increment. All samples were weighed then air dried, followed by oven drying at 40^{o}C to constant weight, re-weighed to allow the calculation of dry/wet ratios and homogenised by mortar and pestle before sub-sampling for further analysis. Dry/wet ratios were used in preference to wet/dry ratios as it was the weight of solid that was of interest rather than water loss, and these were calculated by division of the dry weight (after oven drying at 40^{o}C) by the original wet weight. Dried sub samples were also furnaced at 450^{o}C to determine loss on ignition and ash values.

(a) **(b)** **(c)**

Figure 2-1 (a) Insertion of core tube (b) Excavation of area around core tube (c) Exposure of clean vertical face for low resolution sampling

2.2 Gamma spectroscopy system

The detector used for gamma spectroscopy was a low background EG&G Ortec LO-AX n-type High-Purity germanium gamma photon detector as shown in Figure 2-2. A schematic cross section view of the detector and shielding is shown in Figure 2-3 along with the electronic components in the gamma spectroscopy system.

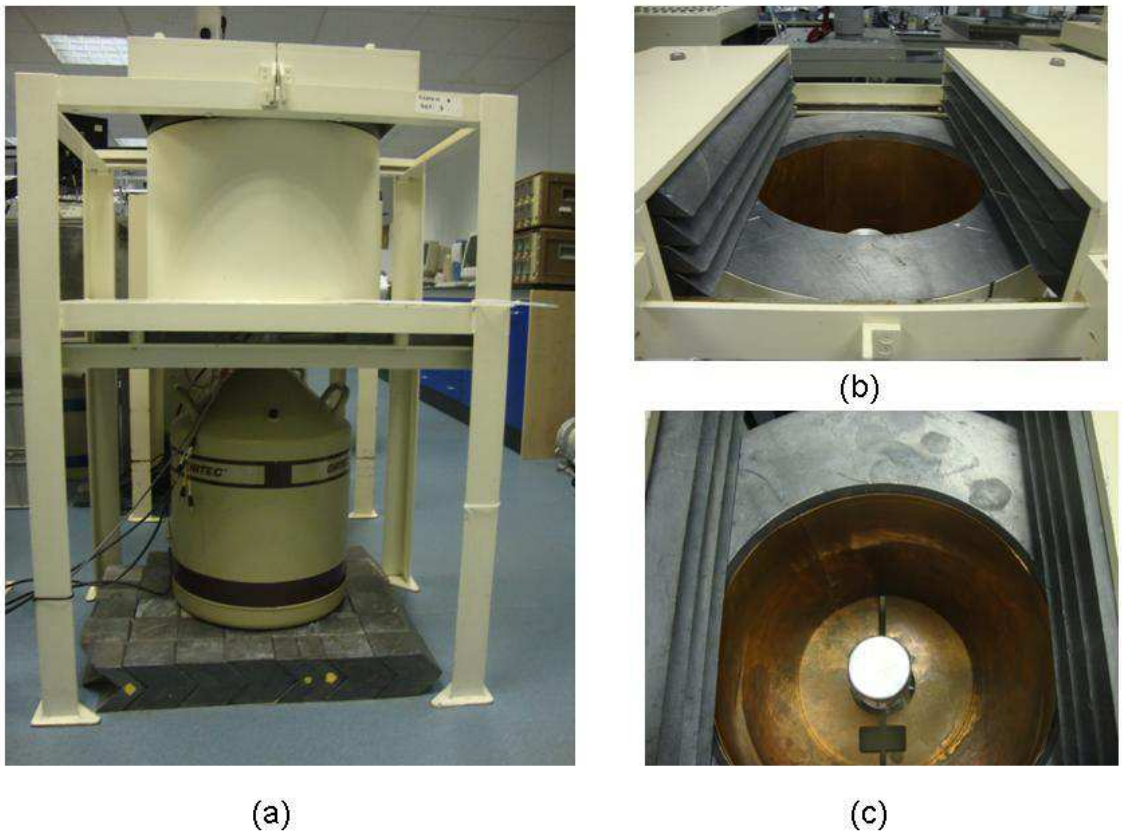

Figure 2-2 (a) EG&G Ortec LO-AX n-type High-Purity germanium gamma photon detector (b) 10cm Pb shielding (c) Ariel view of detector end cap

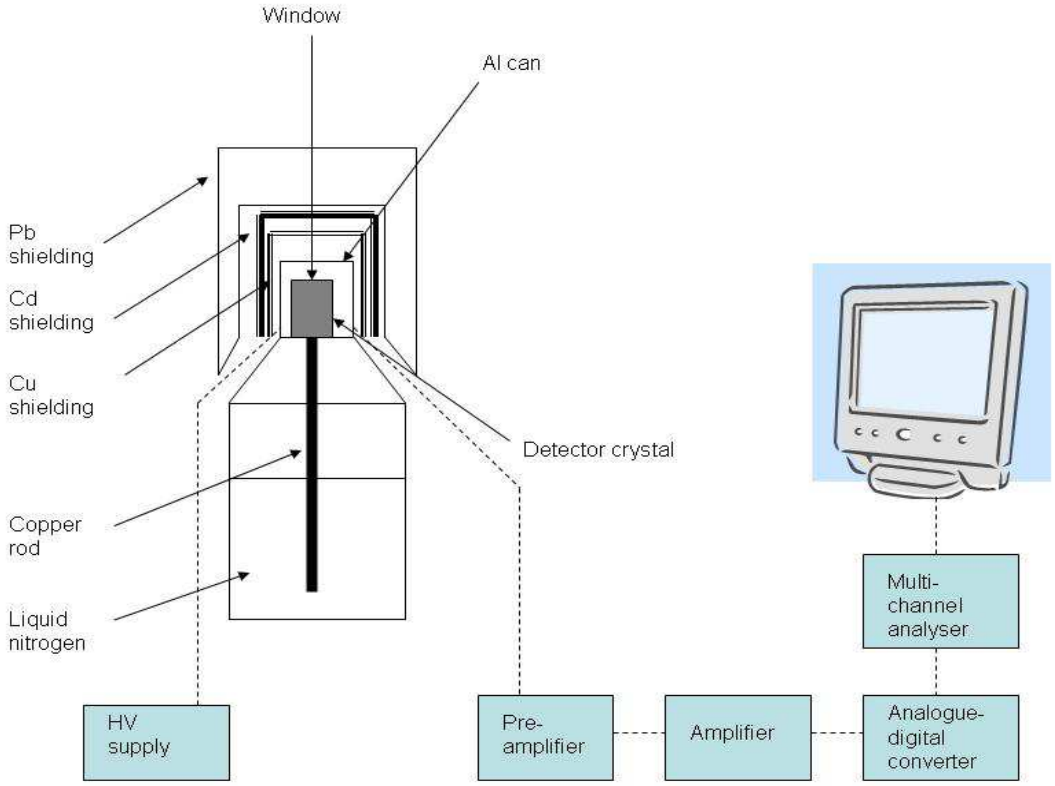

Figure 2-3 Schematic cross section view of the detector and shield and of the electronic components of the gamma spectroscopy system

The detector has a planar geometry with a diameter of 51.4 mm and depth of 19.4 mm. It has a 0.5 mm Be window to minimise gamma photon absorption and a distance of 3 mm from the detector to the end cap. The detector was housed in a 10 cm Pb shield with a Cd – Cu lining to reduce x-ray background and was supported on 10 cm of Pb to further reduce background. The detector has no background peak at the ^{210}Pb energy which is important in obtaining a suitably low limit of detection (MacKenzie et al., 2011). However background peaks did occur for ^{214}Bi and ^{214}Pb. Background spectra were therefore recorded on a regular basis to correct for the background contribution of ^{214}Pb and ^{214}Bi. Analysis times of up to 168 hours were used to obtain counting statistics uncertainties of less than 5%.

2.3 Interaction of radiation with matter and main features in a gamma spectrum

The net photopeak area is used in gamma spectroscopy analysis which is obtained from subtracting the continuum (C) from the gross peak (see Figure 2-4). The photopeak arises when a gamma photon imparts all of its energy to an electron which is then ejected from the atom in which it originated. The electron is normally ejected from the 1s orbital and the resultant vacancy is filled by an electron from an outer orbital giving rise to emission of x-rays. The ejected photoelectron and associated x-rays will induce ionisation in the detector and if this ionisation can be measured it can be related to the gamma photon energy. This is defined as the photoelectric effect. The Compton continuum is generated when gamma photons interact with atoms in the detector causing ejection of Compton electrons and scattering of the gamma photons with reduced energy. Maximum transfer of energy to the Compton electrons occurs for 180^{o} scattering of the gamma photon and this gives a defined maximum to the ionisation that can be caused by the electron, producing a sharp end (the Compton edge) to the continuum. The characteristic annihilation peak is a result of pair production i.e. when gamma photons have greater energy than 1.022 MeV, (twice the energy equivalence of the electron rest mass - 0.511 MeV) a positron – electron pair can be spontaneously produced. The gamma photon is completely absorbed and the positron/electron pair impart their energy by ionisation of the atoms in the sample. When the energy of the positron becomes low it combines with an electron to produce two gamma photons of energy 0.511 MeV, this is known as the annihilation process (Choppin et al., 1995).

The constituent parts of a typical gamma spectrum are shown schematically in Figure 2-4.

G = gross area

N = net area

C = area under continuum

G = N + C

N = G - C

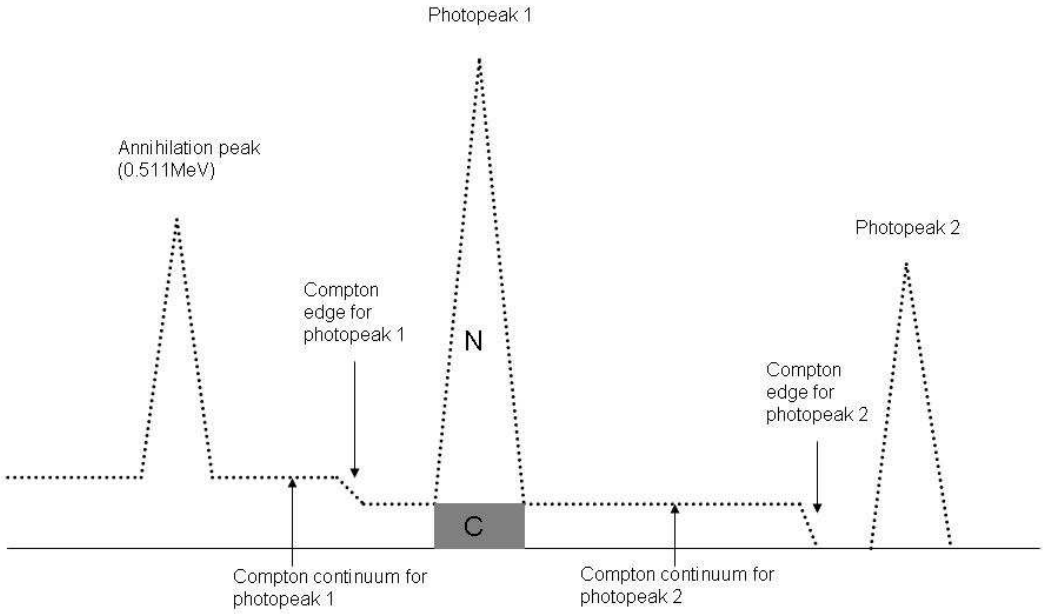

Figure 2-4 Constituent parts of a typical gamma spectrum

Figure 2-5 shows the ^{210}Pb photopeak for a sub section of core UL2

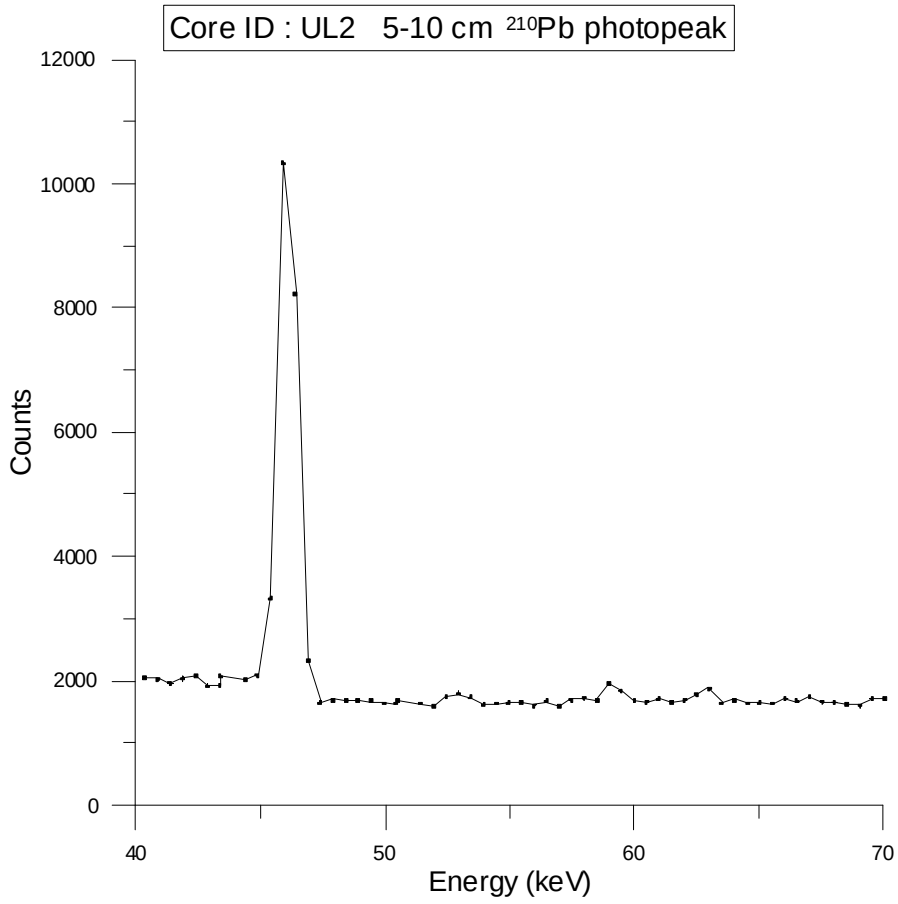

Figure 2-5 ^{210}Pb photopeak for sub section of core UL2

Detection efficiency (E) is defined as follows:

$$E = \frac{C}{A} x\, 100\,\% \qquad (2.1)$$

where C is the photopeak net count rate (cps) and A is the source activity (Bq). Detection efficiency varies with distance (d) from the detector according to the following:

$$E\ \alpha\ \frac{1}{d^2} \qquad (2.2)$$

The limit of detection for ^{210}Pb will vary depending upon factors such as sample weight, sample chemical composition and counting time. In the present work, limit of detection was taken as the value at which the propagated 1 σ error reached 50%. This gave limits of detection of about 5 Bq kg^{-1}.

2.4 Sample preparation for gamma spectroscopy

Samples of ground, dried peat were prepared in a reproducible geometry which, where sample weight allowed, was a pelleted disc, or loose where there was insufficient material to pelletise. A highly reproducible geometry is important and minimising sample depth through pelleting will maximise detection efficiency. To optimise the desired reproducible geometry the pelleted discs were formed using an Enerpac hydraulic disc press by compression in an assembly of stainless steel parts as pictured in Figures 2-6 (a) to 2-6 (i). The hydraulic press unit is shown in Figure 2-6 (a) and the component parts (1-5) of the pelleting assembly are shown in Figure 2-6 (b). The procedure for producing a pellet is:

- Solid cylinder 1 is placed on the base of the press unit (Figure 2-6 (c)).
- Hollow cylinder 3 is then positioned on top of part 2 to form a well into which the sample is placed (Figure 2-6 (d)).
- Plunger 4 is then inserted into the well, compressing the sample (Figure 2-6 (e)).

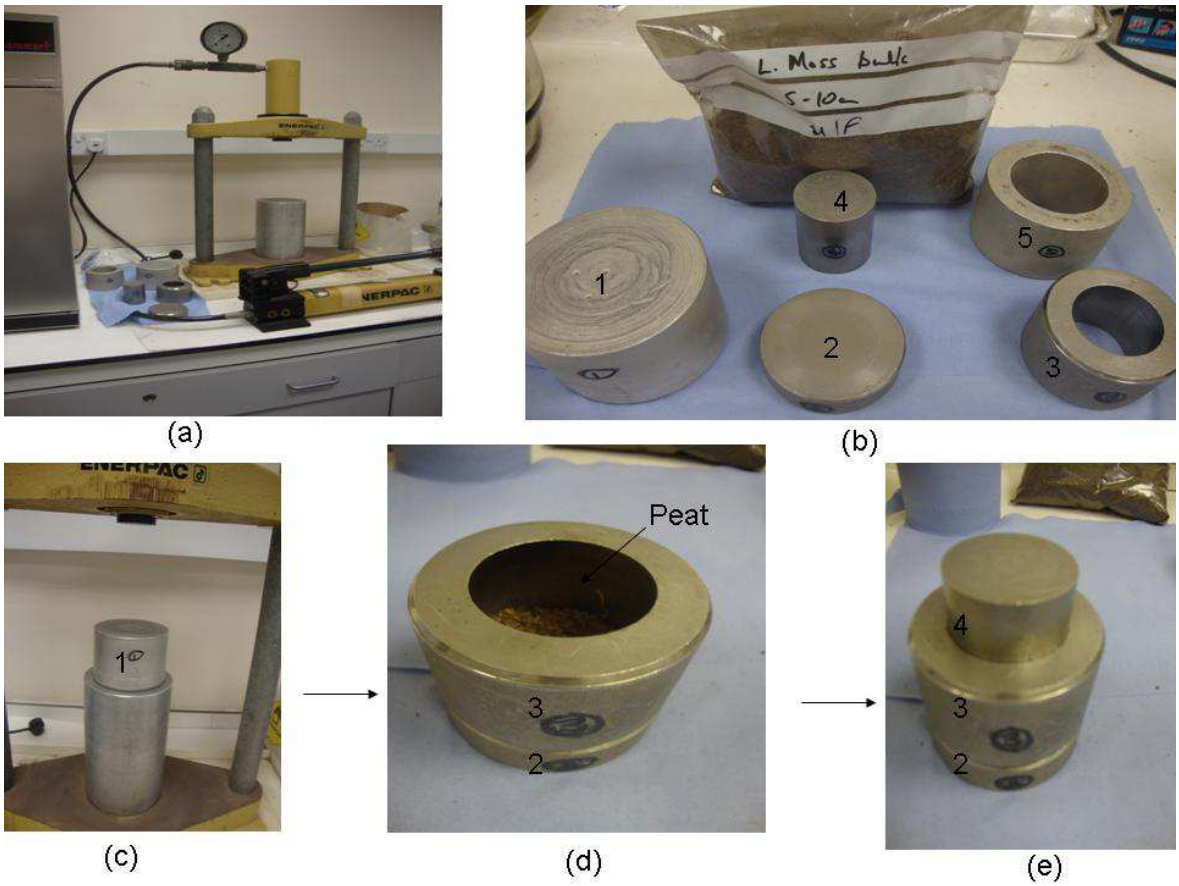

Figure 2-6 Enerpac hydraulic disc press and components for pelleted disc preparation – Part 1

- This combined assembly is then positioned on top of solid cylinder 1 (Figure 2-7(f)) and a pressure of 10-12 tons applied to complete the compression of the sample.

- On release of pressure the assembled unit comprising parts 2,3 & 4 is inverted and placed on the press base unit (after the removal of solid cylinder part 1) and part 5 is placed in-between parts 2 and 3 as a spacer unit (Figure 2-7 (g)).

- Gentle pressure is then applied to the assembly which forces part 3 to drop, releasing the pelleted sample disc (Figure 2-7(h)).

- The pelleted discs or loose samples were transferred to 55 mm diameter unvented petri dishes(Figure 2-7 (i)), which were then sealed using epoxy resin adhesive (Figure 2-7(j)).

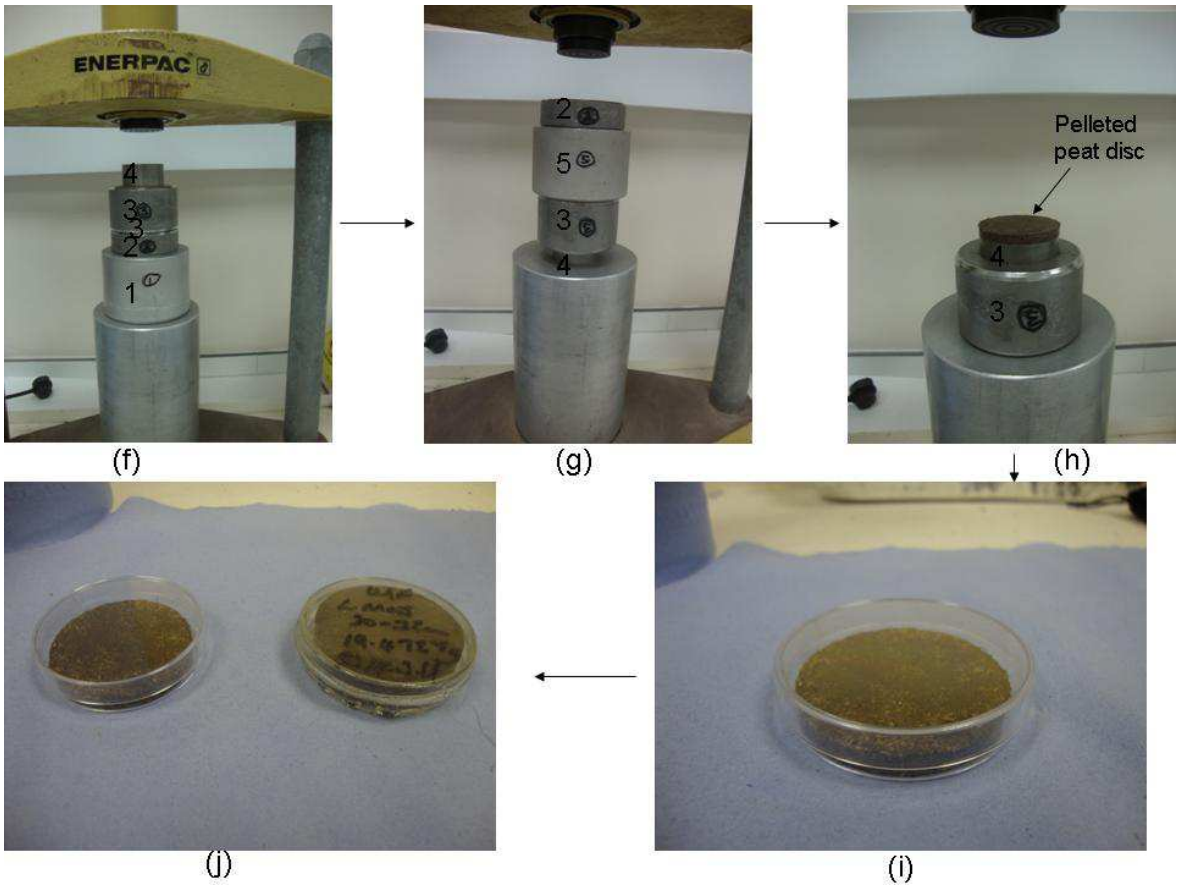

Figure 2-7 Enerpac hydraulic disc press and components for pelleted disc preparation – Part 2

The sealed samples were stored for a minimum of three weeks to ensure radioactive equilibrium between ^{222}Rn and ^{226}Ra. After reaching equilibrium samples were accurately placed in a reproducible position on the end window of the detector.

2.5 Gamma spectroscopy standards and detection efficiencies

Detection efficiencies were established using standards prepared by adding known activities of the radionuclides of interest, using dilutions of certified radionuclide standard solutions, to peat of an age such that no unsupported ^{210}Pb

or anthropogenic radionuclides were present. Details of the detection efficiencies obtained for each radionuclide are shown in Table 2-2 as well as information on the source of the radionuclide standard solutions.

Radionuclide	Half-life	Gamma Energy (keV)	Gamma Intensity (%)	Detection Efficiency 20g pellet (%)	Standard solution source	Standard solution code
^{210}Pb	22.3 *2* y	46.52	4.05	0.456	Amersham	S6(B)35-53
^{214}Pb	26.8 *9* min	351.87	37.1	0.546	Harwell	88/226/10
^{214}Bi	19.9 *4* min	609.311	46.1	0.296	Harwell	88/226/10
^{137}Cs	30.0 *2* y	661.660	85.21	0.718	Amersham	137/22199
^{241}Am	432.7 *5* y	59.5364	35.7	4.329	Harwell	95/241/49

(Half-lives and decay information were taken from Browne and Firestone, 1986)

Table 2-2 Detection efficiencies and Standard solution sources

The accuracy and validity of the method would ideally have been assessed by using a Certified Reference Material (CRM) but at the time the research was undertaken there was no suitable CRM available[1].

[1] IAEA has subsequently produced CRM IAEA-447 for radionuclides in moss- soils (Shakhashiro et al., 2012)

2.6 Metal analysis

Sub samples were analysed for a range of metals using Inductively coupled plasma – optical emission spectroscopy (ICP-OES). A schematic diagram of the main components of the ICP-OES instrument is shown in Figure 2-8.

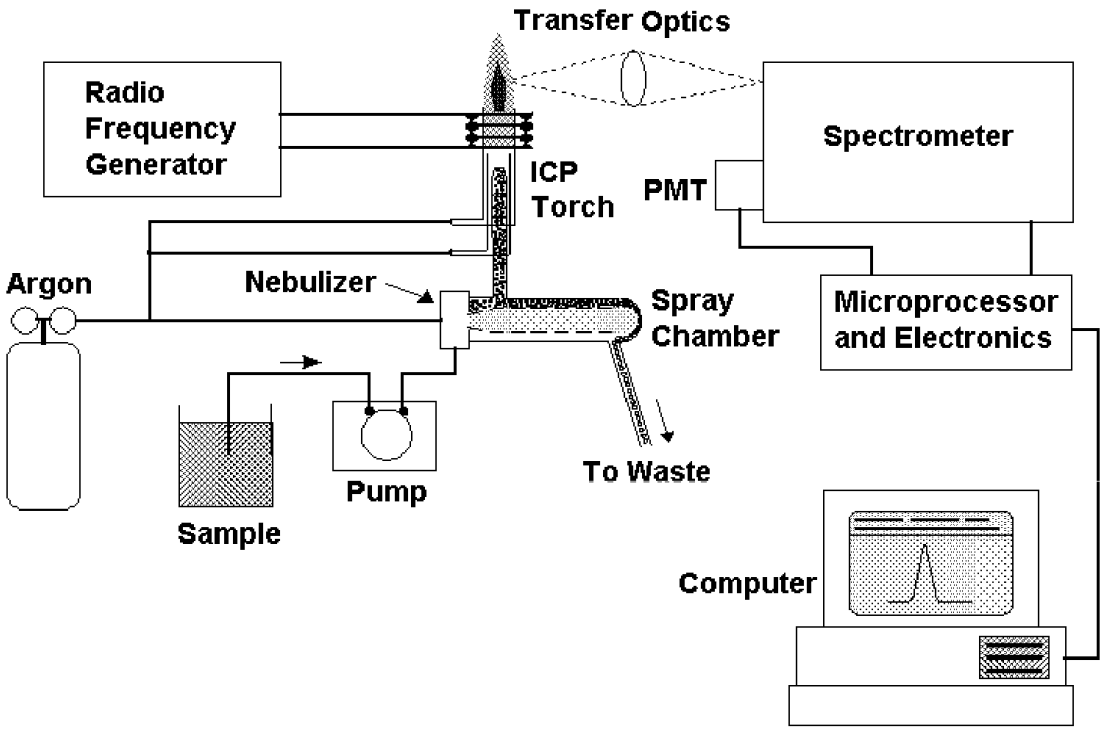

Figure 2-8 Main components of ICP-OES instrument

To prepare samples for ICP-OES analysis, the established method used in the SUERC ICP-MS/OES laboratory was used. 0.1 g sub-samples of dried, ground homogenised peat were refluxed for 8 hours in 2 ml of an aqua regia solution (Aristar grade 12M HCl: 16M HNO_3, 50:50) in a covered Teflon beaker. The refluxed solutions were then diluted to 10 ml with Milli Q (R=18.2 Mohms.cm@25^{o}C) water and filtered through a Whatman 542 grade hardened ashless filter paper to separate from the peat residue, the residues rinsed with Milli Q water and the combined filtered solutions and rinsings made up to a final volume of 100 ml with Milli Q water in an A -grade volumetric flask. Blanks and a Certified Reference Material, CRM049-050 (metals in soil- RTC, Laramie, WY

82070- used in house for inter-comparison of various soil matrices) were also analysed in the same manner. The resulting solutions were analysed for Pb, Zn, Fe, Mn, Cu, Ni, Cr, Cd, Ca and Mg using a Perkin Elmer 5300DV ICP-OES instrument, with a Scott style spray chamber and gem tip cross flow nebuliser under the conditions in Table 2-3.

Torch gas flow rate	Auxiliary gas flow rate	Nebuliser Gas flow rate	RF power Watts	Viewing distance	Plasma view	Sample flow
15 l min^{-1}	0.2 l min^{-1}	0.8 l min^{-1}	1300 watts	15mm	Axial	1.5ml min^{-1}

Table 2-3 ICP-OES instrument conditions- metal analysis

The spectroscopic lines used for analysis of each element are detailed in Table 2-4.

Analyte Element	Atomic Spectroscopic Line (nm)
Pb	220.353
Zn	206.200
Fe	238.204
Mn	257.610
Cu	327.393
Ni	231.604
Cr	267.716
Cd	228.802
Ca	317.933
Mg	285.213

Table 2-4 ICP-OES elemental spectroscopic lines

Peak area was integrated over 3 points with a 2 point background correction. Calibration of the instrument was carried out using 0.1, 1.0 and 10.0 mg l^{-1} standards prepared from NIST traceable Alfa Aesar Specpure® 1000 mg l^{-1} standards for each of the metals under analysis. For quality control purposes the

validity of the method was assessed by analysis of a Certified Reference Material- CRM049-050 (Metals on Soil) with results detailed in Table 2-5.

CRM049-050 Metals on Soil			Units: mg kg^{-1}		(n = 4)	
Element	**Certified Reference value**	**Standard Deviation**	**Confidence Interval**	**Prediction Interval**	**Average measured value**	**Standard Deviation**
Pb	111	6.69	109 - 112	97.5 - 124	118	7.12
Zn	542	28.9	534 - 549	485 - 599	616	41.0
Fe	9170	774	8950 - 9380	7630 - 10700	8791	391
Mn	636	37.7	625 - 646	561 - 710	628	33.3
Cu	88.5	5.39	87.1 - 89.8	77.8 - 99.1	83.4	4.87
Ni	344	19.9	339 - 349	304 - 383	349	28.4
Cr	355	20.7	350 - 360	314 - 396	355	13.7
Cd	80.0	4.28	78.9 - 81.0	71.5 - 88.4	80.3	4.25
Ca	4790	392	4680 - 4910	4020 - 5570	5126	682
Mg	899	61.4	881 - 916	777 - 1020	842	38.1

Table 2-5 Results for certified reference material CRM049-050 (Metals on Soil)

For Mn, Ni, Cr and Cd the average measured value (n=4) for the Certified Reference Material fell within the Confidence Interval range, while for Pb, Fe, Cu, Ca and Mg the value fell outwith the Confidence Interval range but within the Prediction Interval. For Zn, the value fell outwith both of these ranges suggesting a blank problem.

2.7 Pb isotope analysis

Sub samples were analysed for Pb isotopes using Inductively coupled plasma – mass spectroscopy (ICP-MS) and a schematic diagram of the instrument is shown in Figure 2-9.

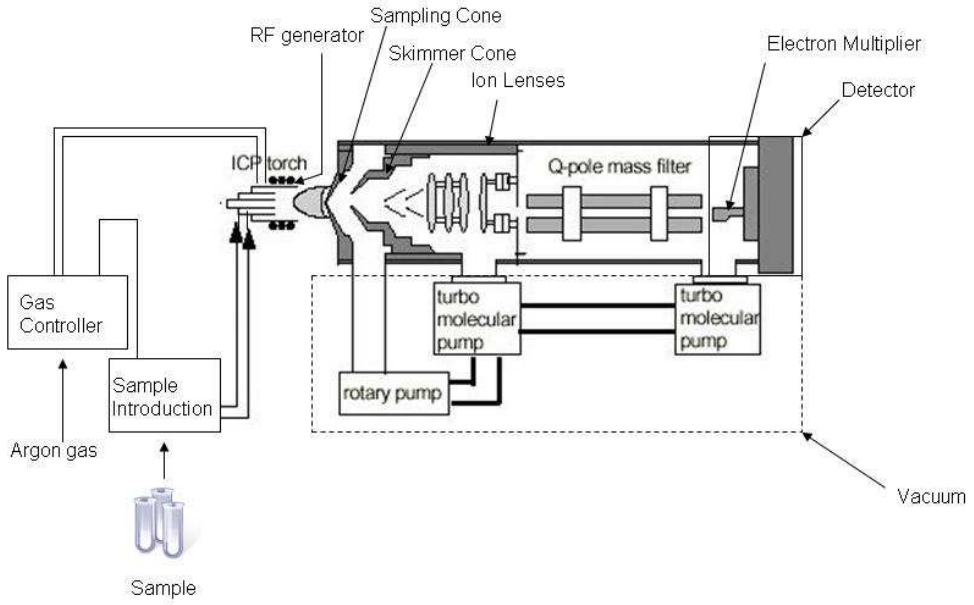

Figure 2-9 Main components of ICP-MS instrument

To prepare samples for Pb isotope analysis, 0.1 g sub-samples of dried, ground homogenised peat were prepared by the method used in section 1.6. Blanks were also analysed in the same manner. Further dilutions were carried out on samples and blanks as required to bring the final Pb concentrations (as measured by ICP-OES analysis) to 5 µg l^{-1}. This value was established by the ICP-MS group at SUERC to be the optimum concentration in terms of providing suitable counting statistics while minimising the effects of blocking the inlet system of the ICP-MS instrument. The resulting solutions were analysed for Pb isotopes using an Agilent 7500CE ICP-MS instrument fitted with an Aspire nebuliser at 0.1 ml min^{-1} flow rate. The instrument was run in "peak jumping mode" with 3 point peak integration over 25 replicates. A NIST Standard Reference Material 981 (common lead isotope standard) was used for quality control and to correct for instrument drift. The certified ratio values for $^{206}Pb/^{207}Pb$, $^{208}Pb/^{207}Pb$ and $^{208}Pb/^{206}Pb$ for the reference material are 1.093, 2.370 and 2.168 respectively. Values in the ranges 1.090-1.113, 2.366-2.389 and 2.146-2.175 were measured

for $^{206}Pb/^{207}Pb$, $^{208}Pb/^{207}Pb$ and $^{208}Pb/^{206}Pb$ respectively for the reference material during the analysis.

2.8 Biogenic silica extraction from lake sediment

A previous study compared alkaline extraction methods using different concentrations of NaOH, Na_2CO_3 and NH_4OH on different sample matrices and concluded the method described below to be most effective, particularly in sediments high in biogenic silica (H Rossiter, pers comm). 40 mg samples of sediment were used and 40 ml Na_2CO_3 (0.5 M) was added. Samples of silica gel were prepared similarly as a proxy for biogenic silica. Samples were shaken in a shaking water bath at 85^{o}C for 2 hours and sub sampled for ICP-OES analysis. Samples were then filtered and the volume reduced to ~ 5 ml. Silica was then precipitated by dropwise addition of Aristar grade HCl (37% / 12M). The precipitate was then collected, rinsed, dried and weighed.

In order to establish the method in the present research, it was applied to a Mexican lake sediment core- ZAC/2 (supplied by Professor S Metcalfe, Nottingham University), which was composed dominantly of biogenic silica.

2.9 Application of extraction method to Peat

When trying to adapt the above biogenic silica extraction method to peat samples some problems were encountered, the most challenging being the opacity of the solution after extraction. The need for larger sample weights to give the required quantities of biogenic silica also exacerbated this problem. The reason for this opacity is due to the presence of humic material in the composition of peat as described in Chapter 1. Humic substances are weak acids so it was recognised that dissolution of organic matter was likely to be a problem during the alkaline digestion. This proved to be the case in this study so in order to overcome this problem the peat was furnaced to destroy organic matter. For this to be a viable option it had to be proved that no silica was lost during the furnacing process. This was validated by an experiment during which the following combinations of biogenic silica proxies and peat were furnaced at 450^{o}C- see Table 2-6.

BSi furnace experiment		450°C					
Sample number	**BSi proxy type**	**BSi proxy weight (g)**	**Peat weight (g)**	**Total weight (g)**	**Weight after furnace (g)**	**Weight loss (g)**	**Weight loss (%)**
1	Fine kiln sand	5.1077	0	5.1077	5.1002	0.0075	0.15
2	Coarse sand	5.1977	0	5.1977	5.1694	0.0283	0.54
3	Silica gel	5.6704	0	5.6704	5.5677	0.1027	1.81
4	None	0	5.1329	5.1329	0.3676	4.7653	92.84
5	Fine kiln sand	2.5117	2.5901	5.1018	2.549	2.5528	50.04
6	Coarse sand	2.2626	2.5745	4.8371	2.4412	2.3959	49.53
7	Silica gel	2.3931	2.6083	5.0014	2.6128	2.3886	47.76
8	Fine kiln sand + Silica gel	2.6115 +2.5384	0	5.1499	5.1109	0.0390	0.76

Table 2-6 Results from biogenic silica furnace experiment

Sub samples from the biogenic silica extraction method were analysed for Si using Inductively coupled plasma – optical emission spectroscopy (ICP-OES) under the conditions shown in table 2-7. The instrument is described in section 2.6. The atomic spectroscopic line used for analysis was 251.611 nm. The accuracy and validity of the method would ideally have been assessed by using a Certified Reference Material (CRM) but at the time the research was undertaken there was no suitable CRM available.

Torch gas flow rate	Auxiliary gas flow rate	Nebuliser Gas flow rate	RF power Watts	Viewing distance	Plasma view	Sample flow
15 l min^{-1}	0.2 l min^{-1}	0.75 l min^{-1}	1400 watts	15mm	Axial	1.5ml min^{-1}

Table 2-7 ICP-OES instrument conditions - Si

3 Results

Results - Part 1

The results for cores UH, UL1, UL2, FH and FL are presented in tabulated form in the first part of this chapter. For all of the cores there are results for the following analyses

- Dry / wet ratio, Loss on ignition and Dry bulk density
- Ash content
- Gamma analysis- ^{210}Pb, ^{137}Cs and ^{241}Am
- ^{210}Pb flux and inventory
    - The 295 keV photopeak was rejected from the calculation of the ^{210}Pb supported component since it is subject to interference from the 294 keV peak of ^{234}Pa. The supported component was therefore calculated from the average of the 352 keV and 609 keV peaks.
    - Cumulative mass values are quoted in g m^{-2} and g cm^{-2} for ease of comparison with published work as both are used in literature.
- ^{137}Cs inventory

For cores UH, UL1, FH and FL there are also results for the following analyses

- Metal concentrations
- Pb inventory

For cores UH and FH there are also results for the following analysis

- Pb isotopes

3.1 Core UH

Core ID : UH Depth (cm)	Cumulative mass (g cm $^{-2}$)	Dry / wet ratio	Loss on ignition (%)	Dry bulk density (g cm^{-3})
0-2	0.02	0.21	97.18	0.019
2-4	0.07	0.22	98.99	0.032
4-6	0.15	0.22	98.48	0.049
6-8	0.32	0.19	97.37	0.117
8-10	0.59	0.17	93.08	0.151
10-12	0.90	0.17	92.87	0.163
12-14	1.22	0.18	94.37	0.155
14-16	1.51	0.17	95.47	0.139
16-18	1.77	0.17	95.75	0.125
18-20	2.08	0.17	96.01	0.178
20-22	2.41	0.18	95.98	0.156
22-24	2.71	0.17	98.13	0.147
24-26	3.01	0.16	99.20	0.148
26-28	3.30	0.15	99.34	0.142
28-30	3.53	0.13	99.34	0.093
30-32	3.77	0.14	99.39	0.144
32-34	4.04	0.13	99.33	0.127
34-36	4.25	0.09	99.57	0.082
36-38	4.41	0.08	99.75	0.075
38-40	4.57	0.09	98.96	0.082
40-42	4.74	0.11	98.93	0.095
42-44	4.96	0.11	98.94	0.122
44-46	5.18	0.10	98.82	0.098

Table 3-1 Core UH Dry / wet ratio, Loss on ignition and Dry bulk density

Core ID:UH Depth (cm)	Cumulative mass ($g\ cm^{-2}$)	Ash content (%)
0-2	0.02	2.82
2-4	0.07	1.01
4-6	0.15	1.52
6-8	0.32	2.63
8-10	0.59	6.92
10-12	0.90	7.13
12-14	1.22	5.63
14-16	1.51	4.53
16-18	1.77	4.25
18-20	2.08	3.99
20-22	2.41	4.02
22-24	2.71	1.87
24-26	3.01	0.80
26-28	3.30	0.66
28-30	3.53	0.66
30-32	3.77	0.61
32-34	4.04	0.67
34-36	4.25	0.43
36-38	4.41	0.25
38-40	4.57	1.04
40-42	4.74	1.07
42-44	4.96	1.06
44-46	5.18	1.18

Table 3-2 Core UH Ash content

Core ID:UH	URANIUM SERIES				
Depth (cm)	^{210}Pb (46keV)	^{214}Pb (295 keV)	^{214}Pb (352 keV)	^{214}Bi (609 keV)	^{137}Cs (662keV)
0-2	246±16	BDL	BDL	BDL	419±9
2-4	222±9	25±7	BDL	BDL	338±6
4-6	292±10	37±7	BDL	BDL	299±6
6-8	303±7	19±4	BDL	BDL	291±5
8-10	257±5	13±3	6±3	BDL	203±3
10-12	109±4	17±3	8±3	7±4	89±2
12-14	52±3	15±2	7±3	5±4	37±1
14-16	38±3	18±3	6±3	BDL	26±1
16-18	17±3	11±2	BDL	BDL	15±1
18-20	9±2	12±2	BDL	5±3	12±1
20-22	11±2	11±2	4±3	BDL	13±1
22-24	BDL	BDL	BDL	BDL	10±1
24-26	BDL	14±3	BDL	BDL	10±1
26-28	BDL	13±3	BDL	BDL	10±1
Units :- Bq kg^{-1} Uncertainty 1σ BDL :- Below detection limit					

Table 3-3 Core UH Gamma analysis : ^{210}Pb and ^{137}Cs

Core ID	Cumulative mass (g cm^{-2})	Depth (cm)	^{241}Am (Bq kg^{-1})
UH	0.586	8-10	2.54±0.38
UH	0.900	10-12	1.92±0.40

Table 3-4 Core UH Gamma analysis : ^{241}Am

ID : UH	Core diameter : 10.0cm				Area : 0.00785m^2 (78.5cm^2)		^{210}Pb flux : 83 Bq m^{-2}y^{-1}		
Depth	Total ^{210}Pb	Supported ^{210}Pb	Unsupported ^{210}Pb	Section activity	Section activity/area	Cumulative activity/area	Dry weight/area	Cumulative mass	
(cm)	Bq kg^{-1}	Bq kg^{-1}	Bq kg^{-1}	Bq	Bq m^{-2}	Bq m^{-2}	g m^{-2}	g m^{-2}	g cm^{-2}
0-2	246±16	BDL	246	0.74	94	94	382	191	0.019
2-4	222±9	BDL	222	1.13	143	237	646	705	0.071
4-6	292±10	BDL	292	2.26	288	525	985	1520	0.152
6-8	303±7	BDL	303	5.57	710	1235	2343	3184	0.318
8-10	257±5	5±3	252	5.96	760	1994	3014	5862	0.586
10-12	109±4	7±3	102	2.61	333	2327	3262	9001	0.900
12-14	52±3	6±3	46	1.12	142	2469	3090	12177	1.218
14-16	38±3	5±3	33	0.72	91	2561	2772	15108	1.511
16-18	17±3	BDL	17	0.33	43	2603	2502	17745	1.775
18-20	9±2	BDL	9	0.25	32	2635	3550	20771	2.077
20-22	11±2	BDL	11	0.27	34	2669	3112	24103	2.410
22-24	0	BDL	0	0.00	0	2669	2946	27132	2.713
24-26	0	BDL	0	0.00	0	2669	2954	30082	3.008
26-28	0	BDL	0	0.00	0	2669	2843	32981	3.298

Table 3-5 Core UH ^{210}Pb flux and inventory

ID : UH	Core diameter : 10.0cm		Area : 0.00785m^2 (78.5cm^2)			
Depth	Cumulative mass	Cumulative mass	^{137}Cs	Section activity	Section activity/area	Cumulative activity/area
(cm)	g cm^{-2}	g m^{-2}	Bq kg^{-1}	Bq	Bq m^{-2}	Bq m^{-2}
0-2	0.019	191	419±9	1.26	160	160
2-4	0.071	705	338±6	1.71	218	378
4-6	0.152	1520	299±6	2.31	294	673
6-8	0.318	3184	291±5	5.35	682	1355
8-10	0.586	5862	203±3	4.80	612	1966
10-12	0.900	9001	89±2	2.28	290	2257
12-14	1.218	12177	37±1	0.90	114	2371
14-16	1.511	15108	26±1	0.57	72	2443
16-18	1.775	17745	15±1	0.29	38	2481
18-20	2.077	20771	12±1	0.33	43	2523
20-22	2.410	24103	13±1	0.32	40	2564
22-24	2.713	27132	10±1	0.23	29	2593
24-26	3.008	30082	10±1	0.23	30	2623
26-28	3.298	32981	10±1	0.22	28	2651

Table 3-6 Core UH ^{137}Cs inventory

Core ID: UH Units: mg kg^{-1}										
Cumulative mass (g cm^{-2})	**Pb**	**Zn**	**Fe**	**Mn**	**Cu**	**Ni**	**Cr**	**Cd**	**Ca**	**Mg**
0.02	85±4	63±0.4	346±4	96±1.25	9±0.6	0±0.2	2±0.5	6±0.1	1418±23	932±11
0.07	72±10	57±1.1	335±3	82±0.49	10±0.4	BDL	1±0.3	5±0.3	1399±25	808±12
0.15	97±6	72±1.8	534±12	83±1.91	12±0.1	2±1.6	2±0.9	7±0.4	1726±47	794±25
0.32	133±3	97±1.5	1936±15	35±0.14	13±0.5	5±0.4	3±0.1	7±0.2	1972±14	841±4
0.59	313±6	151±1.2	7982±16	47±0.33	28±0.4	8±0.8	10±0.5	8±0.9	1726±21	785±5
0.90	317±12	97±1.6	5263±95	23±0.09	29±0.3	8±0.5	8±0.4	6±0.3	1151±32	587±11
1.22	285±9	80±1.8	1226±7	6±0.16	19±0.1	7±0.2	6±0.3	7±0.2	1148±20	604±8
1.51	233±9	90±1	836±6	5±0.1	9±0.5	6±0.9	4±0.2	6±0.3	1367±37	630±9
1.77	146±2	70±0.3	500±5	3±0.05	5±0.7	4±0.6	3±0.1	6±0.5	1144±40	618±9
2.08	103±2	76±1.1	512±5	3±0.04	3±0.2	4±0.1	3±0.4	5±0.5	1226±16	613±4
2.41	97±5	75±0.6	1048±10	5±0.08	4±0.2	4±0.9	4±0.6	5±0.1	1159±23	600±8
2.71	80±4	87±1.4	579±25	2±0.04	3±0.3	5±1.5	5±0.4	5±0.6	1532±34	743±22
3.01	74±15	71±1.2	523±1	2±0.08	3±0.2	3±0.9	2±0.7	5±0.6	1315±5	748±7
3.30	48±6	58±0.2	596±5	2±0.04	3±0.8	2±0.4	2±0.7	5±0.4	1401±6	861±6
3.53	40±5	52±1.9	580±5	1±0.05	2±0.2	BDL	1±0.1	3±0.3	1422±31	911±16
3.77	56±4	56±0.6	666±7	2±0.11	3±0.4	2±0.8	1±0.4	4±0.2	1709±17	1016±19
4.04	59±4	48±0.8	641±8	1±0.05	2±0.2	BDL	1±0.3	5±0.2	1584±55	1030±30
4.25	61±11	44±1.6	636±13	1±0.13	3±0.2	BDL	1±0.2	5±0.5	1663±43	1078±29
4.41	57±10	34±1.8	614±2	1±0.02	3±0.3	4±1.6	1±0.4	4±0.5	1546±5	1101±2
4.57	76±7	60±1.7	635±8	1±0.12	3±0.8	BDL	1±0.5	5±0.7	2090±33	1137±16
4.74	64±7	34±2.2	712±5	1±0.11	3±0.2	BDL	1±0.5	4±0.3	1902±11	1234±15
4.96	65±2	39±0.5	775±12	2±0.04	3±0.4	1±0.4	7±0.1	4±0.6	2001±24	1229±23
5.18	54±3	25±0.8	729±14	2±0.17	3±0.3	BDL	12±0.4	4±0.2	1888±34	1246±27
Inventory (mg m^{-2})	6696	3747	76328	579	427	182	208	280	79536	44276

Table 3-7 Core UH Metal concentrations

Core ID : UH		Core diameter = 10cm			area=	0.00785m
Cumulative mass	Pb	Dry weight	Section concentration	Section concentration/area	Cumulative concentration/area	
g cm^{-2}	mg kg^{-1}	g	mg	mg m^{-2}	mg m^{-2}	mg cm^{-2}
0.02	85±4	3	0.26	32	32	0.003
0.07	72±10	5.07	0.37	47	79	0.008
0.15	97±584	7.73	0.75	96	175	0.017
0.32	133±3	18.39	2.45	312	486	0.049
0.59	313±6	23.66	7.41	943	1429	0.143
0.90	317±12	25.61	8.12	1034	2464	0.246
1.22	285±9	24.26	6.91	881	3344	0.334
1.51	233±9	21.76	5.07	646	3990	0.399
1.77	146±2	19.64	2.87	365	4356	0.436
2.08	103±2	27.87	2.87	366	4721	0.472
2.41	97±5	24.43	2.37	302	5023	0.502
2.71	80±4	23.13	1.85	236	5259	0.526
3.01	74±15	23.19	1.72	219	5477	0.548
3.30	48±6	22.32	1.07	136	5614	0.561
3.53	40±5	14.66	0.59	75	5689	0.569
3.77	56±4	22.6	1.27	161	5850	0.585
4.04	59±4	19.96	1.18	150	6000	0.600
4.25	61±11	12.93	0.79	100	6100	0.610
4.41	57±10	11.75	0.67	85	6186	0.619
4.57	76±7	12.85	0.98	124	6310	0.631
4.74	64±7	14.97	0.96	122	6432	0.643
4.96	65±2	19.12	1.24	158	6590	0.659
5.18	54±3	15.36	0.83	106	6696	0.670

Table 3-8 Core UH Pb inventory

Core ID: UH			
Cumulative mass			
g cm^{-2}	$^{206}Pb/^{207}Pb$	$^{208}Pb/^{207}Pb$	$^{208}Pb/^{206}Pb$
0.02	1.143±0.062	2.423±0.129	2.121±0.066
0.07	1.148±0.033	2.448±0.053	2.133±0.052
0.15	1.145±0.013	2.440±0.025	2.130±0.017
0.32	1.135±0.008	2.419±0.016	2.131±0.011
0.59	1.142±0.006	2.430±0.013	2.127±0.007
0.90	1.153±0.006	2.438±0.013	2.115±0.010
1.22	1.157±0.006	2.445±0.014	2.114±0.011
1.51	1.158±0.007	2.449±0.011	2.114±0.013
1.77	1.156±0.009	2.448±0.016	2.117±0.014
2.08	1.160±0.007	2.448±0.012	2.110±0.012
2.41	1.155±0.007	2.441±0.018	2.113±0.013
2.71	1.156±0.010	2.450±0.020	2.120±0.018
3.01	1.154±0.010	2.450±0.023	2.123±0.016
3.30	1.156±0.011	2.438±0.023	2.110±0.018

Table 3-9 Core UH Pb isotope ratios

3.2 Core UL1

Core ID : UL1 Depth (cm)	Cumulative mass (g cm $^{-2}$)	Dry / wet ratio	Loss on ignition (%)	Dry bulk density (g cm^{-3})
0-5	0.10	0.08	98.73	0.040
5-10	0.36	0.11	97.74	0.063
10-15	0.85	0.11	91.66	0.135
15-21	1.91	0.13	95.35	0.241
21-27	3.50	0.14	98.28	0.289
27-33	5.08	0.10	98.61	0.236

Table 3-10 Core UL1 Dry / wet ratio, Loss on ignition and Dry bulk density

Core ID:UL1 Depth (cm)	Cumulative mass (g cm^{-2})	Ash content (%)
0-5	0.10	1.27
5-10	0.36	2.26
10-15	0.85	8.34
15-21	1.91	4.65
21-27	3.50	1.72
27-33	5.08	1.39

Table 3-11 Core UL1 Ash content

Core ID:UL1	URANIUM SERIES				
Depth (cm)	^{210}Pb (46keV)	^{214}Pb (295 keV)	^{214}Pb (352 keV)	^{214}Bi (609 keV)	^{137}Cs (662keV)
0-5	210±8	BDL	BDL	BDL	247±3
5-10	326±8	BDL	BDL	3±1	222±3
10-15	173±5	5±2	5±1	5±1	147±2
15-21	17±4	3±1	2±1	BDL	28±1
21-27	BDL	BDL	2±1	3±1	10±1
27-33	BDL	2±1	3±1	5±1	13±1
Units :- Bq kg^{-1} Uncertainty 1σ BDL :- Below detection limit					

Table 3-12 Core UL1 Gamma analysis : ^{210}Pb and ^{137}Cs

Core ID	Cumulative mass (g cm^{-2})	Depth (cm)	^{241}Am (Bq kg^{-1})
UL1	0.855	10-15	3.16±0.48

Table 3-13 Core UL1 Gamma analysis : ^{241}Am

ID : UL1	Section area:10x10x5cm				Area : 0.01m^2 (100cm^2)		^{210}Pb flux : 87 Bq m^{-2}y^{-1}		
Depth	Total ^{210}Pb	Supported ^{210}Pb	Unsupported ^{210}Pb	Section activity	Section activity/area	Cumulative activity/area	Dry weight/area	Cumulative mass	
(cm)	Bq kg^{-1}	Bq kg^{-1}	Bq kg^{-1}	Bq	Bq m^{-2}	Bq m^{-2}	g m^{-2}	g m^{-2}	g cm^{-2}
0-5	210±8	0	210	4.19	419	419	1995	998	0.100
5-10	326±8	3	323	10.24	1024	1443	3170	3580	0.358
10-15	173±5	5	168	11.36	1136	2579	6762	8546	0.855
15-21	17±4	2.5	14.5	2.09	209	2788	14441	19147	1.915
21-27	0	2.5	-2.5	0	0	2788	17313	35024	3.502
27-33	4±4	3.33	0.67	0.09	9	2797	14141	50751	5.075

Table 3-14 Core UL1 ^{210}Pb inventory and flux

ID : UL1	Sectionarea:10x10x5cm		Area : 0.01m^2 (100cm^2)			
Depth	Cumulative mass	Cumulative mass	^{137}Cs	Section activity	Section activity/area	Cumulative activity/area
(cm)	g cm^{-2}	g m^{-2}	Bq kg^{-1}	Bq	Bq m^{-2}	Bq m^{-2}
0-5	0.100	998	247±3	4.93	493	493
5-10	0.358	3580	222±3	7.04	704	1196
10-15	0.855	8546	147±2	9.94	994	2190
15-21	1.915	19147	28±1	4.04	404	2595
21-27	3.502	35024	10±0	1.73	173	2768
27-33	5.075	50751	13±0	1.84	184	2952

Table 3-15 Core UL1 ^{137}Cs inventory

Core ID: UL1 Units : mg kg $^{-1}$										
Cumulative mass (g cm^{-2})	**Pb**	**Zn**	**Fe**	**Mn**	**Cu**	**Ni**	**Cr**	**Cd**	**Ca**	**Mg**
0.10	3±0.1	39±0.4	214±3	49±0.63	4±0.04	1±0.02	1±0.01	0.12±0.009	1045±6	659±5
0.36	24±0.1	70±0.5	1560±17	55±0.44	8±0.09	2±0.02	2±0.01	0.38±0.006	1436±17	650±8
0.85	237±0.7	121±0.2	9259±79	50±0.5	28±0.3	12±0.07	12±0.09	1.02±0.027	1336±12	699±7
1.91	88±0.8	49±0.4	1296±21	6±0.06	7±0.1	4±0.06	4±0.02	0.52±0.018	1108±20	649±14
3.50	14±0.1	46±0.2	569±5	2±0.02	1±0.01	3±0.02	1±0.01	0.41±0.002	1163±16	725±9
5.08	4±0.1	40±0.1	585±6	3±0.03	1±0.004	2±0.02	1±0.01	0.16±0.01	1342±13	869±8
Inventory (mg m^{-2})	3256	3182	104814	776	361	230	171	25	70782	42314

Table 3-16 Core UL1 Metal concentrations

Core ID: UL1		10x10x5cm		area =0.01m		
Cumulative mass	Pb	Dry weight	Section concentration	Section concentration/area	Cumulative concentration/area	
g cm^{-2}	mg kg^{-1}	g	mg	mg m^{-2}	mg m^{-2}	mg cm^{-2}
0.10	3±0.1	19.95	0.05	5	5	0.0005
0.36	24±0.1	31.70	0.77	77	82	0.0082
0.85	237±0.7	67.62	16.04	1604	1686	0.1686
1.91	88±0.8	144.41	12.78	1278	2964	0.2964
3.50	14±0.1	173.13	2.36	236	3200	0.3200
5.08	4±0.1	141.41	0.57	57	3256	0.3256

Table 3-17 Core UL1 Pb inventory

3.3 Core UL2

Core ID : UL2 Depth (cm)	Cumulative mass (g cm $^{-2}$)	Dry / wet ratio	Loss on ignition (%)	Dry bulk density (g cm^{-3})
0-5	0.15	0.14	99.17	0.059
5-10	0.59	0.13	96.82	0.120
10-15	1.15	0.15	93.21	0.104
15-20	1.67	0.16	95.17	0.101
20-25	2.21	0.15	97.46	0.114
25-30	2.71	0.12	97.80	0.088
30-35	3.11	0.10	98.85	0.070

Table 3-18 Core UL2 Dry / wet ratio, Loss on ignition and Dry bulk density

Core ID:UL2 Depth (cm)	Cumulative mass (g cm^{-2})	Ash content (%)
0-5	0.15	0.83
5-10	0.59	3.18
10-15	1.15	6.79
15-20	1.67	4.83
20-25	2.21	2.54
25-30	2.71	2.20
30-35	3.11	1.15

Table 3-19 Core UL2 Ash content

Core ID:UL2	URANIUM SERIES				
Depth (cm)	^{210}Pb (46keV)	^{214}Pb (295 keV)	^{214}Pb (352 keV)	^{214}Bi (609 keV)	^{137}Cs (662keV)
0-5	169±6	BDL	BDL	BDL	314±5
5-10	299±6	23±3	4±3	BDL	256±3
10-15	67±4	13±3	BDL	BDL	46±1
15-20	31±3	13±4	BDL	BDL	30±1
20-25	19±3	14±3	4±3	BDL	17±1
25-30	4±3	BDL	BDL	BDL	13±1
30-35	10±2	9±3	BDL	BDL	17±1
Units :- Bq kg^{-1} Uncertainty 1σ BDL :- Below detection limit					

Table 3-20 Core UL2 Gamma analysis : ^{210}Pb and ^{137}Cs

Core ID	Cumulative mass (g cm^{-2})	Depth (cm)	^{241}Am (Bq kg^{-1})
UL2	0.594	5-10	1.48±0.48
UL2	1.154	10-15	1.27±0.44

Table 3-21 Core UL2 Gamma analysis : ^{241}Am

ID : UL2	Section area : 20x20x5cm				Area : 0.04m^2 (400cm^2)		^{210}Pb flux : 92 Bq m^{-2}y^{-1}		
Depth	Total ^{210}Pb	Supported ^{210}Pb	Unsupported ^{210}Pb	Section activity	Section activity/area	Cumulative activity/area	Dry weight/area	Cumulative mass	
(cm)	Bq kg^{-1}	Bq kg^{-1}	Bq kg^{-1}	Bq	Bq m^{-2}	Bq m^{-2}	g m^{-2}	g m^{-2}	g cm^{-2}
0-5	169±6	BDL	169	19.77	494	494	2925	1463	0.146
5-10	299±6	BDL	299	72.04	1801	2295	6023	5937	0.594
10-15	67±4	BDL	67	13.91	348	2643	5192	11544	1.154
15-20	31±3	BDL	31	6.28	157	2800	5062	16671	1.667
20-25	19±3	BDL	19	4.33	108	2908	5698	22051	2.205
25-30	4±3	BDL	4	0.71	18	2926	4421	27110	2.711
30-35	10±2	BDL	10	1.40	35	2961	3502	31072	3.107

Table 3-22 Core UL2 ^{210}Pb flux and inventory

ID : UL2	Section area:20x20x5cm		Area : 0.04m^2 (400cm^2)			
Depth	Cumulative mass	Cumulative mass	^{137}Cs	Section activity	Section activity/area	Cumulative activity/area
(cm)	g cm^{-2}	g m^{-2}	Bq kg^{-1}	Bq	Bq m^{-2}	Bq m^{-2}
0-5cm	0.146	1463	314±5	36.74	918	918
5-10cm	0.594	5937	256±3	61.68	1542	2460
10-15cm	1.154	11544	46±1	9.55	239	2699
15-20cm	1.667	16671	30±1	6.07	152	2851
20-25cm	2.205	22051	17±1	3.87	97	2948
25-30cm	2.711	27110	13±1	2.30	57	3005
30-35cm	3.107	31072	17±1	2.38	60	3065

Table 3-23 Core UL2 ^{137}Cs inventory

3.4 Core FH

Core ID : FH Depth (cm)	Cumulative mass (g cm $^{-2}$)	Dry / wet ratio	Loss on ignition (%)	Dry bulk density (g cm^{-3})
0-3	0.05	0.14	98.96	0.033
3-5	0.14	0.12	99.34	0.041
5-7	0.25	0.12	98.51	0.066
7-9	0.43	0.14	97.66	0.120
9-11	0.65	0.15	96.46	0.097
11-13	0.84	0.11	96.11	0.099
13-15	1.02	0.10	96.45	0.076
15-17	1.18	0.09	94.60	0.087
17-19	1.43	0.14	96.26	0.166
19-21	1.79	0.16	96.67	0.192
21-23	2.17	0.17	97.02	0.186
23-25	2.51	0.15	97.15	0.155
25-27	2.79	0.13	97.66	0.127
27-29	3.06	0.12	97.90	0.138
29-31	3.28	0.11	98.15	0.079

Table 3-24 Core FH Dry / wet ratio, Loss on ignition and Dry bulk density

Core ID:FH Depth (cm)	Cumulative mass (g cm^{-2})	Ash content (%)
0-3	0.05	1.04
3-5	0.14	0.66
5-7	0.25	1.49
7-9	0.43	2.34
9-11	0.65	3.54
11-13	0.84	3.89
13-15	1.02	3.55
15-17	1.18	5.40
17-19	1.43	3.74
19-21	1.79	3.33
21-23	2.17	2.98
23-25	2.51	2.85
25-27	2.79	2.34
27-29	3.06	2.10
29-31	3.28	1.85

Table 3-25 Core FH Ash content

Core ID:FH	URANIUM SERIES				
Depth (cm)	^{210}Pb (46keV)	^{214}Pb (295 keV)	^{214}Pb (352 keV)	^{214}Bi (609 keV)	^{137}Cs (662keV)
0-3	182±14	60±11	BDL	BDL	112±5
3-5	198±14	59±13	BDL	BDL	114±6
5-7	167±8	41±8	BDL	15±10	105±4
7-9	160±8	BDL	BDL	BDL	128±4
9-11	148±8	BDL	BDL	BDL	142±4
11-13	76±9	BDL	BDL	BDL	56±3
13-15	49±8	29±6	BDL	BDL	46±3
15-17	17±6	BDL	BDL	BDL	31±3
17-19	17±3	16±3	6±3	BDL	21±2
19-21	8±2	10±2	BDL	BDL	12±1
21-23	BDL	15±3	3±2	BDL	13±1
23-25	BDL	BDL	BDL	BDL	15±1
Units :- Bq kg^{-1} Uncertainty 1σ BDL :- Below detection limit					

Table 3-26 Core FH Gamma analysis : ^{210}Pb and ^{137}Cs

Core ID	Cumulative mass (g cm^{-2})	Depth (cm)	^{241}Am (Bq kg^{-1})
FH	0.649	9-11	4.05±1.53

Table 3-27 Core FH Gamma analysis : ^{241}Am

ID : FH	Core diameter : 7.5cm				Area : 0.0044m^2 (44cm^2)		^{210}Pb flux : 49 Bq m^{-2}y^{-1}		
Depth	Total ^{210}Pb	Supported ^{210}Pb	Unsupported ^{210}Pb	Section activity	Section activity/area	Cumulative activity/area	Dry weight/area	Cumulative mass	
(cm)	Bq kg^{-1}	Bq kg^{-1}	Bq kg^{-1}	Bq	Bq m^{-2}	Bq m^{-2}	g m^{-2}	g m^{-2}	g cm^{-2}
0-3	182±14	BDL	182	0.78	178	178	977	489	0.049
3-5	198±14	BDL	198	0.71	161	339	814	1384	0.138
5-7	167±8	BDL	167	0.98	222	561	1330	2456	0.246
7-9	160±8	BDL	160	1.68	383	944	2393	4317	0.432
9-11	148±8	BDL	148	1.27	288	1232	1945	6486	0.649
11-13	76±9	BDL	76	0.66	150	1382	1977	8448	0.845
13-15	49±8	BDL	49	0.33	74	1456	1516	10194	1.019
15-17	17±6	BDL	17	0.13	29	1486	1734	11819	1.182
17-19	17±3	BDL	17	0.25	56	1542	3323	14348	1.435
19-21	8±2	BDL	8	0.13	31	1573	3832	17925	1.793
21-23	0	BDL	0	0	0	1573	3723	21702	2.170
23-25	0	BDL	0	0	0	1573	3102	25115	2.511

Table 3-28 Core FH ^{210}Pb flux and inventory

ID : FH	Core diameter : 7.5cm		Area : 0.0044m^2 (44cm^2)			
Depth	Cumulative mass	Cumulative mass	^{137}Cs	Section activity	Section activity/area	Cumulative activity/area
(cm)	g cm^{-2}	g m^{-2}	Bq kg^{-1}	Bq	Bq m^{-2}	Bq m^{-2}
0-3	0.049	489	112±5	0.48	109	109
3-5	0.138	1384	114±6	0.41	93	202
5-7	0.246	2456	105±4	0.61	140	342
7-9	0.432	4317	128±4	1.35	306	648
9-11	0.649	6486	142±4	1.22	276	924
11-13	0.845	8448	56±3	0.49	111	1035
13-15	1.019	10194	46±3	0.31	70	1105
15-17	1.182	11819	31±3	0.24	54	1159
17-19	1.435	14348	21±2	0.31	70	1228
19-21	1.793	17925	12±1	0.20	46	1274
21-23	2.170	21702	13±1	0.21	48	1323
23-25	2.511	25115	15±1	0.20	47	1369

Table 3-29 Core FH ^{137}Cs inventory

Core ID: FH Units : mg kg^{-1}										
Cumulative mass (g cm^{-2})	Pb	Zn	Fe	Mn	Cu	Ni	Cr	Cd	Ca	Mg
0.05	29±2	219±2	289±3	31±0.19	5±0.49	2±0.28	3±0.3	3±0.2	3314±33	789±9
0.14	46±7	161±1.3	562±7	19±0.15	6±0.18	8±1.34	2±0.2	3±0.6	2285±34	789±17
0.25	85±8	61±0.4	1005±10	41±0.16	7±0.76	BDL	3±0.2	4±0.3	1311±14	701±8
0.43	110±4	83±1.5	1994±34	33±0.4	10±0.13	2±0.86	3±0.6	4±0.6	1449±48	754±21
0.65	237±8	82±2.1	3933±79	11±0.02	13±0.08	6±0.61	4±0.3	5±0.6	1886±62	880±27
0.84	218±3	126±0.4	1593±11	4±0.15	15±0.24	5±0.68	7±0.7	5±0.5	1919±21	788±9
1.02	209±9	51±1.2	1083±27	3±0.02	30±0.36	10±1.6	14±0.5	4±0.6	1607±82	833±28
1.18	167±7	56±1.8	744±6	2±0.08	16±0.58	3±1.75	5±0.3	3±0.8	1780±28	831±8
1.43	144±6	41±0.5	723±5	2±0.04	14±0.14	4±1.28	5±0.5	3±0.4	1770±25	766±8
1.79	74±4	43±0.3	697±5	2±0.03	6±0.04	3±0.14	3±0.7	3±0.7	1863±2	825±6
2.17	51±10	66±3.7	760±3	4±2.79	9±0.49	10±7.96	5±1.8	5±0.8	3052±12	911±1
2.51	40±4	34±1.5	853±5	3±0.03	5±0.82	3±1.43	3±0.4	4±0.1	2217±16	1002±10
2.79	80±4	38±0.7	799±3	2±0.03	3±0.79	3±0.93	2±0.2	5±0.5	1618±13	1063±10
3.06	72±8	41±0.9	807±9	2±0.08	3±0.26	1±0.76	2±0.1	5±0.6	1723±48	1110±17
3.28	70±2	40±0.2	781±8	2±0.13	3±0.2	2±0.96	2±0.5	5±0.8	1856±48	1160±14
Inventory (mg m^{-2})	3530	2133	36626	269	310	140	137	138	66362	29933

Table 3-30 Core FH Metal concentrations

Core ID : FH		Core diameter = 7.5cm			area=	0.0044m
Cumulative mass	Pb	Dry weight	Section concentration	Section concentration/area	Cumulative concentration/area	
g cm^{-2}	mg kg^{-1}	g	mg	mg m^{-2}	mg m^{-2}	mg cm^{-2}
0.05	29±2	4.3	0.12	28	28	0.003
0.14	46±7	3.58	0.16	37	66	0.007
0.25	85±8	5.85	0.50	113	179	0.018
0.43	110±4	10.53	1.16	263	442	0.044
0.65	237±8	8.56	2.03	461	903	0.090
0.84	218±3	8.7	1.90	431	1334	0.133
1.02	209±9	6.67	1.39	317	1651	0.165
1.18	167±7	7.63	1.27	290	1941	0.194
1.43	144±6	14.62	2.11	478	2419	0.242
1.79	74±4	16.86	1.25	284	2703	0.270
2.17	51±10	16.38	0.84	190	2892	0.289
2.51	40±4	13.65	0.55	124	3017	0.302
2.79	80±4	11.21	0.90	204	3220	0.322
3.06	72±8	12.14	0.87	199	3419	0.342
3.28	70±2	6.95	0.49	111	3530	0.353

Table 3-31 Core FH Pb inventory

Core ID: FH	NBS corrected		
Cumulative mass			
g cm^{-2}	$^{206}Pb/^{207}Pb$	$^{208}Pb/^{207}Pb$	$^{208}Pb/^{206}Pb$
0.05	1.148±0.008	2.430±0.019	2.117±0.016
0.14	1.147±0.010	2.418±0.018	2.109±0.016
0.25	1.148±0.006	2.427±0.016	2.115±0.010
0.43	1.153±0.007	2.428±0.012	2.105±0.009
0.65	1.154±0.008	2.442±0.027	2.115±0.022
0.84	1.162±0.006	2.447±0.014	2.107±0.010
1.02	1.168±0.005	2.452±0.015	2.100±0.008
1.18	1.174±0.008	2.459±0.016	2.095±0.015
1.43	1.178±0.008	2.466±0.015	2.094±0.013
1.79	1.173±0.011	2.461±0.021	2.098±0.013
2.17	1.175±0.011	2.457±0.019	2.090±0.016
2.51	1.180±0.012	2.468±0.021	2.091±0.019
2.79	1.196±0.024	2.477±0.047	2.072±0.042
3.06	1.178±0.022	2.445±0.046	2.076±0.042
3.28	1.189±0.032	2.476±0.076	2.082±0.041

Table 3-32 Core FH Pb isotope ratios

3.5 Core FL

Core ID : FL Depth (cm)	Cumulative mass (g cm $^{-2}$)	Dry / wet ratio	Loss on ignition (%)	Dry bulk density (g cm^{-3})
0-5	0.09	0.07	98.38	0.035
5-10	0.35	0.06	97.70	0.071
10-15	0.85	0.08	95.14	0.130
15-20	1.46	0.06	95.72	0.113
20-25	1.97	0.06	96.85	0.091
25-30	2.45	0.07	96.70	0.102
30-35	3.21	0.12	97.42	0.203

Table 3-33 Core FL Dry / wet ratio, Loss on ignition and Dry bulk density

Core ID:FL Depth (cm)	Cumulative mass (g cm^{-2})	Ash content (%)
0-5	0.09	1.62
5-10	0.35	2.30
10-15	0.85	4.86
15-20	1.46	4.28
20-25	1.97	3.15
25-30	2.45	3.30
30-35	3.21	2.58

Table 3-34 Core FL Ash content

Core ID:FL	URANIUM SERIES				
Depth (cm)	^{210}Pb (46keV)	^{214}Pb (295 keV)	^{214}Pb (352 keV)	^{214}Bi (609 keV)	^{137}Cs (662keV)
0-5	196±8	BDL	3±1	9±2	122±2
5-10	181±7	3±2	4±1	4±2	154±2
10-15	181±5	4±1	4±1	5±1	76±1
15-20	101±4	4±1	5±1	6±1	51±1
20-25	93±6	6±2	3±1	7±1	35±1
25-30	41±6	4±2	4±1	6±1	24±1
30-35	11±3	3±1	3±1	6±1	14±1
Units :- Bq kg^{-1} Uncertainty 1σ BDL :- Below detection limit					

Table 3-35 Core FL Gamma analysis : ^{210}Pb and ^{137}Cs

Core ID	Cumulative mass (g cm^{-2})	Depth (cm)	^{241}Am (Bq kg^{-1})
FL	0.351	5-10	2.11±0.83
FL	0.853	10-15	2.64±0.38
FL	1.461	15-20	1.67±0.64

Table 3-36 Core FL Gamma analysis : 241Am

ID : FL	Core area =10x10x5cm				Area =0.01m^2 (100cm^2)		^{210}Pb flux : 103 Bq m^{-2}y^{-1}		
Depth	Total ^{210}Pb	Supported ^{210}Pb	Unsupported ^{210}Pb	Section activity	Section activity/area	Cumulative activity/area	Dry weight/area	Cumulative mass	
(cm)	Bq kg^{-1}	Bq kg^{-1}	Bq kg^{-1}	Bq	Bq m^{-2}	Bq m^{-2}	g m^{-2}	g m^{-2}	g cm^{-2}
0-5	196±8	6	190	3.30	330	330	1737	869	0.087
5-10	181±7	4	177	6.27	627	957	3540	3508	0.351
10-15	181±5	4	177	11.52	1152	2108	6507	8531	0.853
15-20	101±4	5	96	5.42	542	2650	5645	14607	1.461
20-25	93±6	5	88	4.01	401	3052	4560	19709	1.971
25-30	41±6	5	36	1.83	183	3235	5080	24529	2.453
30-35	11±3	4	7	0.71	71	3305	10137	32137	3.214

Table 3-37 Core FL ^{210}Pb flux and inventory

ID : FL	Core area =10x10x5cm		Area =0.01m^2 (100cm^2)			
Depth	Cumulative mass	Cumulative mass	^{137}Cs	Section activity	Section activity/area	Cumulative activity/area
(cm)	g cm^{-2}	g m^{-2}	Bq kg^{-1}	Bq	Bq m^{-2}	Bq m^{-2}
0-5	0.087	869	122±2	2.12	212	212
5-10	0.351	3508	154±2	5.45	545	757
10-15	0.853	8531	76±1	4.95	495	1252
15-20	1.461	14607	51±1	2.88	288	1540
20-25	1.971	19709	35±1	1.60	160	1699
25-30	2.453	24529	24±1	1.22	122	1821
30-35	3.214	32137	14±0	1.42	142	1963

Table 3-38 Core FL ^{137}Cs inventory

Core ID: FL Units : mg kg^{-1}										
Cumulative mass g cm^{-2}	Pb	Zn	Fe	Mn	Cu	Ni	Cr	Cd	Ca	Mg
0.09	7±0.2	45±0.4	446±3	48±0.29	5±0.04	2±0.02	1±0.01	0.02±0.014	1533±21	907±14
0.35	93±1.2	53±0.7	2529±21	13±0.16	6±0.07	3±0.06	2±0.02	0.37±0.009	736±7	744±7
0.85	237±0.8	45±0.1	2866±30	10±0.09	13±0.18	7±0.07	8±0.04	0.27±0.03	941±14	739±13
1.46	226±1	35±0.2	1760±13	7±0.03	16±0.09	5±0.06	8±0.04	0.31±0.023	792±8	729±10
1.97	282±1.6	39±0.2	1250±9	5±0.03	27±0.07	4±0.02	5±0.03	0.55±0.021	997±11	804±11
2.45	174±1.5	32±0.3	893±12	4±0.03	20±0.25	3±0.04	4±0.13	0.46±0.02	979±19	833±12
3.21	72±0.4	33±0.2	908±6	3±0.02	4±0.02	3±0.02	2±0.02	0.39±0.014	1339±12	918±9
Inventory (mg m^{-2})	6056	1430	57760	307	468	150	168	14	38964	30337

Table 3-39 Core FL Metal concentrations

Core ID : FL		10x10x5cm			area=	0.01m
Cumulative mass	Pb	Dry weight	Section concentration	Section concentration/area	Cumulative concentration/area	
g cm^{-2}	mg kg^{-1}	g	mg	mg m^{-2}	mg m^{-2}	mg cm^{-2}
0.09	7±0.2	17.37	0.12	12	12	0.0012
0.35	93±1.2	35.41	3.31	331	343	0.0343
0.85	237±0.8	65.07	15.39	1539	1882	0.1882
1.46	226±1	56.45	12.75	1275	3157	0.3157
1.97	282±1.6	45.60	12.86	1286	4443	0.4443
2.45	174±1.5	50.80	8.82	882	5325	0.5325
3.21	72±0.4	101.37	7.32	732	6056	0.6056

Table 3-40 Core FL Pb inventory

3.6 Biogenic Silica (BSi) results

Results – Part 2

In the second part of this chapter the results for biogenic silica determination are presented in tabulated form:

- Table 3-41 shows the summary results from the BSi extractions from lake sediment core ZAC / 2 which were carried out at various stages throughout the study. There is reasonable agreement between the results over the three different sets of analyses and good agreement in the trend

- Table 3-42 shows the summary data for BSi extractions on unfurnaced and furnaced peat using various sample weights and volumes of extracting solution. It was evident from the unfurnaced analyses (samples 1.1 to 2.4) that humic substances made BSi extraction and purification non viable in peat, therefore the decision to furnace the peat prior to extraction was explored

- Table 3-43 shows the summary data for BSi extractions on core UL2

- Table 3-44 shows the summary data for BSi extractions on core FHb.

Core ID : ZAC/2			40 ml 0.5 M Na_2CO_3										
Year :	2009			2010					2012				
Depth	Weight	Si	Si	Weight	Si	Std	Si	Std	Weight	Si	Std	Si	Std
(cm)	(g)	(mg l^{-1})	(mg kg^{-1})	(g)	(mg l^{-1})	dev	(mg kg^{-1})	dev	(g)	(mg l^{-1})	dev	(mg kg^{-1})	dev
Silica gel	0.0452	7.223	76710	0.0466	5.619	0.1503	289400	7741	0.0455	25.64	0.297	264100	3058
0-5	0.0403	10.61	126400	0.0416	3.545	0.0111	204500	641	0.0407	13.4	0.15	158000	1766
5-10	0.0414	19.07	221100	0.0430	5.094	0.0511	284300	2850	0.0413	19.03	0.176	221200	2049
10-15	0.0417	15.82	182100	0.0413	4.841	0.1192	281300	6928	0.0416	19.38	0.078	223600	906
15-20	0.0401	12.62	151100	0.0434	4.751	0.0767	262700	4242	0.0451	20.38	0.064	216900	681
20-25	0.0438	11.69	128100	0.0479	5.09	0.0405	255000	2027	0.0472	19.42	0.156	197500	1589
25-30	0.0433	12.23	135500	0.0467	5.305	0.0085	272600	438	0.0452	17.53	0.166	186200	1760
30-35	0.0431	15.64	174100	0.0469	5.788	0.1382	296200	7073	0.0451	22.38	0.202	238200	2154
35-40	0.0413	16.14	187600	0.0396	5.733	0.1349	347400	8178	0.0425	21.51	0.139	243000	1568
40-45	0.0415	18.03	208600	0.0454	7.095	0.0876	375100	4631	0.0457	24.03	0.182	252400	1913

Table 3-41 BSi analysis Core ZAC/2 Lake sediment

Sample ID	Weight peat	Furnaced	Weight after furnace	Weight silica gel added	Volume Na_2CO_3	Si	Standard deviation	Si	Standard deviation
	(g)	No/Yes	(g)	(g)	(ml)	mg L^{-1}		mg kg^{-1}	
1.1	1.0041	No	N/A	0	40	0	0	0	0
1.2	5.0074	No	N/A	0	30	0.011	0.0015	3.381	0.4528
1.3	1.0042	No	N/A	0.0134	40	0	0	0	0
1.4	1.0288	No	N/A	0.0249	40	0	0	0	0
1.5	1.0161	No	N/A	0.0396	40	0	0	0	0
1.6	5.0015	No	N/A	0.0109	30	0.011	0.0021	3.164	0.6294
1.7	5.0488	No	N/A	0.0256	30	0	0	0	0
1.8	5.0645	No	N/A	0.0423	30	0	0	0	0
2.1	1.0188	No	N/A	0	100	0	0	0	0
2.2	1.0091	No	N/A	0.0434	100	0	0	0	0
2.3	1.0131	No	N/A	0	150	0.182	0.0024	1350	18
2.4	1.0128	No	N/A	0.0408	150	0	0	0	0
1	25.0628	Yes	2.2678	0	100	0.041	0.0012	8.252	0.2394
2	10.042	Yes	0.7769	0	100	0.284	0.0056	141.4	2.8
3	50.1591	Yes	3.6630	0	100	0.028	0.0008	2.7773	0.0822
4	100.89	Yes	10.1547	0	100	0.021	0.0004	1.042	0.0208
5	97.29	Yes	8.5133	0	100	0.026	0.0022	1.324	0.1112
6.1	102.01	Yes	9.2776	0	100	0.017	0.0013	0.819	0.0641
*6.2	102.01	N/A	N/A	0	100	0.027	0.0014	1.342	0.0697
**6.3	102.01	N/A	N/A	0.048	100	0.034	0.0020	1.66	0.0964
*6.2 = further extraction from 6.1 residue Weight residue = 9.0659g				**6.3 = further extraction from 6.2 residue + 0.0480g silica gel Weight residue = 8.2627g					

Table 3-42 BSi peat extraction data

Core ID: UL2						
Depth	Weight	Volume 0.5 M Na_2CO_3	Si	Standard deviation	Si	Standard deviation
(cm)	(g)	(mls)	(mg L^{-1})		(mg kg^{-1})	
0-5	20.03	200	0.277	0.0040	138.1	1.99
5-10	51.0	200	2.491	0.0047	488.5	0.92
10-15	100.9	200	0.042	0.0018	4.2	0.18
15-20	100.9	200	0.029	0.0012	2.9	0.12
20-25	100.9	200	0.042	0.0019	4.2	0.19
25-30	75.0	200	0.071	0.0023	9.4	0.31
30-35	91.5	200	0.127	0.0043	13.9	0.47

Table 3-43 Core UL2 BSi

Core ID: FHb						
Depth	Weight	Volume 0.5 M Na_2CO_3	Si	Standard deviation	Si	Standard deviation
(cm)	(g)	(mls)	(mg L^{-1})		(mg kg^{-1})	
0-5	5.7815	200	0.177	0.0044	306.5	7.60
5-9	9.7354	200	0.457	0.0042	469.5	4.27
9-13	9.6320	200	0.483	0.0021	501.0	2.20
13-17	9.9046	200	0.593	0.0048	598.7	4.83
17-21	24.6836	200	0.342	0.0013	138.7	0.53
21-25	24.6178	200	0.332	0.0023	135.0	0.92
25-29	19.8383	200	0.321	0.0067	161.7	3.35
29-31	4.8774	200	0.081	0.0011	166.1	2.30

Table 3-44 Core FHb BSi

4 Discussion

4.1 Dry / wet ratios

Dry / wet ratios for the cores varied in the general range of 0.06 – 0.22 (Figure 4-1) with the ranges for each core shown in table 4-1.

Core ID	Dry / wet ratio range
UH	0.08 - 0.22
UL1	0.08 - 0.14
UL2	0.10 - 0.16
FH	0.09 - 0.17
FL	0.06 - 0.12

Table 4-1 Dry / wet ratio range

No general systematic trend was seen for all of the cores although core UH showed a near-constant, high ratio in the top three samples followed by a general decrease with depth, whereas the other cores all showed irregular variations. In particular core FH showed a pronounced minimum at 15-17 cm. All of the cores were collected from sections of peat that were visually above the permanent water table and none of the cores exhibited evidence of a water table in the dry / wet ratios.

4.2 Dry bulk density

Dry bulk densities for the cores varied in the general range of 0.019 – 0.289 (Figure 4-2) with the ranges for each core shown in table 4-2.

Core ID	Dry bulk density range (g cm $^{-3}$)
UH	0.019 - 0.178
UL1	0.040 - 0.289
UL2	0.059 - 0.120
FH	0.033 - 0.192
FL	0.035 - 0.203

Table 4-2 Dry bulk density range

Core UH showed an increase from the surface to 10–12 cm then followed an irregular series of peaks and troughs with a maximum at 18-20cm. Values for core UL1 increased from the surface to reach a maximum at 21-27 cm. Core UL2 showed a minimum at 10-20 cm and reached a maximum at 20-25cm, with an overall trend similar to that in core UH but a muted version. In core FH there was a general increase with depth with a peak at 7-9 cm, dropping to a minimum at 13-15 cm before rising again to a maximum at 19-21 cm. Core FL showed a similar pattern with a maximum at 10-15 cm and a minimum at 20-25 cm.

As there were complex variations in the dry bulk densities it was concluded that results from here on would be more accurately interpreted relative to cumulative mass (g cm^{-2}) rather than depth (cm).

4.3 Loss on ignition

Loss on ignitions for the cores varied in the general range of 91.7% - 99.8% (Figure 4-3) with the ranges for each core shown in table 4-3.

Core ID	Loss on ignition range (%)
UH	92.87 - 99.75
UL1	91.66 - 98.73
UL2	93.21 - 99.17
FH	94.60 - 99.34
FL	95.14 - 98.38

Table 4-3 Loss on ignition range

All cores showed a similar trend, with a decrease from the surface to a minimum at a cumulative mass value of ~ 1 g cm^{-2}, followed by an increase with depth, which is indicative of varying atmospheric deposition of inorganic material as a function of time.

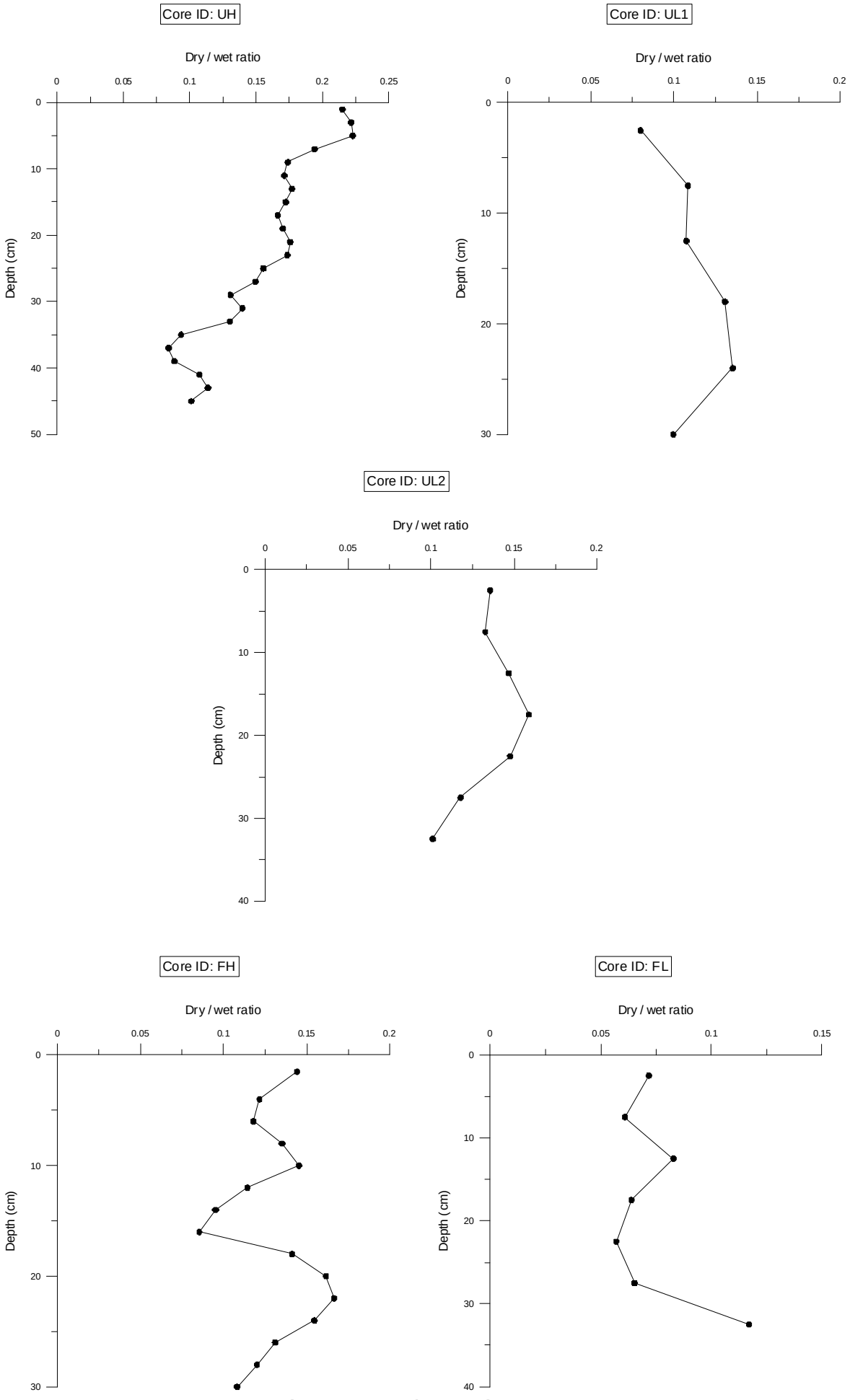

Figure 4-1 Dry / wet ratios

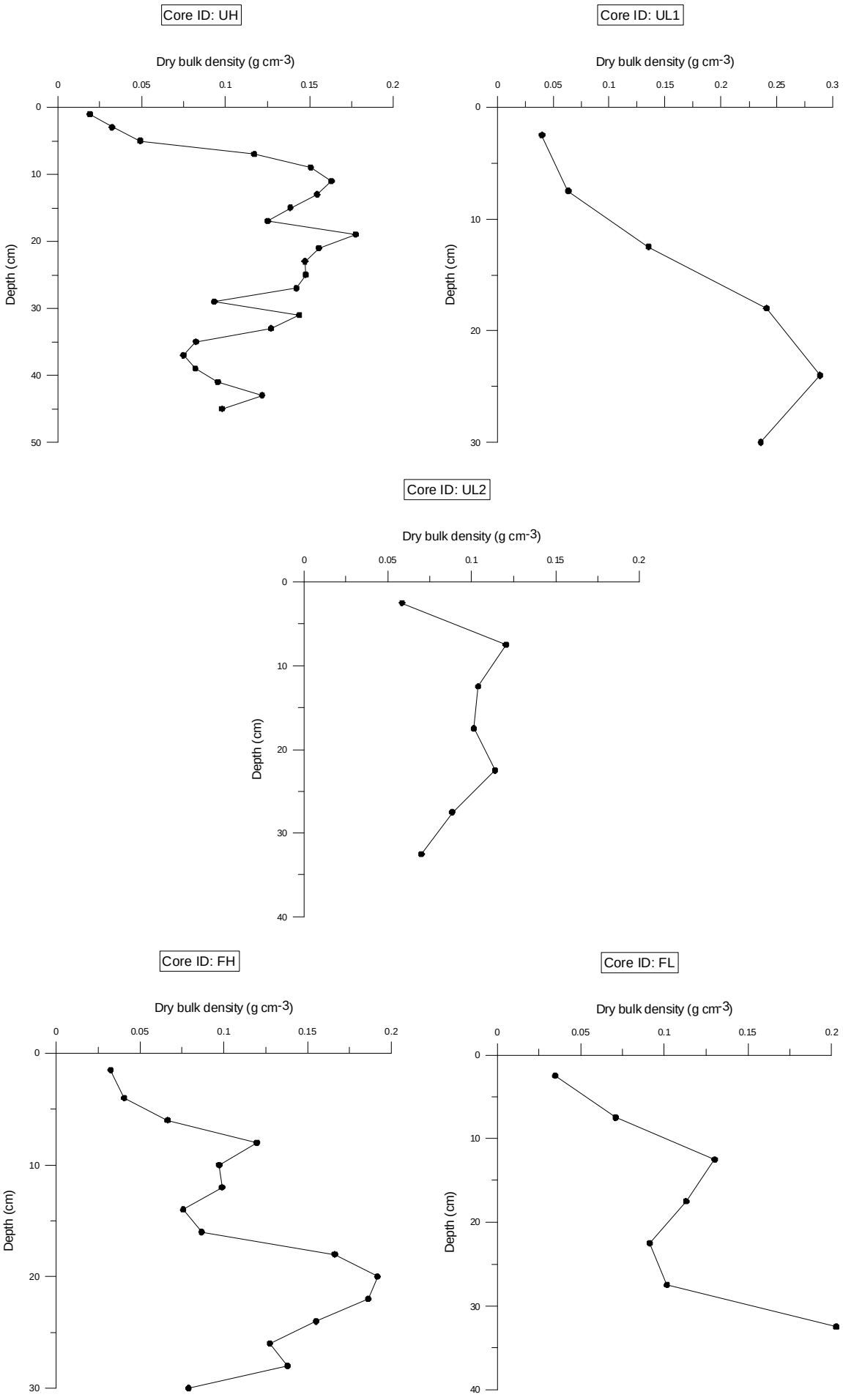

Figure 4-2 Dry bulk densities

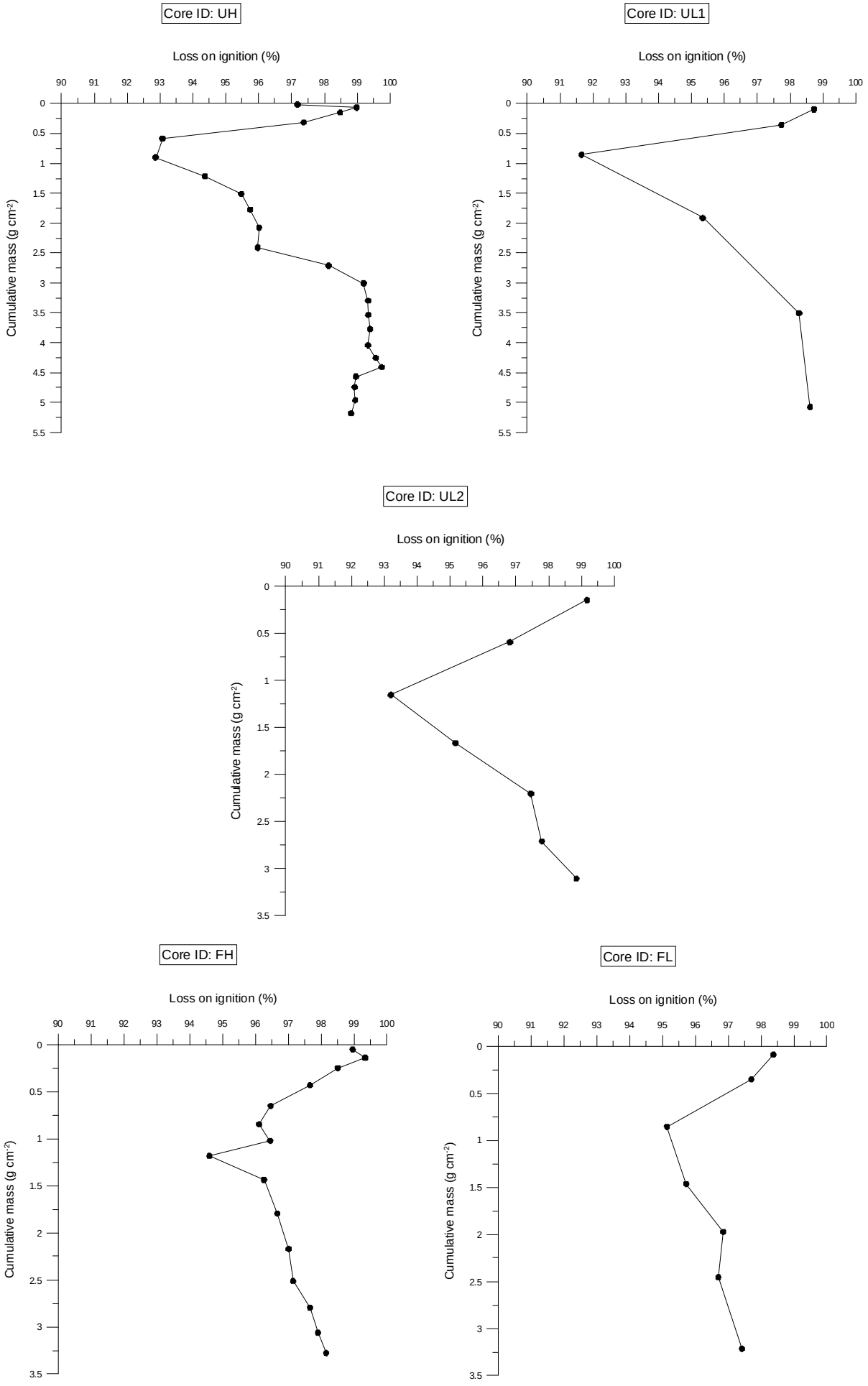

Figure 4-3 Loss on ignitions

4.4 ^{210}Pb chronologies

For the unforested site, all three cores (UH, UL1 and UL2) showed a similar distribution of unsupported ^{210}Pb (Figure 4-4) with maximum values of 300-326 Bq kg^{-1} at a cumulative mass value of ~ 0.5 g cm^{-2}. However, in each case a reversal to lower values in the range 169-246 Bq kg^{-1} was observed nearer the surface. This probably indicates a reduction in ^{210}Pb specific activity because of plant growth (growth dilution) (Grover et al., 2012).

For the forested site, core FH showed near constant values of unsupported ^{210}Pb in the top two sections at 182-198 Bq kg^{-1}, then the specific activity slowly decreased to a value of 148 Bq kg^{-1} at a cumulative mass value of 0.65 g cm^{-2}. This was followed by an approximately exponential decrease to 17 Bq kg^{-1} at a cumulative mass value of 1.18 g cm^{-2}, below which a slow rate of decrease was observed until the limit of detection was reached at a cumulative mass value of 2.2 g cm^{-2}. Core FL showed a similar trend but with less detail. The specific activity in the top section (corresponding to the combined depth of the top two sections in FH) was 196 Bq kg^{-1}, with a slightly lower value of 177 Bq kg^{-1} for the next two samples.

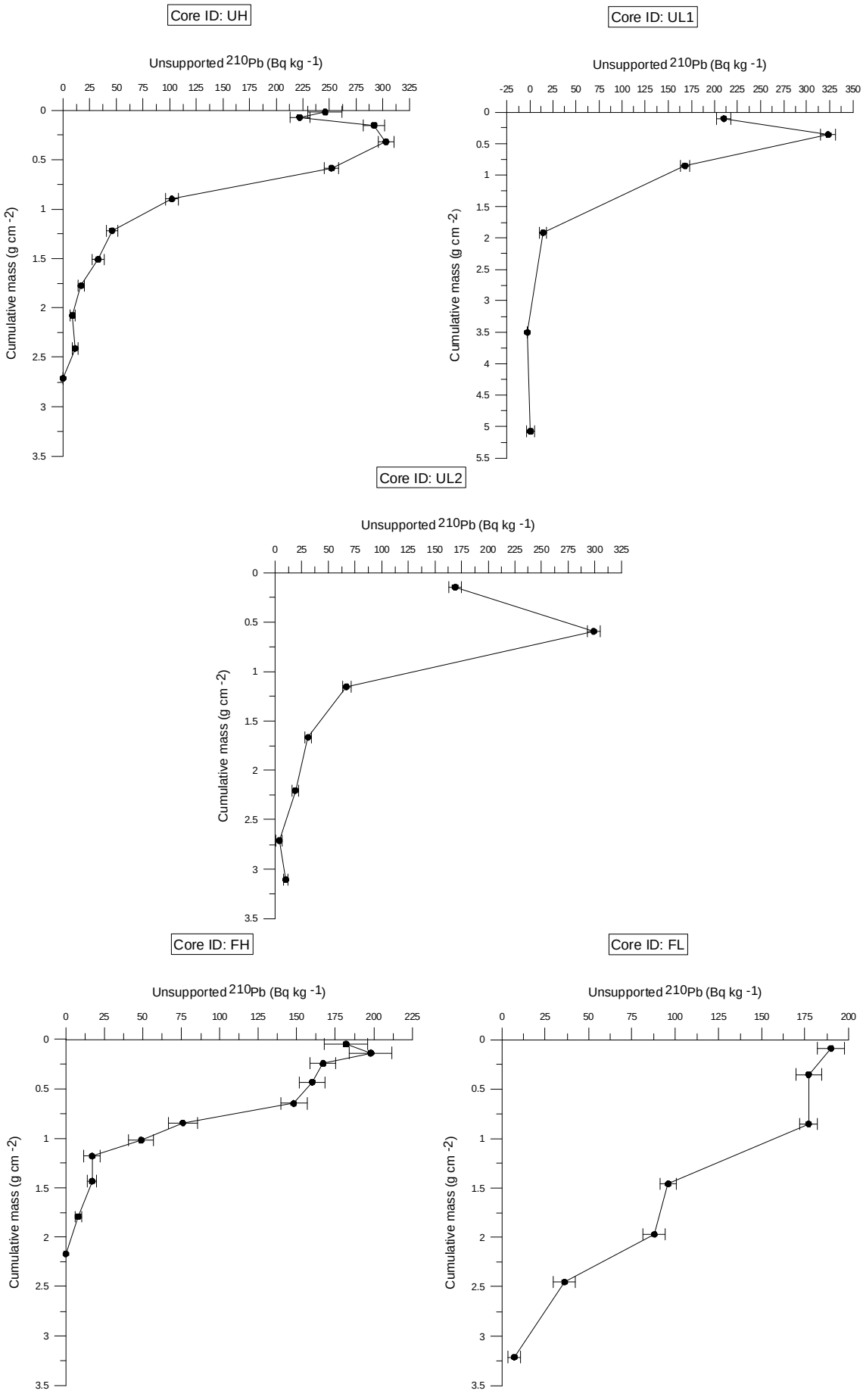

Figure 4-4 Unsupported ^{210}Pb Bq kg^{-1}

4.4.1 CIC calculation

Chronologies were derived for the cores by firstly calculating accumulation rates from interpretation of sections of each core (by application of the CIC equation (1.4) described in Chapter 1.4) and secondly by dividing the cumulative mass (g cm^{-2}) for each section by the calculated accumulation rate (g $cm^{-2}y^{-1}$) to derive the age of each section of the core. Because of the complex nature of the ^{210}Pb profiles near the surface the complete set of data for any individual core could not be used in the calculation. In order to deal with this type of situation McCall et al (1984) adopted the approach of applying the CIC calculation to individual sections of the core which had different density bands. A similar approach was used here and the CIC calculation was therefore applied selectively to those sections of cores that did display an exponential decrease in ^{210}Pb specific activity with increasing cumulative mass. The uncertainty on the chronology was estimated from the error on the gradient of the best fit straight line in the plot of ln activity against cumulative mass.

For core UH, the top three data points, which were apparently affected by growth dilution, were excluded from the calculation as was the bottom point which showed a slight increase in ^{210}Pb specific activity against the preceding decreasing trend. The remaining section (Figure 4-5) gave an accumulation rate of 0.015 ± 0.00076 g cm^{-2} y^{-1}. This was then applied to the entire core to derive an age profile. There is of course an uncertainty of the accuracy of the chronology derived by applying the calculated accumulation rate to the surface section affected by growth dilution. However, as this section only accounted for less than 5% of the total cumulative mass of the core any inaccuracy in the chronology will be small. To attempt to demonstrate this quantitatively; the average ^{210}Pb in the top three sections is approximately 20% lower than that for the fourth section (6-8cm), if this is translated into a 20% increase in the accumulation rate for this section (from 0.015 g cm^{-2} y^{-1} to 0.018 g $cm^{-2}y^{-1}$) it would alter the age by three years, i.e. from a value of 21 years to one of 18 years.

Core ID: UH (Middle section 2)

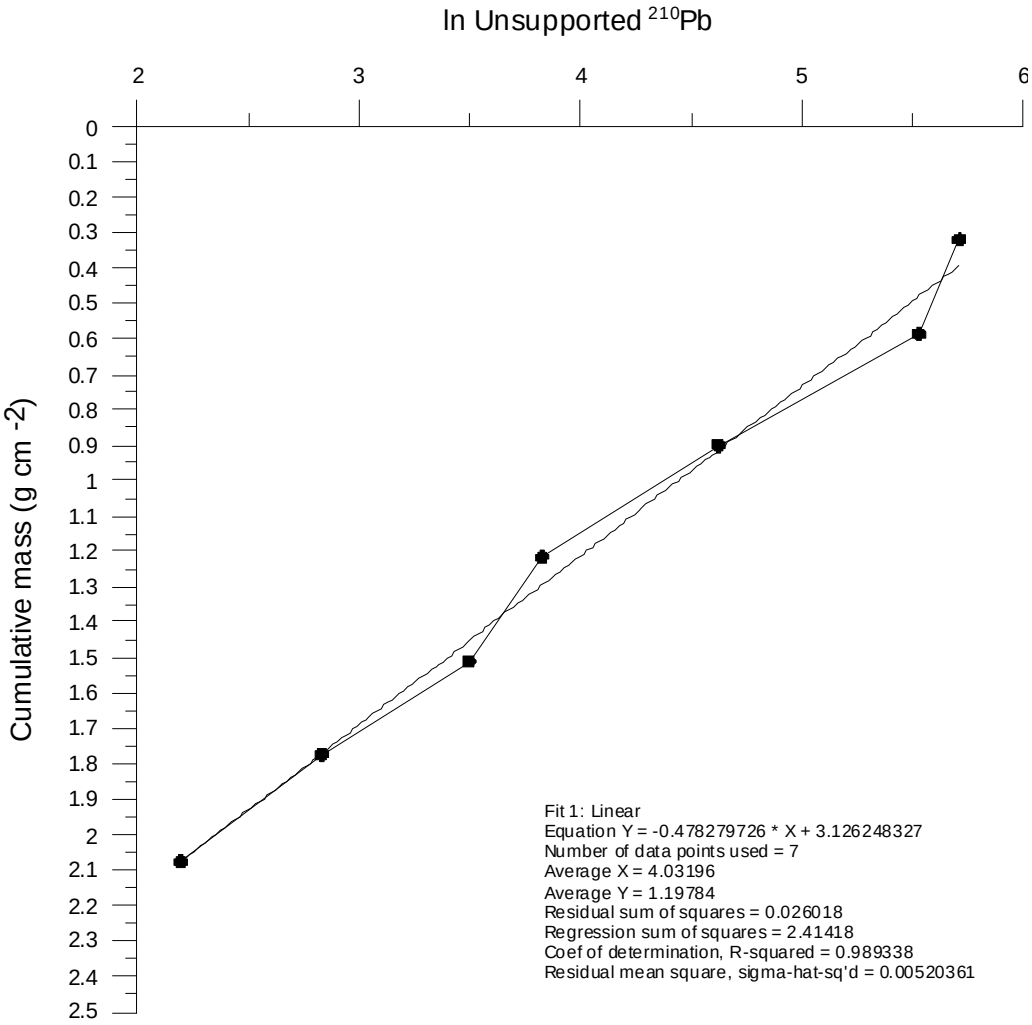

Figure 4-5 Core UH ln unsupported ^{210}Pb

For core UL1, the top data point was excluded from the calculation as were the bottom two which had error values of greater than 50% and the remaining section (Figure 4-6) gave an accumulation rate of 0.015 ± 0.0016 g cm^{-2} y^{-1} which is in excellent agreement with the accumulation rate derived for core UH and was applied to the entire core to derive an age profile.

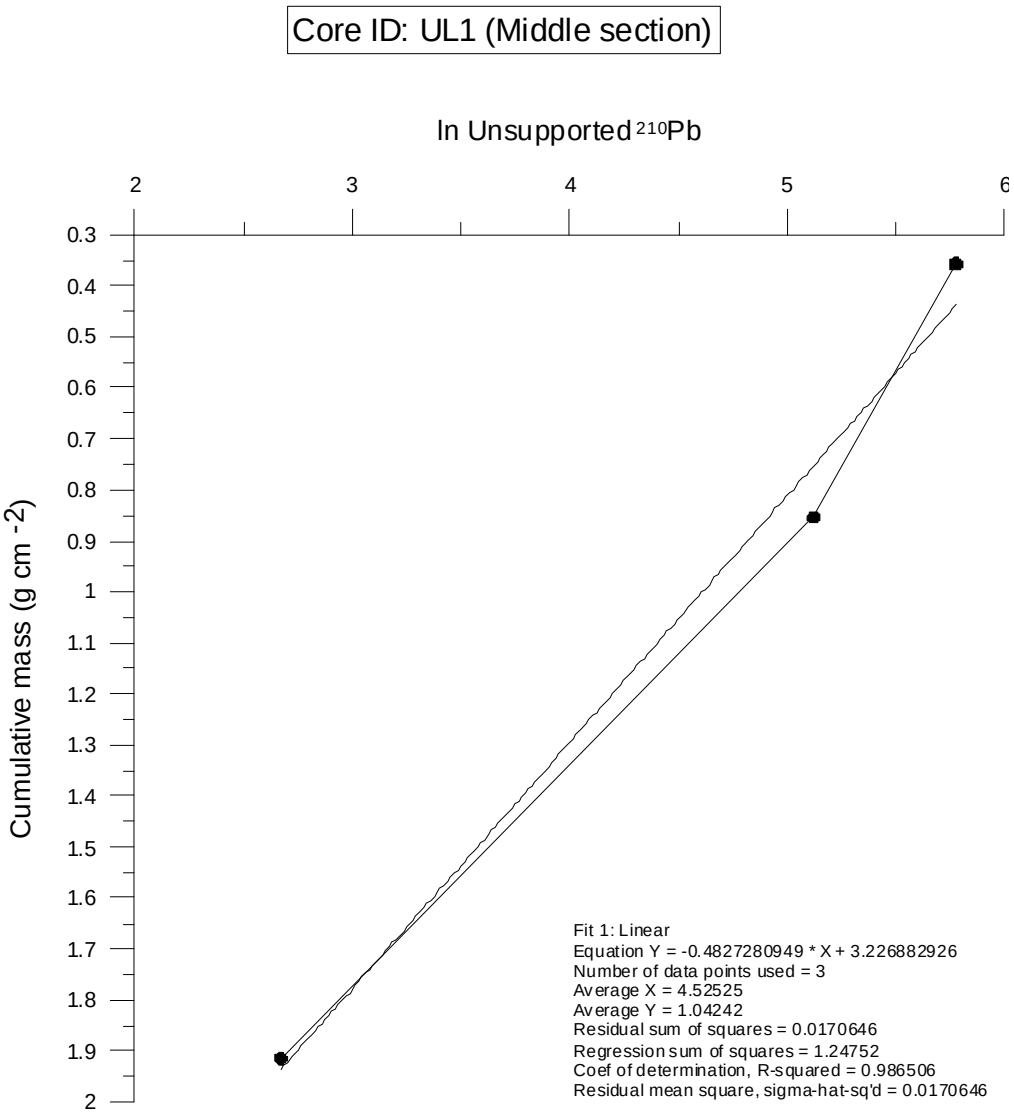

Figure 4-6 Core UL1 ln unsupported ^{210}Pb

For core UL2, the top data point was excluded from the calculation as were the bottom two, one of which had an error of greater than 50% and the other showed a slight increase in ^{210}Pb specific activity against the preceding decreasing trend. The remaining section (Figure 4-7) gave an accumulation rate of 0.017 ± 0.007 g cm^{-2} y^{-1}. The uncertainty in this case, based on the error on the gradient in the CIC graph was relatively high at 41%, but the derived accumulation rate was again in good agreement with the accumulation rate derived for core UH and was applied to the entire core to derive an age profile.

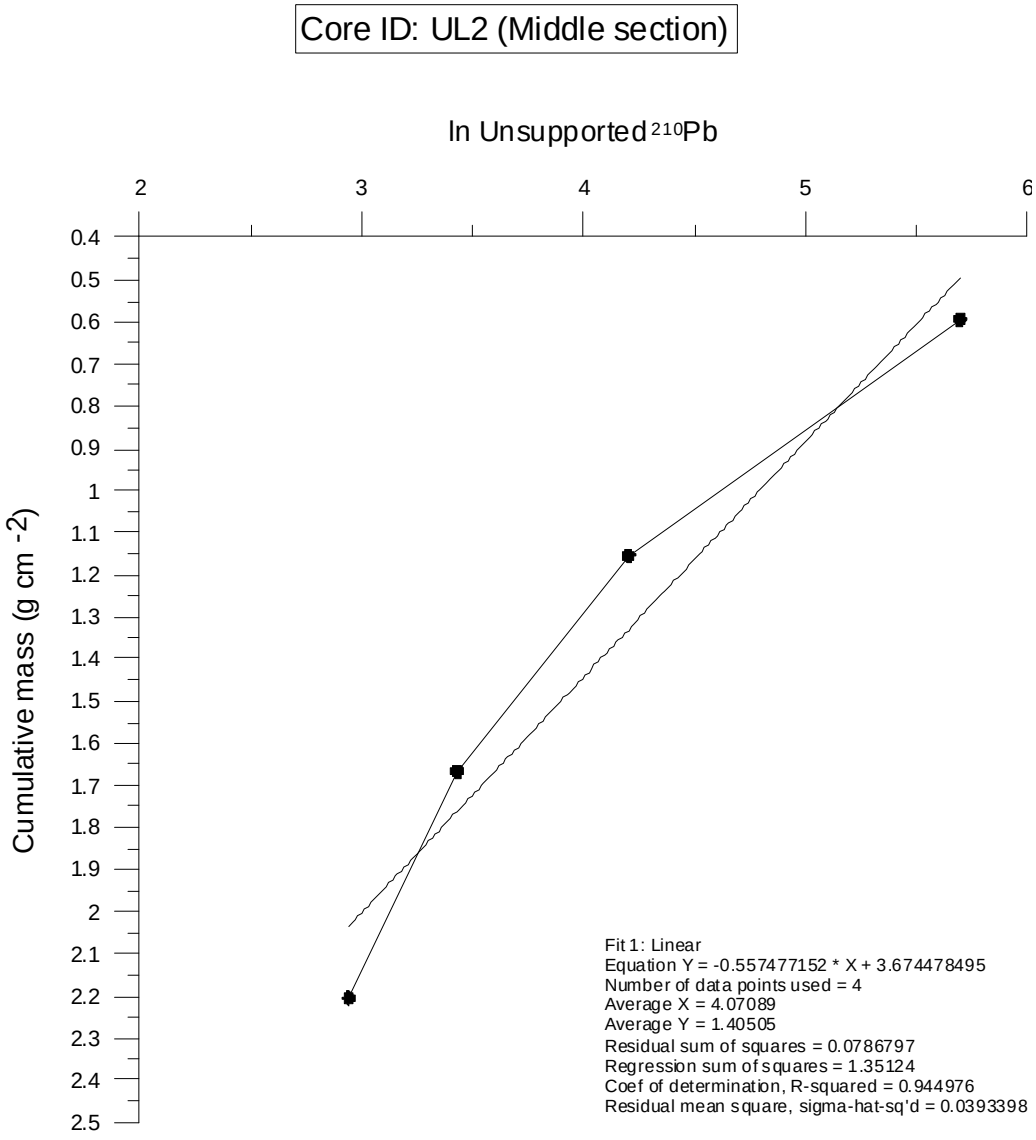

Figure 4-7 Core UL2 ln unsupported ^{210}Pb

For core FH, the top sample, which appeared to be affected by growth dilution, was excluded. The remaining samples showed a profile that approximates to an exponential trend with small perturbations at about 0.2 – 0.4 g cm^{-2} and 1.8 g cm^{-2}. On the basis of attempting to fit an exponential to selected sections of the core, there was no obvious basis for treating the data on a sectional basis, so the CIC calculation was applied to all of the data except the top sample (Figure 4-8), to give an average accumulation rate of 0.014 ± 0.0014 g cm^{-2} y^{-1}. This average accumulation rate is within error the same as that of 0.015 g cm^{-2} y^{-1} for the unforested core UH, implying that peat accumulation has continued at a relatively constant rate when the forest was present.

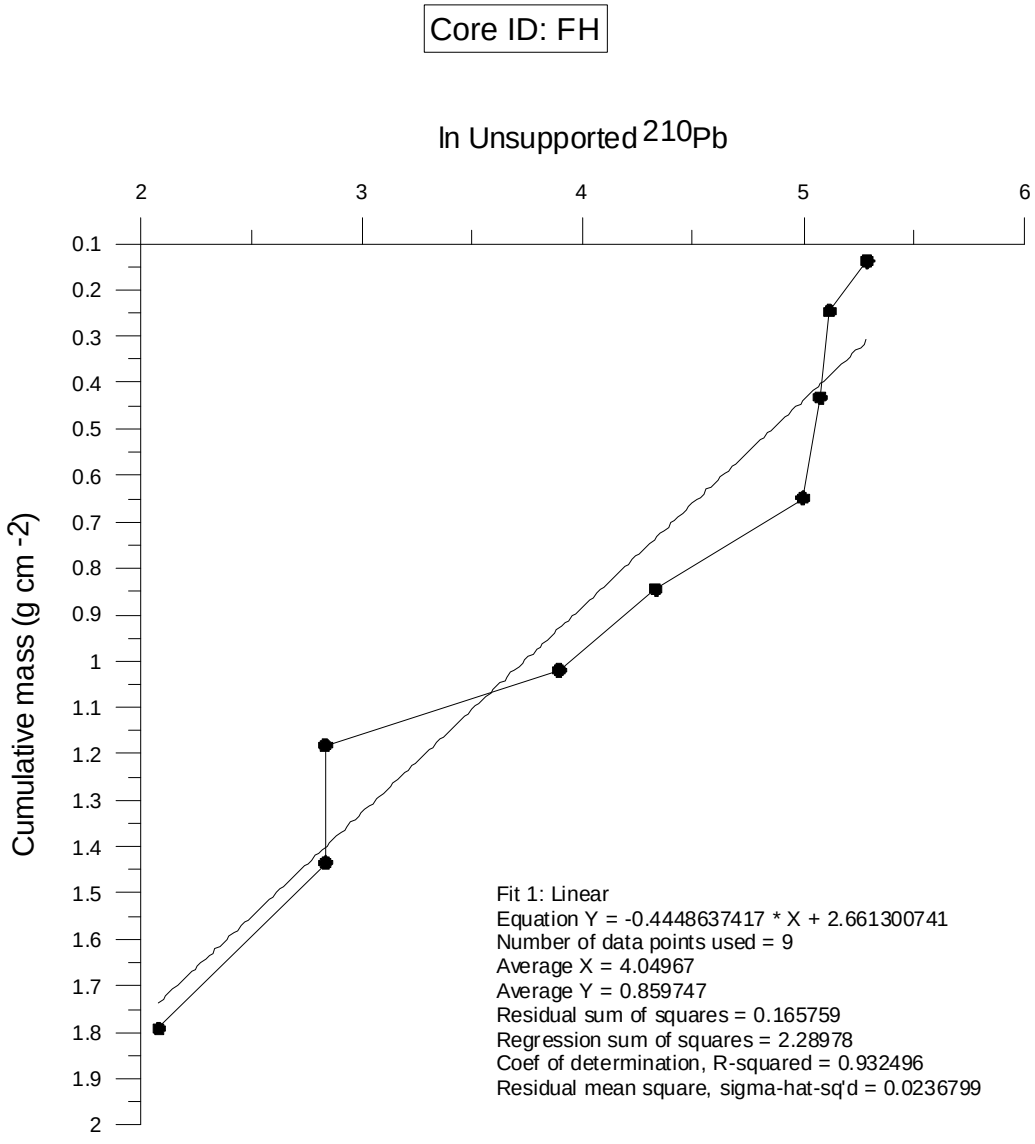

Figure 4-8 Core FH ln unsupported ^{210}Pb

For core FL, the top three data points were almost constant being within 2 σ error of each other so could not be used in the interpretation although like core FH this core appeared to have two distinct zones. The accumulation rate calculated for the middle (Figure 4-9) section was 0.021 ± 0.0037 g cm^{-2} y^{-1}. This was then applied to derive an age profile for the entire core.

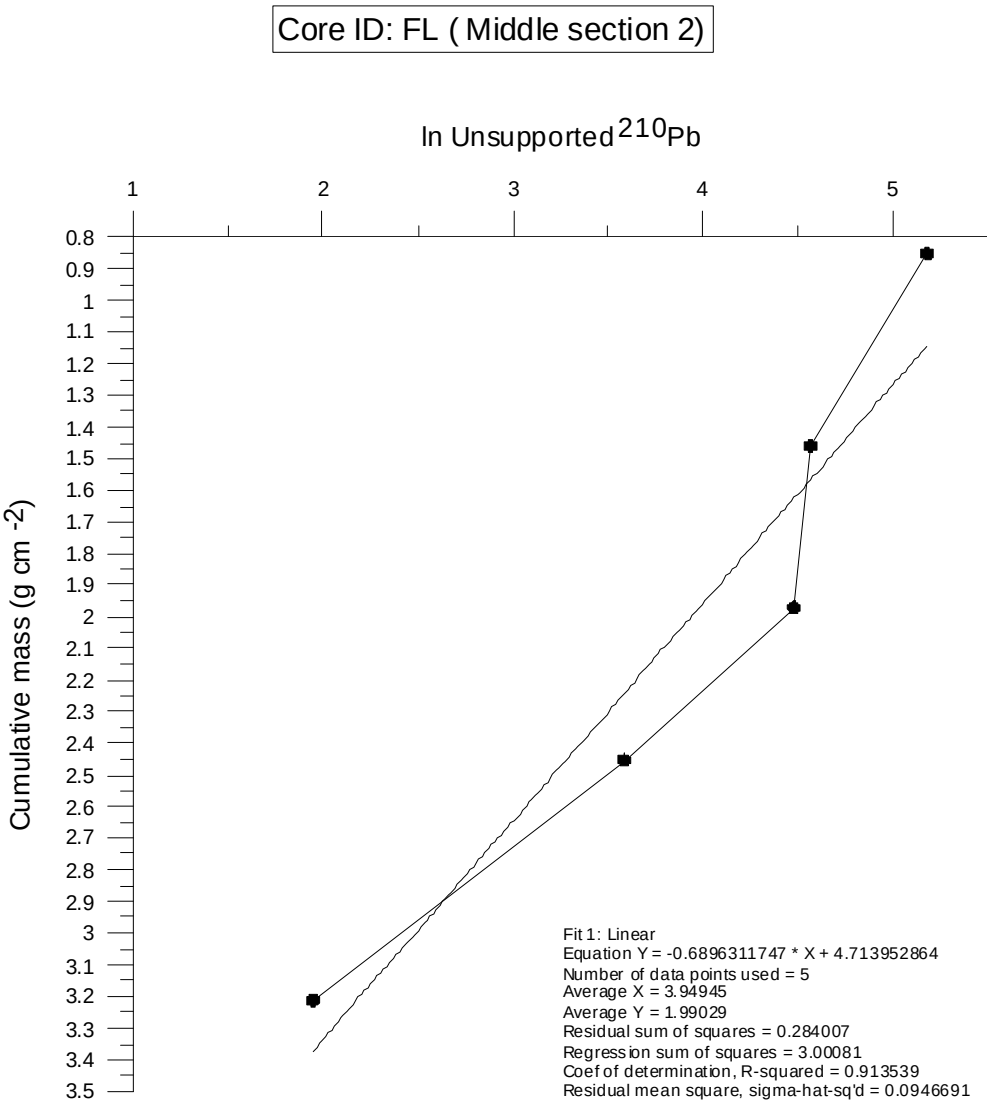

Figure 4-9 Core FL ln unsupported ^{210}Pb

The chronologies that were derived are shown in Tables 4-4 to 4-8.

Core ID:UH	
Cumulative mass	CIC age
g cm^{-2}	y
0.019	1.27±0.06
0.071	4.73±0.24
0.152	10.1±0.5
0.318	21.2±1.1
0.586	39±2
0.900	60±3
1.218	81±4
1.511	101±5
1.775	118±6
2.077	138±7
2.410	161±8

Table 4-4 Core UH CIC ages

CoreID:UL1	
Cumulative mass	CIC age
g cm^{-2}	y
0.100	6.67±0.73
0.358	23.9±2.6
0.855	57±6
1.915	127±14

Table 4-5 Core UL1 CIC ages

CoreID:UL2	
Cumulative mass	CIC age
g cm^{-2}	y
0.146	8.6±3.5
0.594	35±14
1.154	68±28
1.667	98±40
2.205	130±53
2.711	159±65
3.107	183±74

Table 4-6 Core UL2 CIC ages

CoreID:FH	
Cumulative mass	CIC age
g cm^{-2}	y
0.049	3.55±0.36
0.138	10±1
0.246	18±2
0.432	31±3
0.649	47±5
0.845	61±6
1.019	74±8
1.182	86±9
1.435	104±11
1.793	130±13

Table 4-7 Core FH CIC ages

CoreID:FL	
Cumulative mass	CIC age
g cm^{-2}	y
0.087	4.14±0.73
0.351	17±3
0.853	41±7
1.461	70±12
1.971	94±17
2.453	117±21
3.214	153±27

Table 4-8 Core FL CIC ages

4.4.2 CRS calculation

CRS ages were calculated using inventories (Bq m^{-2}) as described in Chapter 1.4 using equation (1.5) and the results for each core are tabulated below (Tables 4-9 to 4-13) .

Core ID : UH	
Cumulative mass	CRS age
g cm^{-2}	y
0.019	0.57±0.01
0.071	2.06±0.05
0.152	4.96±0.12
0.318	12.9±0.4
0.586	30±1
0.900	53±4
1.218	74±7
1.511	92±12
1.775	110±18
2.077	128±29
2.410	162±74

Table 4-9 Core UH CRS ages

Core ID : UL1	
Cumulative mass	CRS age
g cm^{-2}	y
0.100	2.50±0.13
0.358	13.0±0.8
0.855	41±5
1.915	103±76

Table 4-10 Core UL1 CRS ages

Core ID : UL2	
Cumulative mass	CRS age
g cm^{-2}	y
0.146	2.80±0.08
0.594	20.5±0.8
1.154	58±4
1.667	81±9
2.205	107±23
2.711	136±46
3.107	165±66

Table 4-11 Core UL2 CRS ages

Core ID: FH	
Cumulative mass	**CRS age**
g cm^{-2}	**y**
0.049	1.87±0.08
0.138	5.8±0.2
0.246	10.8±0.5
0.432	21±1
0.649	38±3
0.845	57±6
1.019	75±10
1.182	88±14
1.435	106±23
1.793	149±75

Table 4-12 Core FH CRS ages

Core ID: FL	
Cumulative mass	**CRS age**
g cm^{-2}	**y**
0.087	1.65±0.06
0.351	7.0±0.3
0.853	20.0±0.9
1.461	41±3
1.971	64±8
2.453	97±30
3.214	146±154

Table 4-13 Core FL CRS ages

CRS accumulation rates were calculated by dividing Δ cumulative mass values (representing the cumulative mass increment) by the Δ t values (representing the time increment) for each section of the cores (where Δ represents the difference obtained by subtracting the respective values for cumulative mass and time in each layer from those in the following deeper layer) and the results are tabulated below (Tables 4-14 to 4-18).

Core ID:UH	Δt	Section accumulation rate
Δ Cumulative mass (g cm^{-2})	y	g $cm^{-2}y^{-1}$
0.052	1.49	0.035
0.081	2.90	0.028
0.166	7.91	0.021
0.268	17.00	0.016
0.314	23.46	0.013
0.318	20.23	0.016
0.293	18.12	0.016
0.264	18.30	0.014
0.302	17.85	0.017
0.333	34.62	0.010

Table 4-14 Core UH CRS accumulation rates

Core ID:UL1	Δt	Section accumulation rate
Δ Cumulative mass (g cm^{-2})	y	g $cm^{-2}y^{-1}$
0.258	10.52	0.025
0.497	27.79	0.018
1.060	62.10	0.017

Table 4-15 Core UL1 CRS accumulation rates

Core ID:UL2	Δt	Section accumulation rate
Δ Cumulative mass (g cm^{-2})	y	g $cm^{-2}y^{-1}$
0.448	17.69	0.025
0.560	37.26	0.015
0.513	23.16	0.022
0.538	25.96	0.021
0.506	28.64	0.018
0.396	29.55	0.013

Table 4-16 Core UL2 CRS accumulation rates

Core ID:FH	Δt	Section accumulation rate
Δ Cumulative mass (g cm^{-2})	y	g $cm^{-2}y^{-1}$
0.089	3.90	0.023
0.108	5.07	0.021
0.186	10.10	0.018
0.217	16.90	0.013
0.196	19.33	0.010
0.174	17.64	0.010
0.163	13.24	0.012
0.253	17.63	0.014
0.358	43.31	0.008

Table 4-17 Core FH CRS accumulation rates

Core ID:FL	Δt	Section accumulation rate
Δ Cumulative mass (g cm^{-2})	y	g $cm^{-2}y^{-1}$
0.264	5.31	0.050
0.502	13.08	0.038
0.608	20.90	0.029
0.510	22.90	0.022
0.482	33.10	0.015
0.761	48.94	0.016

Table 4-18 Core FL CRS accumulation rates

4.4.3 Comparison of CRS and CIC chronologies

To enable comparison of the chronologies derived from both the CIC and the CRS methods the results are tabulated below (Tables 4-19 to 4-23).

Core ID:UH		
Cumulative mass	CRS age	CIC age
g cm^{-2}	y	y
0.019	0.57±0.01	1.27±0.06
0.071	2.06±0.05	4.73±0.24
0.152	4.96±0.12	10.1±0.5
0.318	12.9±0.4	21.2±1.1
0.586	30±1	39±2
0.900	53±4	60±3
1.218	74±7	81±4
1.511	92±12	101±5
1.775	110±18	118±6
2.077	128±29	138±7
2.410	162±74	161±8

Table 4-19 Core UH CRS and CIC comparison

CoreID:UL1		
Cumulative mass	CRS age	CIC age
g cm^{-2}	y	y
0.100	2.50±0.13	6.67±0.73
0.358	13.0±0.8	23.9±2.6
0.855	41±5	57±6
1.915	103±76	127±14

Table 4-20 Core UL1 CRS and CIC comparison

CoreID:UL2		
Cumulative mass	CRS age	CIC age
g cm^{-2}	y	y
0.146	2.80±0.08	8.6±3.5
0.594	20.5±0.8	35±14
1.154	58±4	68±28
1.667	81±9	98±40
2.205	107±23	130±53
2.711	136±46	159±65
3.107	165±66	183±74

Table 4-21 Core UL2 CRS and CIC comparison

Core ID:FH		
Cumulative mass	CRS age	CIC age
g cm^{-2}	y	y
0.049	1.87±0.08	3.55±0.36
0.138	5.8±0.2	10±1
0.246	10.8±0.5	18±2
0.432	21±1	31±3
0.649	38±3	47±5
0.845	57±6	61±6
1.019	75±10	74±8
1.182	88±14	86±9
1.435	106±23	104±11
1.793	149±75	130±13

Table 4-22 Core FH CRS and CIC comparison

Core ID:FL		
Cumulative mass	CRS age	CIC age
g cm-2	y	y
0.087	1.65±0.06	4.14±0.73
0.351	7.0±0.3	17±3
0.853	20.0±0.9	41±7
1.461	41±3	70±12
1.971	64±8	94±17
2.453	97±30	117±21
3.214	146±154	153±27

Table 4-23 Core FL CRS and CIC comparison

The CRS v CIC results are shown graphically in Figure 4-10. There was good agreement between the CIC and CRS derived chronologies for the high resolution core, UH, from the unforested site. There was reasonable agreement between the CIC and CRS chronologies for the high resolution core, FH, from the forested site. However in this case the CIC ages were slightly higher than the CRS ages over the 0 – 70 y timespan. There was good agreement between 70 and 100 y but the CRS age was significantly older for the deepest sample, consistent with the expected deviation due to underestimation of I_T and I_i in the CRS equation, however, the uncertainty on the CRS age for this sample was large. There was generally much poorer agreement between the CRS and CIC chronologies for the low resolution cores (UL1, UL2 and FL). The error bar for the CRS age of the deepest section of core FL was omitted from the graph as it was large but the point was shown for comparison with the CIC age. When comparing R-squared values for the plots the best fits were achieved for cores UH, UL1 and UL2 (0.995, 0.998 and 0.996 respectively), although there was more of a deviation away from the centre line of the plot for the three low resolution cores(UL1, UL2 and FL) . The R-squared values for the other cores were in the range of 0.961 – 0.988. One of the major factors influencing the accuracy of the calculation was that of obtaining a good limit of detection, it was therefore important to ensure minimisation of the unquantifiable contribution of unsupported ^{210}Pb below the detection limit by using a low background detector (MacKenzie et al., 2011). The consistent results achieved between the CIC and CRS chronologies for core UH would imply this to have been the case. Another factor that could have impacted on the accuracy of the chronology calculation was that of inaccuracies in defining the core area. These inaccuracies were significantly smaller when the defined geometry of a core tube was used but larger for the cores measured and sectioned manually in the field. This is almost certainly the cause of the better agreement between CRS and CIC chronologies for the cores collected using a coring tube (UH and FH) relative to the cores which were sectioned in the field.

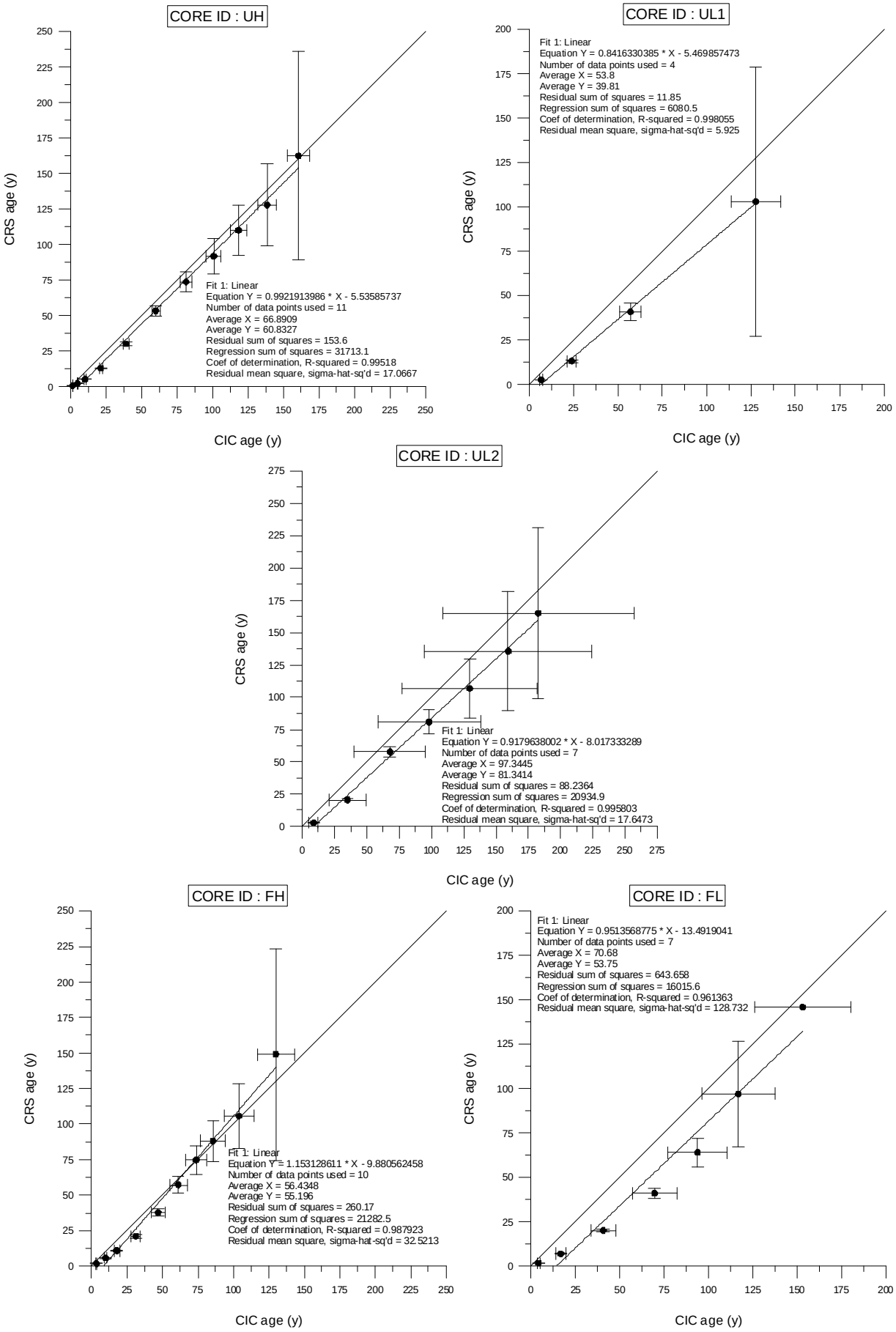

Figure 4-10 CRS and CIC comparisons

4.5 Anthropogenic – ^{137}Cs

For the unforested site all three cores (UH, UL1 and UL2) showed a similar distribution of ^{137}Cs (Figure 4-11) with maximum values of 247-419 Bq kg^{-1} at the surface followed by a continuous exponential decrease with increasing depth.

For the forested site both cores (FH and FL) showed a similar trend to the unforested cores but with a reversal to lower values nearer the surface (Figure 4-11). The sub surface maximum values of ~ 150 Bq kg^{-1} were seen in the dry bulk density range 0.35 – 0.65 g cm^{-2} below which there is an exponential decrease. The maximum values observed for both forested cores are lower than those observed in the unforested cores and both FH and FL exhibit the bend back towards the surface.

If the ^{137}Cs profile represented temporal variations in deposition, distinct peaks would have been observed for weapons testing (1963) and Chernobyl (1986) fallout. None of the profiles showed a distribution consistent with this pattern of input.

It was concluded that ^{137}Cs profiles could not be used for chronological purposes. The observed profiles almost certainly represent a combined weapons testing plus Chernobyl fallout profile generated by downward movement of ^{137}Cs since deposition.

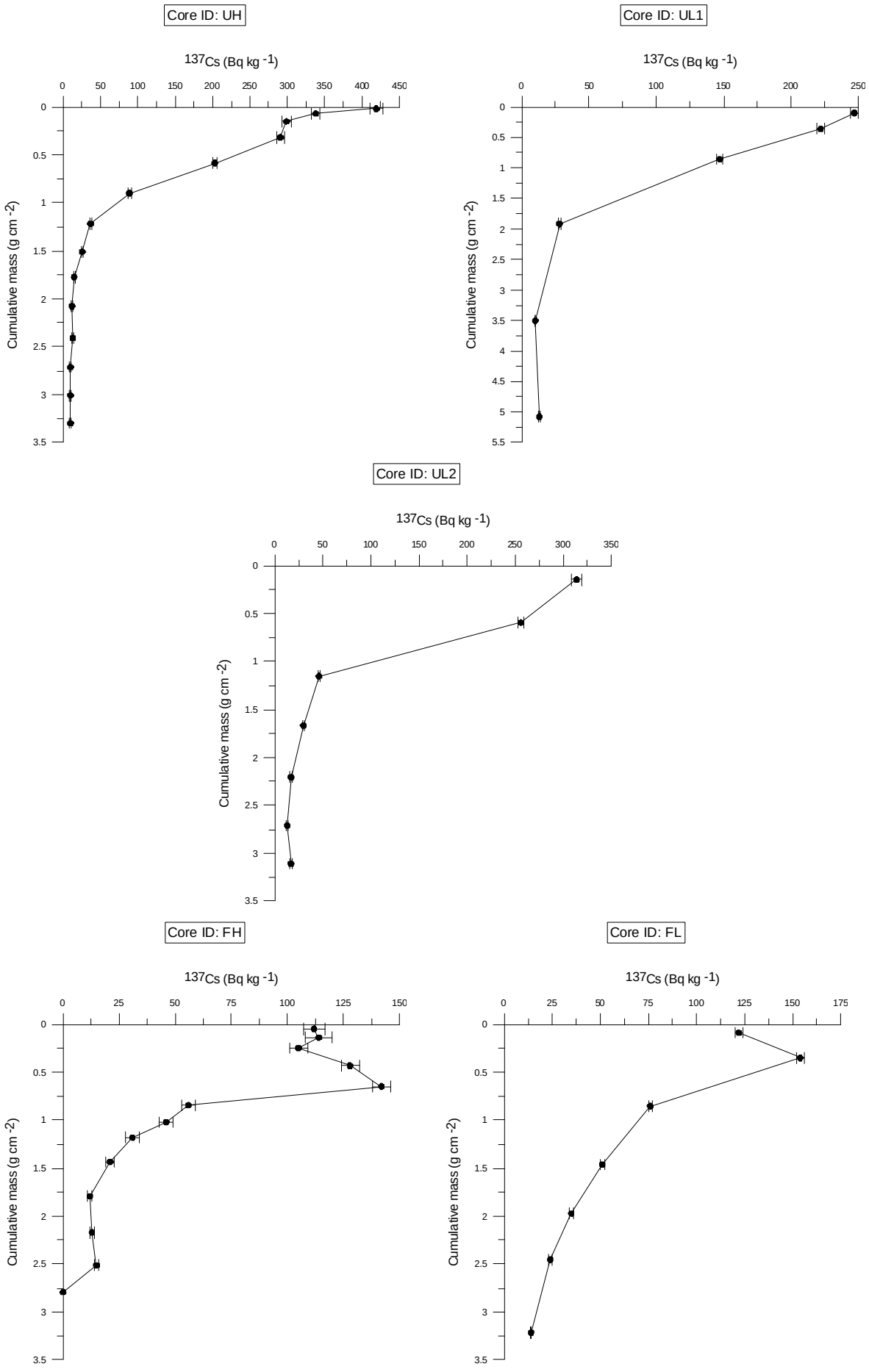

Figure 4-11 ^{137}Cs (Bq kg^{-1}) profiles

4.6 Anthropogenic – ^{241}Am

As detailed in the introduction ^{241}Am was not deposited directly from fallout but has been growing in as a result of decay of ^{241}Pu. Previously ^{241}Am was not widely used for chronologies in peat because of its low activities but ingrowth is now approaching maximum activity and ^{241}Am was detected in all five cores (Figure 4-12).

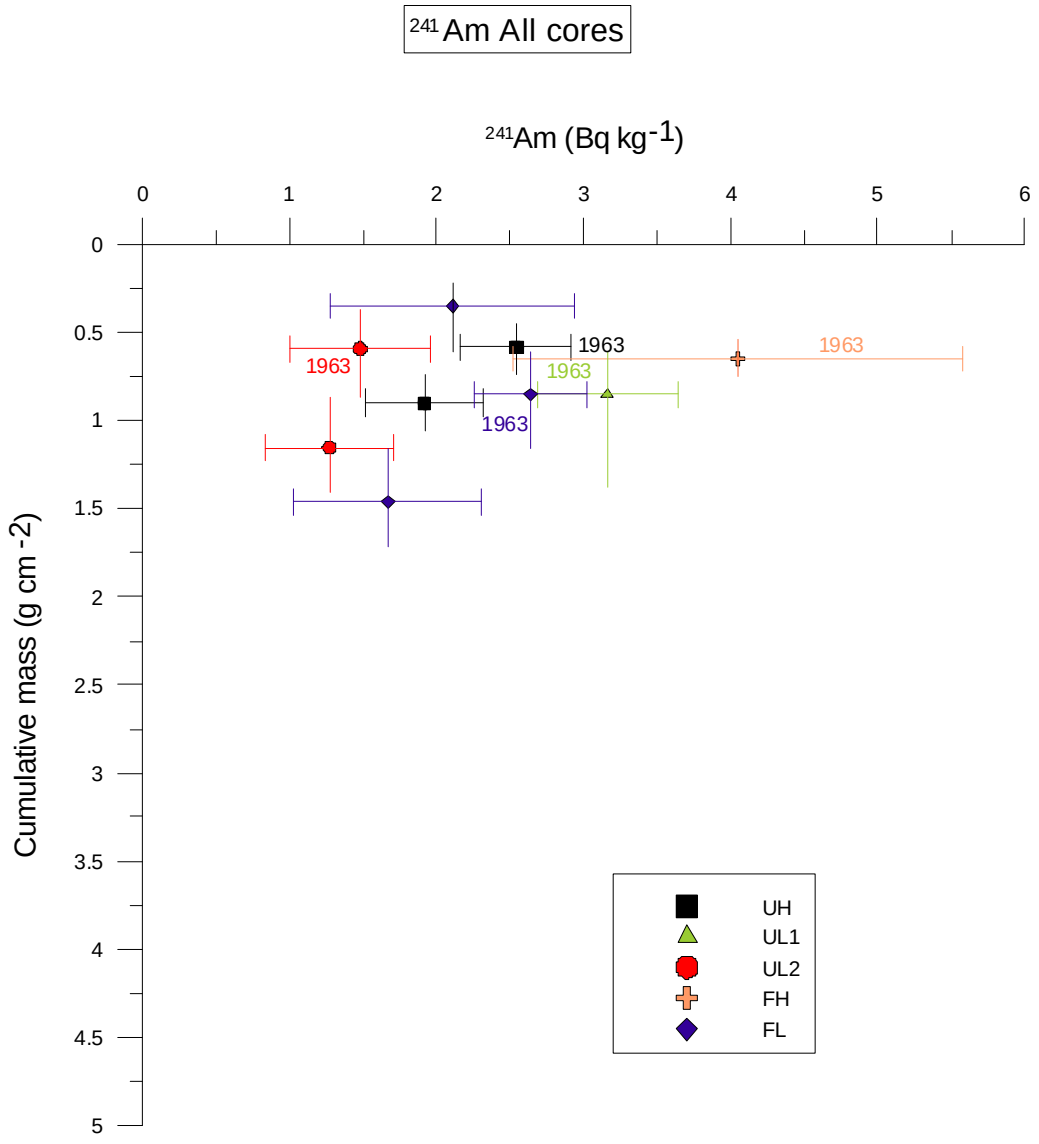

Figure 4-12 Distribution of ^{241}Am in cores

The vertical line through each point on the plot represents the cumulative mass range covered by the core section and the section with the maximum specific activity is labelled as 1963 on the graph. All of the cores exhibited maximum

^{241}Am values over the relatively narrow range of 0.586 g cm^{-2} to 0.855 g cm^{-2} cumulative mass.

Figure 4-13 shows the CIC chronologies for the three unforested cores (UH, UL1 and UL2) and the CRS chronology for core UH. The graphs also show the cumulative mass range at which the maximum ^{241}Am specific activity was observed for each of the cores plotted at the time corresponding to 1963. There was excellent agreement between the three cores for the CIC method and also between the CIC and CRS chronologies for high resolution core UH. Importantly, the independent chronology provided by the ^{241}Am was in agreement with all three CIC chronologies and with the CRS chronology for core UH, providing a high degree of confidence in the accuracy of the chronologies.

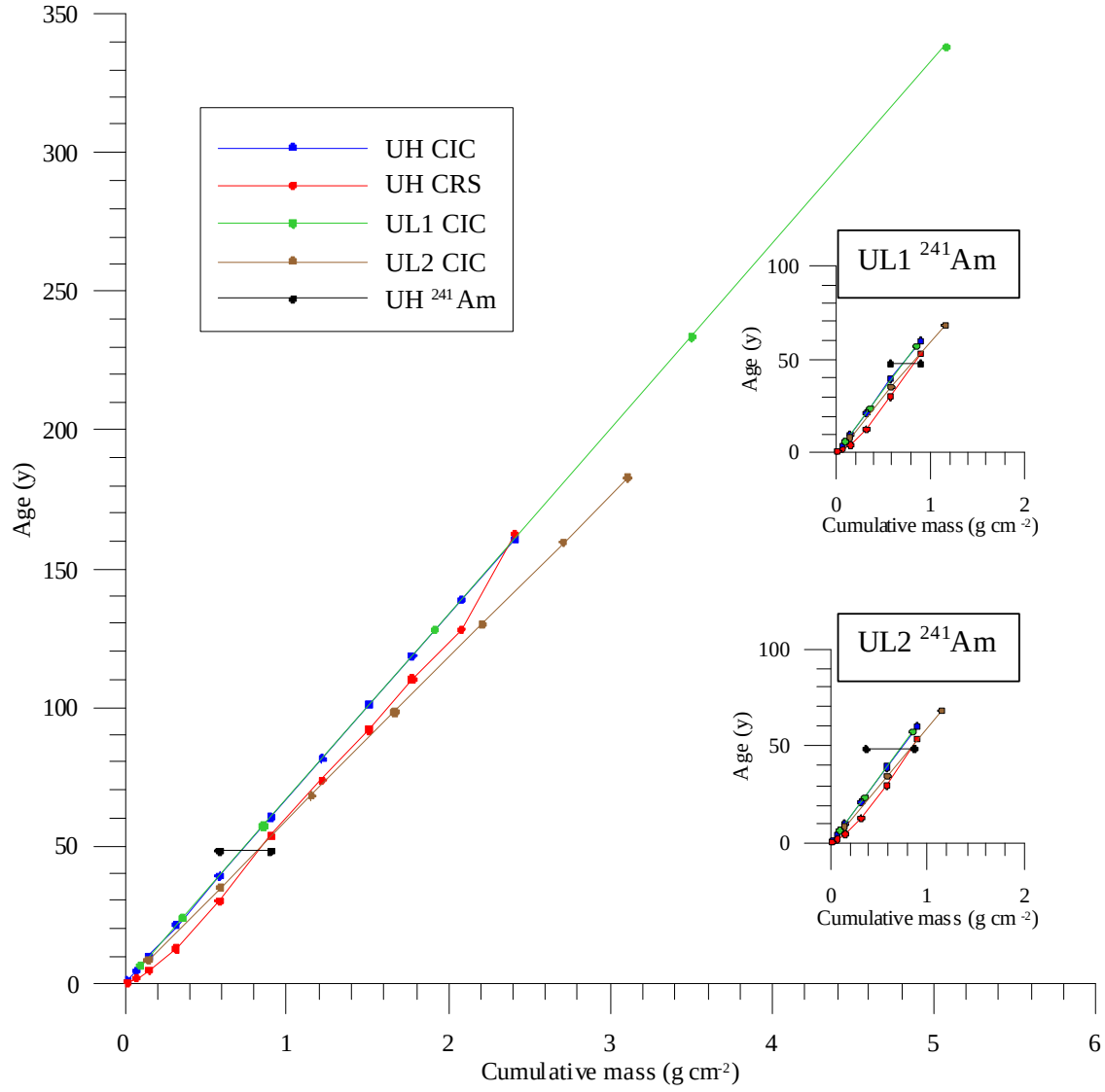

Figure 4-13 Comparison of UH, UL1 and UL2 CIC, UH CRS and UH ^{241}Am chronologies

Figure 4-14 shows the CIC chronology for core UH and the CRS chronologies for all of the unforested cores (UH, UL1 and UL2) along with the ^{241}Am chronology for core UH. It is apparent that there was much poorer agreement between the low resolution CRS chronologies (UL1 and UL2) and the CRS and CIC chronologies for core UH. Also, the CRS chronologies for core UL1 and UL2 were inconsistent with the ^{241}Am chronology, casting doubt on their accuracy. This supports the suggestion that the high resolution sampling method using a defined geometry core tube gave a more reliable CRS chronology than the low resolution method where the chronology is more vulnerable to errors in defining precise area and depth.

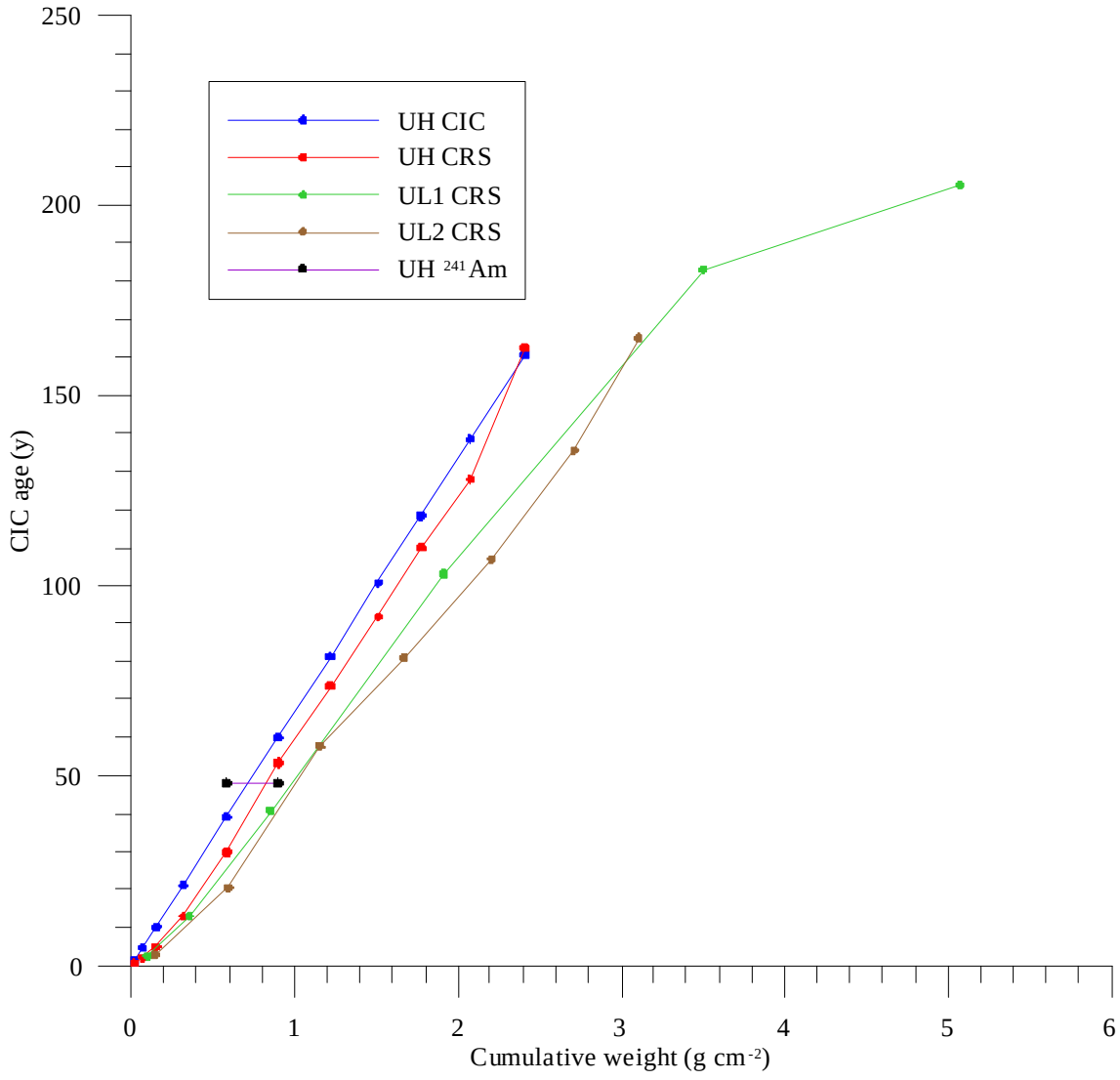

Figure 4-14 Comparison of UH, UL1 and UL2 CRS, UH CIC and UH ^{241}Am chronologies

Figure 4-15 shows the CIC and CRS chronologies for the forested cores (FH and FL) along with the ^{241}Am chronology for core FH. The graph also shows the 1955 and 1995 horizons which correspond to the time of afforestation and deforestation, respectively. There was reasonable agreement between the CIC and CRS chronologies for core FH, but with a slight offset of CRS ages to younger values over about the first 70 years of the chronologies. This covers the period of afforestation and deforestation and may reflect disturbance of the peat during the forestry operation. For the low resolution core (FL) there was poor agreement between the CIC and CRS chronologies as well as poor agreement with the CIC and CRS chronologies for core FH. Neither the CIC nor CRS chronologies for core FL agreed with the ^{241}Am chronology for core FH.

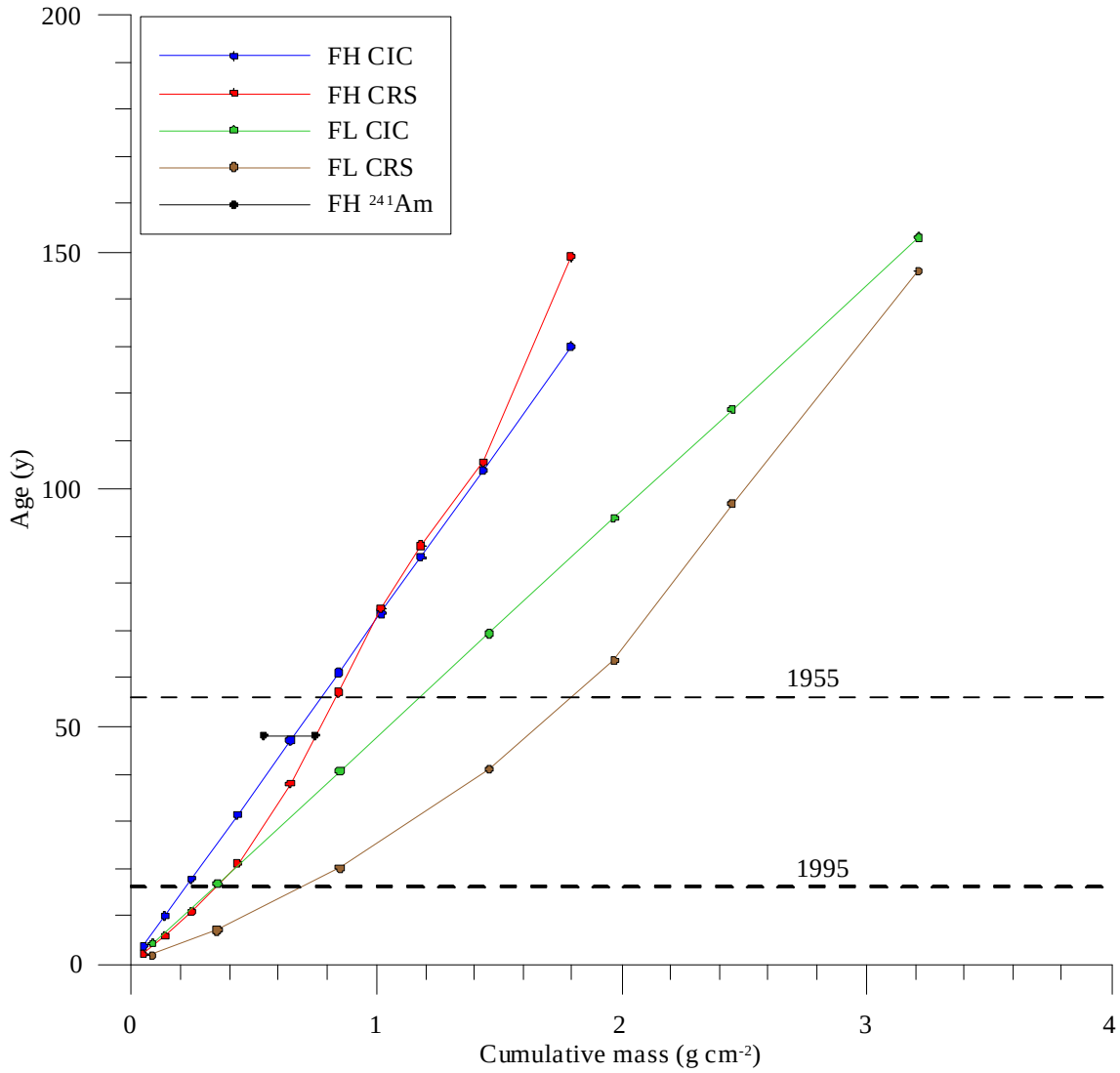

Figure 4-15 Comparison of FH CIC and CRS, FL CIC and CRS and FH ^{241}Am chronologies

The CIC and CRS chronologies for core FL did overlap with the ^{241}Am chronology for this core (Figure 4-16), but in this case the large sample increment meant that the horizon corresponding to 1963 covered a large range of cumulative mass.

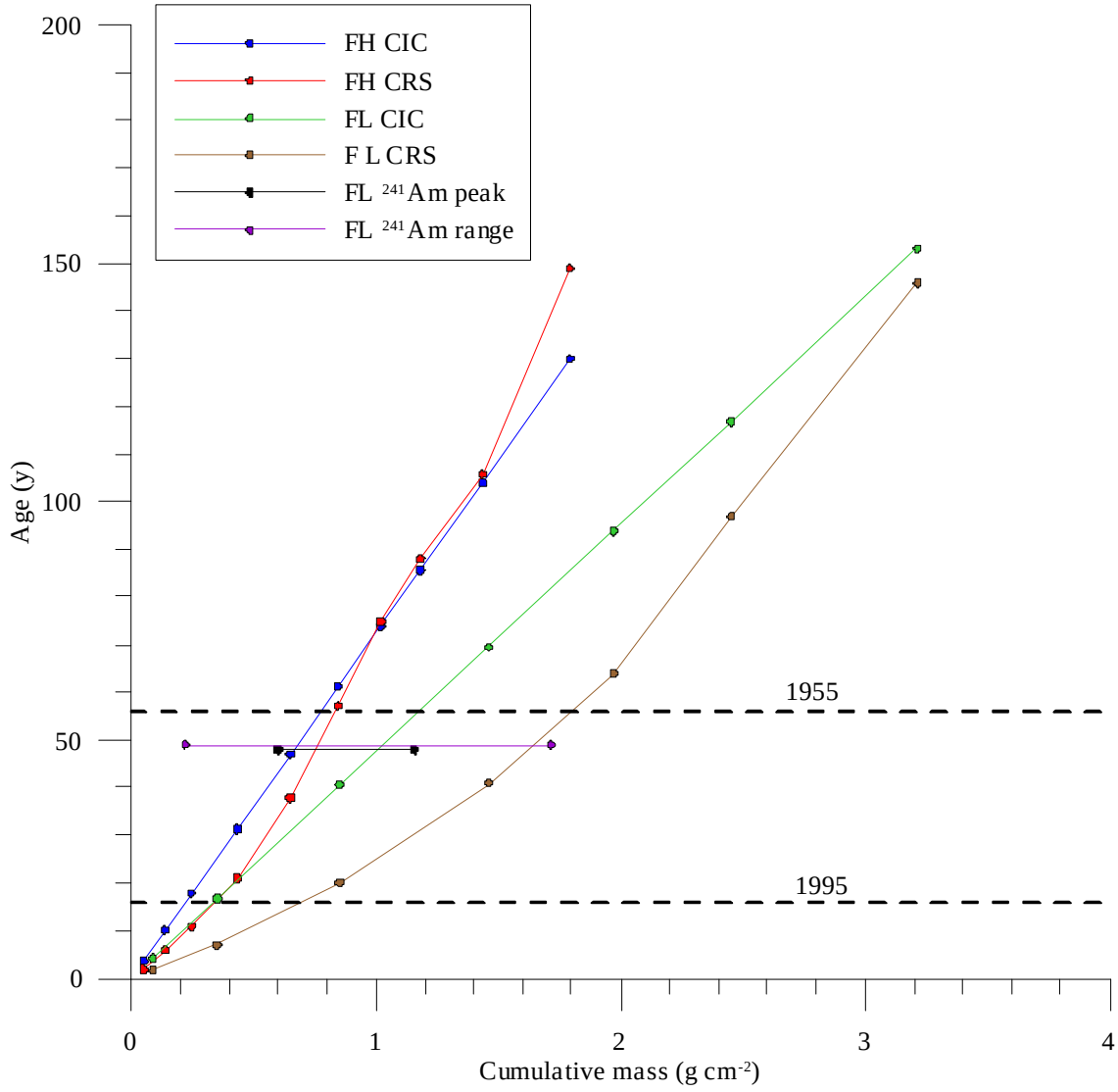

Figure 4-16 Comparison of FH CIC and CRS, FL CIC and CRS and FL ^{241}Am chronologies

4.7 Ash content

The distribution of anthropogenic contaminants was established to assess the compatibility of the chronologies with known historical trends in input and with trends derived in other peat and lake sediment studies.

Deposition of inorganic material (ash) will vary in response to conditions in the atmosphere, with greater deposition at times of high pollutant releases from activities such as the burning of coal. On the basis of ash distribution in a ^{210}Pb dated peat core from Eaglesham Moor, Central Scotland, MacKenzie et al (1998 (b)) observed good correlation of ash content with the expected trend since the start of the industrial revolution, ~1850 (Russell, 2000), with peak deposition in the mid 20th century but a decrease after the introduction of the clean air acts in 1956 and 1968.

It was concluded in section 4.6 that the high resolution cores gave reliable and consistent chronologies for both the CIC and CRS models. CIC chronologies were used to establish the trend of ash deposition within this study and the trends were consistent with that found by MacKenzie et al (1998 (b)). Given the relatively good agreement between the CIC and CRS chronologies for the high resolution cores, a similar conclusion would have been reached had the CRS chronologies been used. For the three unforested cores UH, UL1 and UL2 (Figure 4-17) the trends were similar and showed a gradual increase in ash content from the onset of the industrial revolution, with a maximum in the 1950s for cores UH and UL1, and in the 1940s for core UL2, before rapidly falling away at a time corresponding to the introduction of the clean air acts (1956 and 1968). For the forested cores, FH and FL, (Figure 4-17) there was a similar general trend in ash content to that in the unforested cores with core FH reaching a maximum value in 1924 and core FL in 1969.

In general the implied variations in ash deposition correspond well with the known history of industrial emissions, providing further confidence in the chronologies.

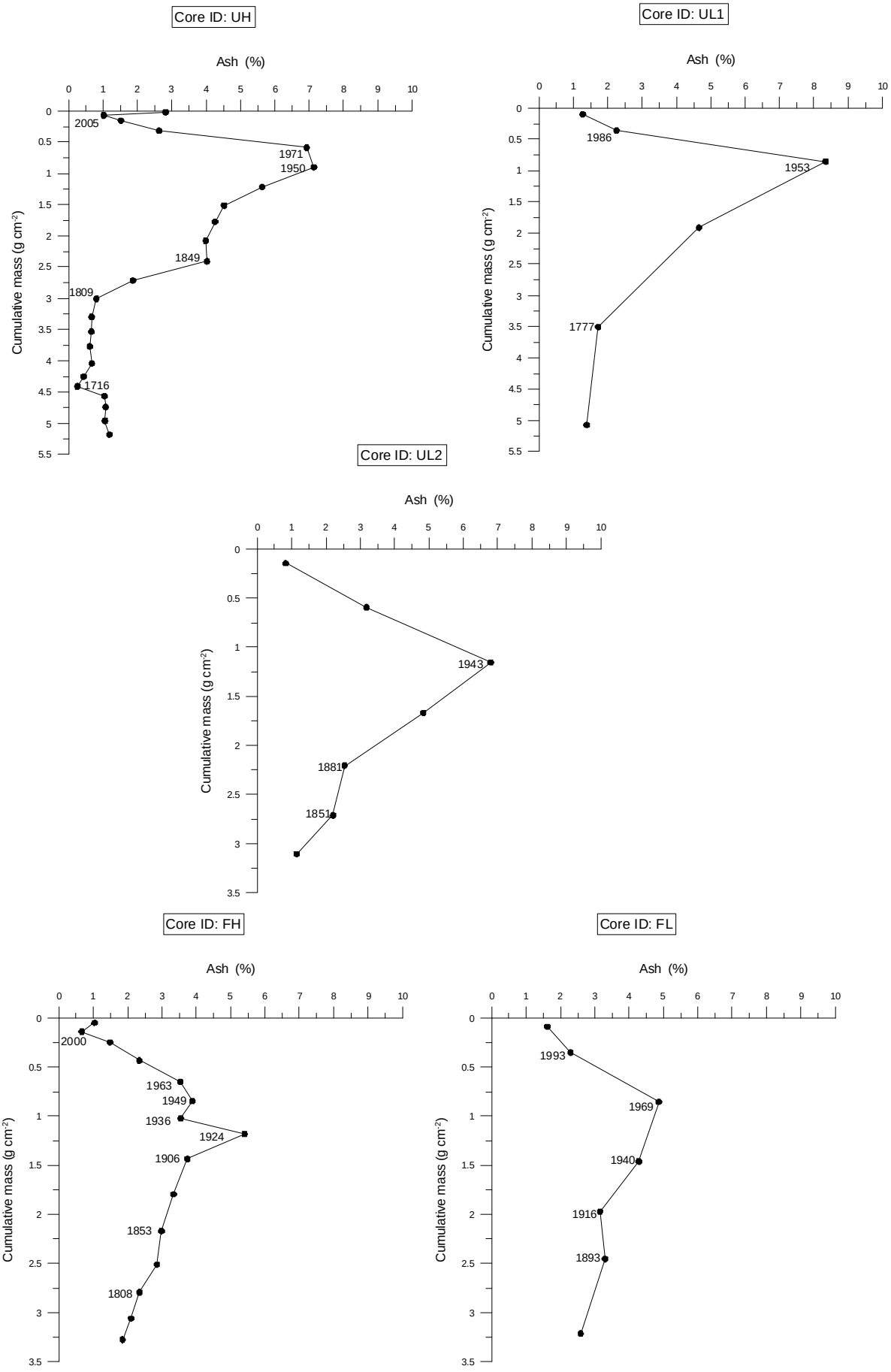

Figure 4-17 Comparison of Ash content (%) with CIC chronologies

4.8 Pb concentrations

Pb concentration analysis was carried out on cores UH, UL1, FH and FL (Figure 4-18). All cores showed the general trend of a gradual rise in Pb concentrations from the time marking the onset of the industrial revolution, and with the exception of core FL, reached a peak in concentration in the 1950s before rapidly falling away. For cores UH, UL1 and FH the maximum Pb concentrations were reached in 1960, 1953 and 1963, respectively, and for core FL the maximum was reached in 1916 before decreasing until 1940 and rising again to peak in 1969, followed by a rapid decrease. The trends in cores UH, UL1 and UL2 were consistent with chronologies observed in numerous other studies of peat bogs and lake sediments in Scotland as exemplified by the study of four Scottish ombrotrophic peat bogs by Cloy et al (2005, 2008) where Pb concentrations were seen to peak in the mid 20th century.

For the two unforested cores (UH and UL1) there was excellent agreement between the Pb concentration profiles and the ash profiles. There were similarities when comparing the Pb concentration profiles of the forested cores (FH and FL) with the corresponding ash profiles however the agreement was not as good as for the unforested cores, suggesting that forested sites give less reliable records of atmospheric deposition. This is possibly attributable to a canopy effect causing complex variations in deposition (Hyvarinen, 1990).

As with the ash profiles, the implied temporal variations in Pb deposition are consistent with known historical trends, providing further support for the accuracy of the chronologies.

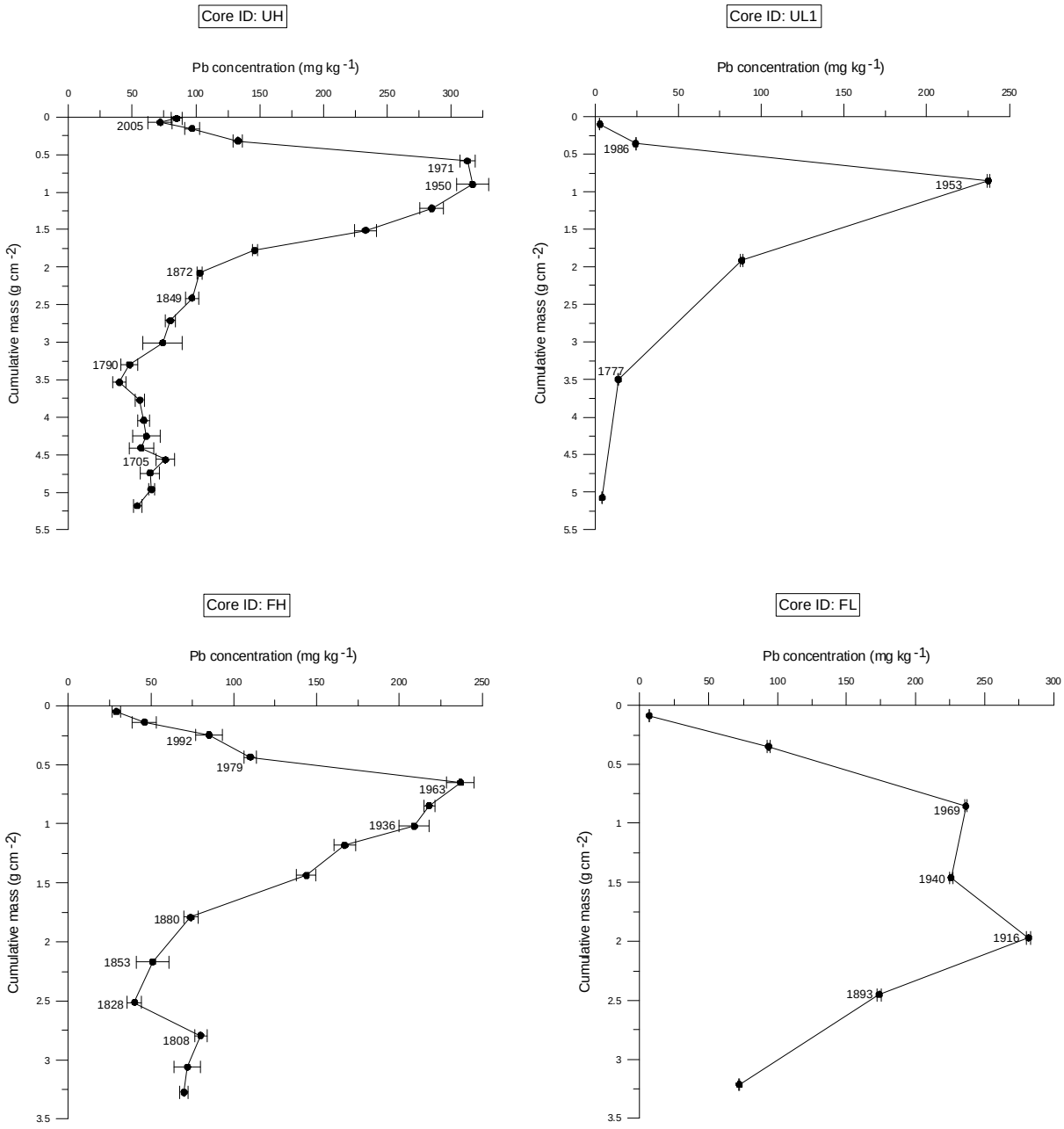

Figure 4-18 Comparison of Pb concentrations (mg kg^{-1}) with CIC chronologies

4.9 Pb isotopes

Pb isotope analysis was carried out on the two high resolution cores (UH and FH). Figure 4-19 shows a plot of the $^{206}Pb/^{207}Pb$ ratio versus $^{208}Pb/^{207}Pb$ ratio for core UH. This shows a trend consistent with the Pb being a binary mixture of industrial Pb and petrol Pb, with the industrial Pb defined as an average of coal burning and industrial emissions. Emissions from coal combustion and industrial

sources will be mixed before being deposited in the atmosphere therefore an average value for these sources was calculated based on data presented in the preceding references. One point lying outwith the mixing line appears to be an analytical artefact as it does not correspond to an expected value for any likely known source of Pb to this peat. It has been well established from other studies (Sugden et al., 1993; Farmer et al., 1996, 1999, 2000, 2005, 2006; MacKenzie et al., 1997, 1998(a); MacKenzie and Pulford, 2002; Cloy et al.,2008) that Pb archives in peat cores in this area contain Pb predominantly from petrol, industrial emmisions and coal combustion. The isotopic composition of petrol Pb is relatively well established (Farmer et al., 2000).

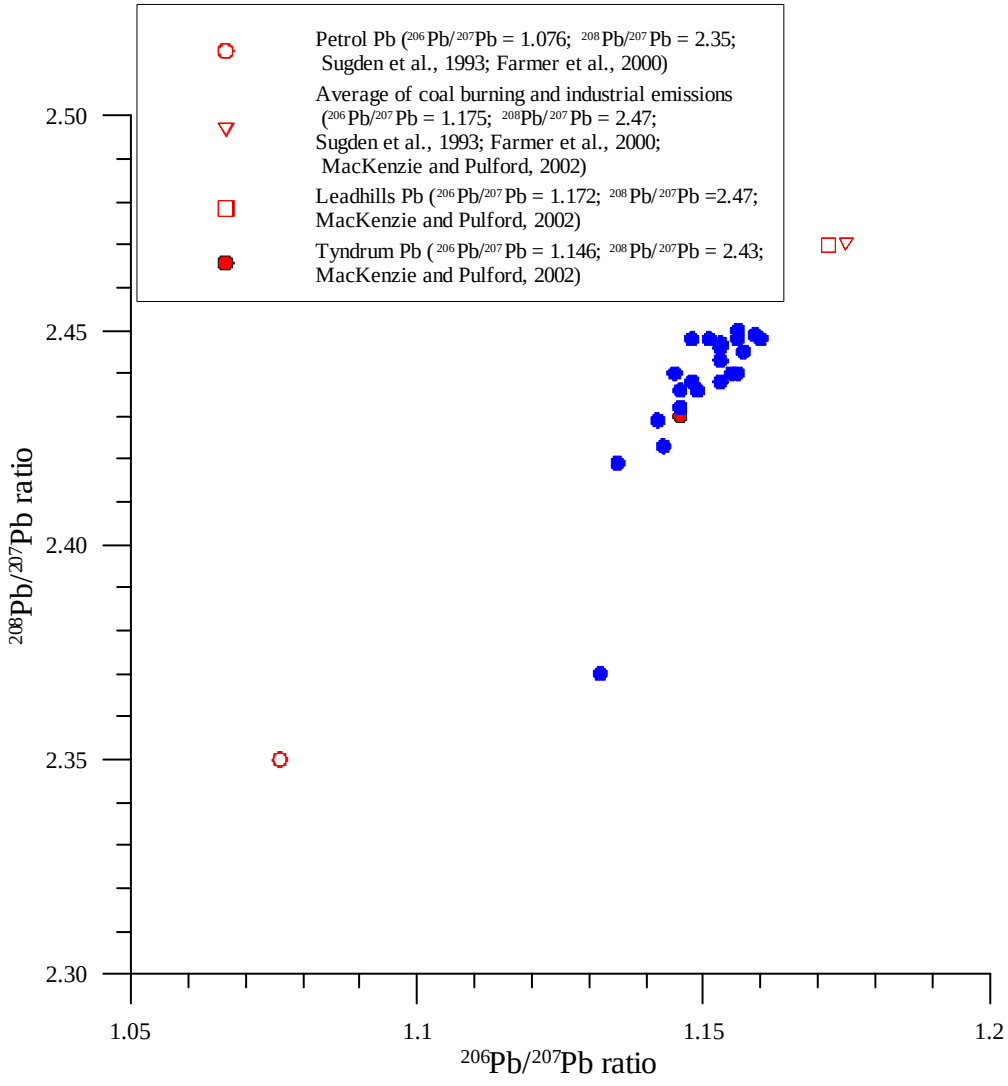

Unforested

Figure 4-19 Core UH $^{206}Pb/^{207}Pb$ v $^{208}Pb/^{207}Pb$

Figure 4-20 shows the corresponding plot of the $^{206}Pb/^{207}Pb$ ratio versus $^{208}Pb/^{207}Pb$ ratio for core FH. This shows a similar trend to that for core UH however some of the values are outwith the expected binary mixing zone.

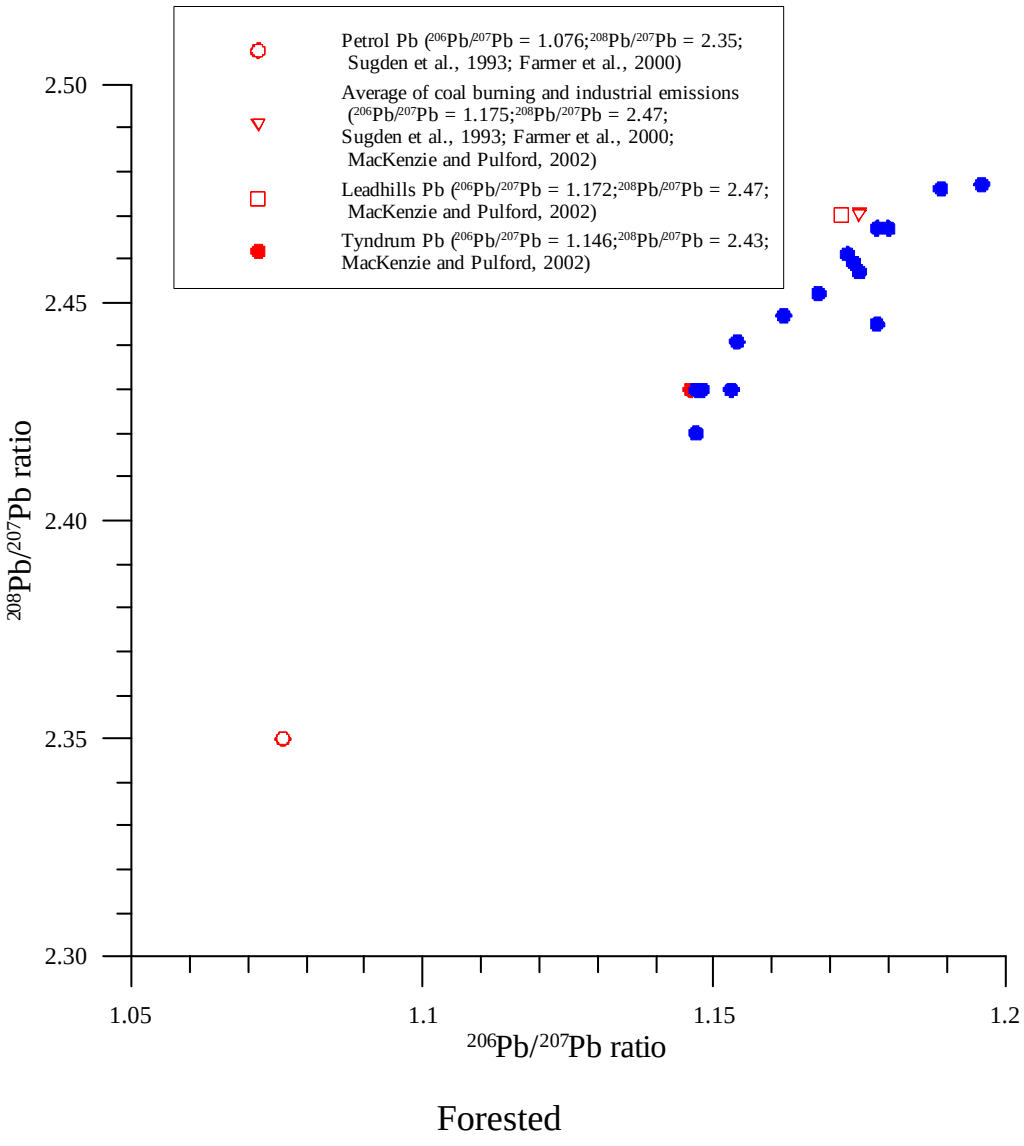

Figure 4-20 Core FH $^{206}Pb/^{207}Pb$ v $^{208}Pb/^{207}Pb$

Figures 4-21 and 4-22 show plots of $^{206}Pb/^{207}Pb$ ratios versus cumulative mass for cores UH and FH respectively. The trend observed in other studies was a fall in $^{206}Pb/^{207}Pb$ ratios from a value ~1.17 in the 19th century (arising from activities such as coal combustion and the smelting of Pb ores) to lower values (~ 1.12 - 1.13) in the 1970s and 1980s as the influence of leaded petrol was seen, followed by a gradual rise in the ratio as leaded petrol was phased out and eventually banned, which resulted in a typical ratio of 1.15 in the late 20th / early 21st century (Farmer et al., 2002). Both cores did exhibit trends consistent with those observed by Farmer et al (2002) and reflected the lowering effect on the $^{206}Pb/^{207}Pb$ ratio of imported Australian lead ores from the late 19th century. A rise to higher $^{206}Pb/^{207}Pb$ ratios nearer the surface was also consistent with the effect of phasing out and eventual ban on the sale of leaded petrol in 2000 (this effect was more pronounced in core UH). However, the values obtained, particularly for core UH, showed an offset relative to the values that would have been expected on the basis of other studies. The $^{206}Pb/^{207}Pb$ ratios for core UH prior to 1950, in the range 1.154 to 1.160, are approximately 0.01 to 0.02 lower than other studies have reported for peat of corresponding age from Scotland, and archive moss samples of corresponding age (Sugden et al., 1993; Farmer et al., 1996, 1999, 2000, 2005, 2006; MacKenzie et al., 1997, 1998(a); MacKenzie and Pulford, 2002; Cloy et al.,2008). The only recognised source of Pb to Scottish peats with a low $^{206}Pb/^{207}Pb$ ratio was petrol Pb and the sections of core affected are in the early 20th and late 19th centuries, before the introduction of leaded petrol. Therefore there is no obvious source to explain the observed low $^{206}Pb/^{207}Pb$ ratios suggesting the possibility of an analytical artefact. For core FH, most of the $^{206}Pb/^{207}Pb$ ratios were consistent with previously reported values, but two of the deeper samples gave values slightly higher than expected. Given the relatively short distance between the two sample sites, it's very unlikely they would be affected by different atmospheric deposition of Pb. The section of core FH with the anomalous ratio corresponds to ages before disturbance by forestation.

Overall, the implied temporal trends in the Pb isotopes were consistent with expected variations, again providing support for the accuracy of the chronologies. There is, however, some doubt about the accuracy of some of the data and these analyses will be repeated before this work is presented for publication in the open literature.

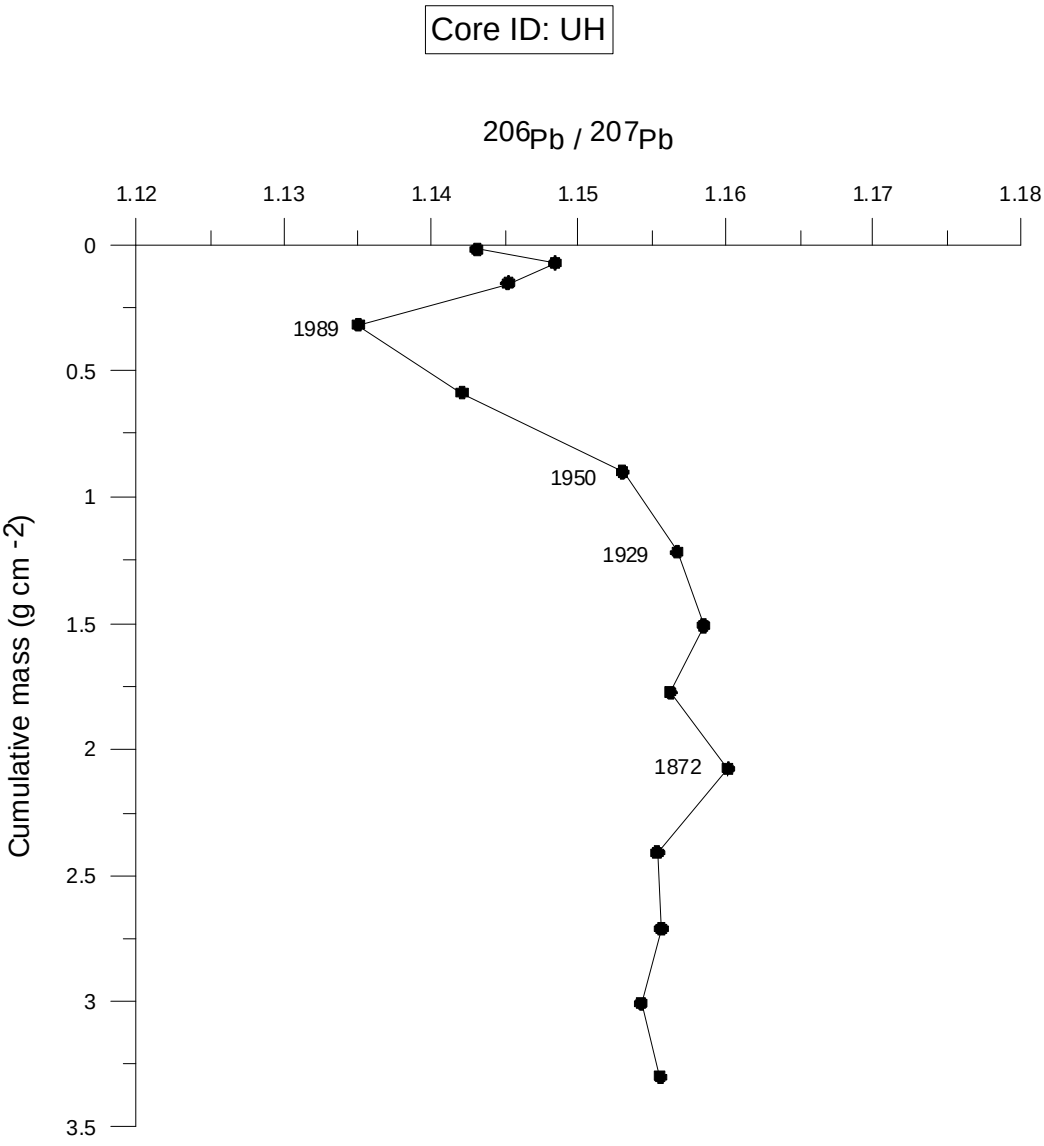

Figure 4-21 Comparison of $^{206}Pb/^{207}Pb$ ratios with CIC chronology for core UH

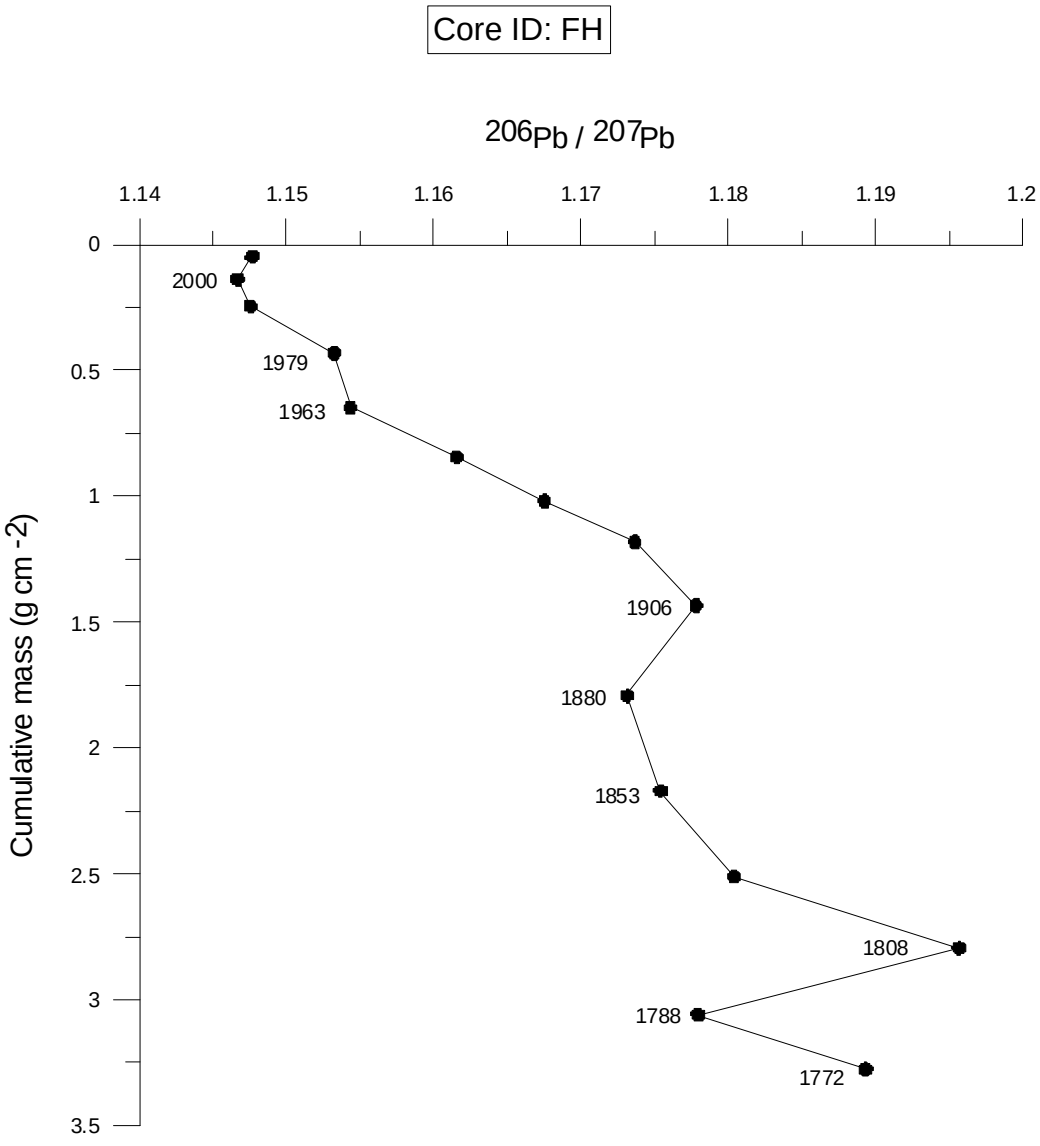

Figure 4-22 Comparison of $^{206}Pb/^{207}Pb$ ratios with CIC chronology for core FH

4.10 Biogenic silica (BSi)

Biogenic silica (BSi) extraction was carried out on core UL2 (Figure 4-23) and a composite core, FHb (Figure 4-24) which was the result of combining sections of the original FH core in order to provide samples of sufficient mass for BSi extraction.

For core UL2, BSi was detected at 138 – 489 mg kg^{-1} near the surface but fell to very low values in the range 2.9 to 13.9 mg kg^{-1} in deeper sections. This distribution suggests production of BSi by growing plants in a form that is unstable under acidic conditions in peat causing subsequent redissolution. This being the case would rule out the possibility of ^{32}Si being suitable as a method of deriving chronologies in peat.

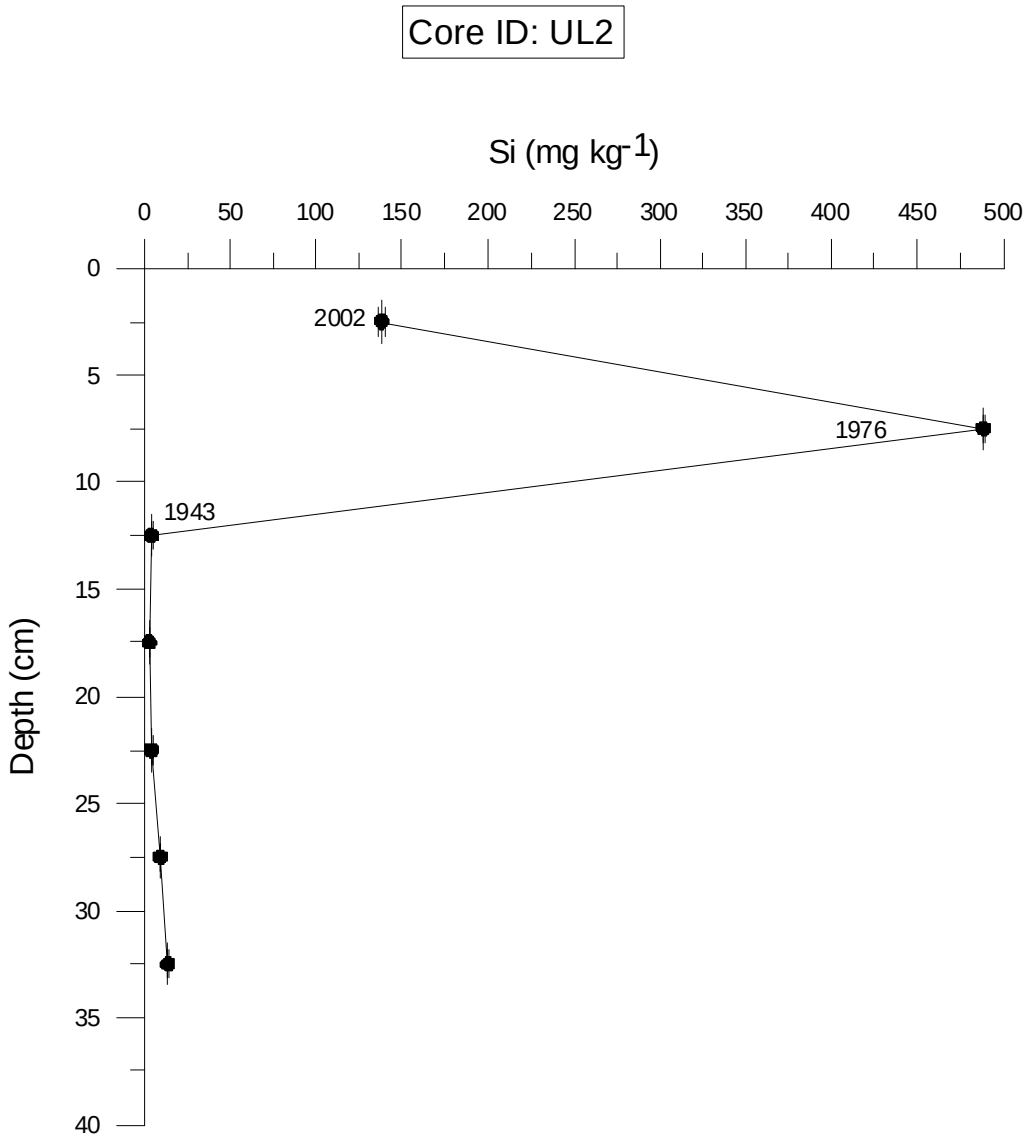

Figure 4-23 Core UL2 BSi profile

For composite core FH(b) there were higher levels of BSi detected throughout the core which could be indicative of BSi production by trees during the period when the site was forested. High values in the range 307 - 599 mg kg^{-1} were found in the sections of the core above 17 cm, while relatively constant values in the range 135 – 166 mg kg^{-1} were observed in deeper sections. Comparison with the CIC chronology indicates that the high levels of BSi were present in layers deposited long before the forest was planted. Thus, if the origin of the BSi was the trees, then the results imply significant mobility of the BSi so the conclusion again is that BSi being unstable under peat conditions would rule out the possibility of ^{32}Si from BSi being suitable as a method of deriving chronologies in peat.

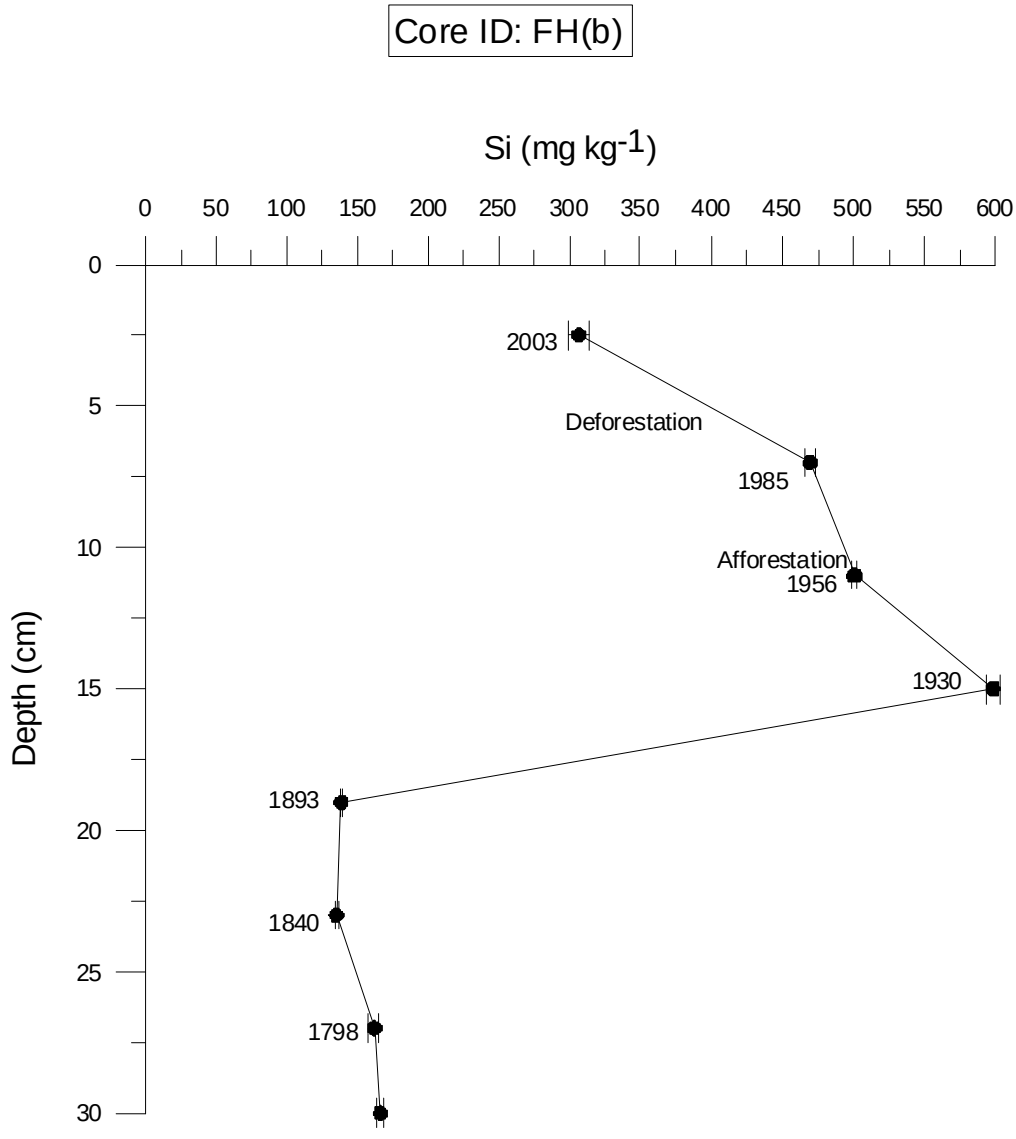

Figure 4-24 Core FHb BSi profile

4.11 Inventories

Comparison of the inventories for the two high resolution cores revealed significantly higher values for the unforested site with ratio values for unforested / forested of 1.7, 1.9 and 1.9 for ^{210}Pb, Pb and ^{137}Cs respectively (Table 4-24). This could represent a real difference between the sites but could be an artefact produced by comparison of inventories over the entire core length which represents different timespans.

Core ID	^{210}Pb	Pb	^{137}Cs
	Bq m^{-2}	mg m^{-2}	Bq m^{-2}
UH	2669	6696	2651
FH	1573	3530	1369
UH/FH	1.7	1.9	1.9

Table 4-24 ^{210}Pb, Pb and ^{137}Cs inventory comparison

To give a more accurate comparison for Pb, the unforested / forested ratios were calculated for specific key dates (Table 4-25). Ratios of 1.7, 1.7, 1.8 and 2.7 were calculated for 1850-2010, 1900-2010, 1950-2010 and 2000-2010 respectively (taking an average where a specific date fell in the middle of a range) for the high resolution cores (UH and FH). For the time periods 1850-1900 and 1900-1950 the UH/FH ratios were 2.2 and 1.4 respectively. Inventories were not compared for the low resolution cores due to the uncertainty of area and depth for each section giving a large uncertainty in the inventories, as corroborated by the errors found in the CRS results. The inventory data for specific time intervals reveal that the higher values observed for the unforested than the forested site has been a systematic, long term feature, not related to the afforestation / deforestation period. This implies a significant difference in metal deposition at the two locations within the same bog. Bindler et al. (2004) reported a similar level of variability in Pb and Hg inventories in cores from a Swedish peat bog. Martínez Cortizas et al. (2012) found similar variations in a multi core study of an ombrotrophic peat bog in Spain, and cited various authors who cast doubt on using peat core inventories as definitive records of contaminant deposition when there are many factors which can influence the archive (e.g. vegetation and topography). He concluded that there are

limitations in extrapolation of data from a single core to estimate regional levels of contaminant deposition and multi core high resolution sampling resulted in more accurate records of atmospheric metal deposition.

Pb Inventories - Comparison by date						
Cumulative Inventory Units : mg m^{-2}						
Core / Year	1850-2010	1900-2010	1950-2010	2000-2010	1850-1900	1900-1950
UH	5023	3990-4356	2464	175	1033	1527
FH	2892	2419	1334	66	474	1085
UH/FH	1.7	1.7	1.8	2.7	2.2	1.4

Table 4-25 Pb inventory comparison by date

When the metal inventories were compared for the high resolution cores UH and FH (Table 4-26) the range of values for the unforested / forested ratio was between 1.2 and 2.2 with an overall average of 1.67.

Core ID	Zn	Fe	Mn	Cu	Ni	Cr	Cd	Ca	Mg
	mg m^{-2}	mg m^{-2}	mg m^{-2}	mg m^{-2}	mg m^{-2}	mg m^{-2}	mg m^{-2}	mg m^{-2}	mg m^{-2}
UH	3747	76328	579	427	182	208	280	79536	44276
FH	2133	36626	269	310	140	137	138	66362	29933
UH/FH	1.8	2.1	2.2	1.4	1.3	1.5	2.0	1.2	1.5

Table 4-26 Metal inventory comparison

4.12 Conclusions

With a limit of detection of 5 Bq kg^{-1} or better and rigorous control of sampling variables using a core tube giving a well defined area and sampling increment, (2cm) good agreement was achieved for the CIC, CRS and ^{241}Am chronologies for the high resolution cores UH and FH. The CIC method chronologies were improved by non inclusion of surface samples showing evidence of growth dilution.

This provides confidence in both the CIC and CRS ^{210}Pb dating methods and highlights the value of ^{241}Am as an independent chronology. ^{241}Am has not previously been routinely exploited for peat but now has optimum potential for chronologies as its activities approach peak detectable level of ingrowth from ^{241}Pu.

^{210}Pb and ^{241}Am chronologies indicated essentially identical accumulation rates of 0.015 g cm^{-2} y^{-1} and 0.014 g cm^{-2} y^{-1} for the unforested and forested locations respectively, indicating that the presence of trees over a limited time period had little influence on the long term accumulation rate of peat.

For the less constrained sampling technique of measuring the area in the field and using a trowel for sectional removal, there was consistency with the high resolution chronologies for the CIC method but for not for the CRS method. This was almost certainly a result of the inaccuracies in definition of area and depth due to the sampling technique.

The study confirmed that ^{137}Cs does not provide a means of establishing chronologies in peat with the profiles suggesting downward migration of ^{137}Cs. ^{137}Cs was still detectable in layers of peat deposition as long ago as 1828, on the basis of the CIC chronology.

The chronologies were consistent with known temporal variations of input of anthropogenic species, specifically ash, Pb and stable Pb isotope composition, based upon other environmental archive studies and known historical trends of industrial and vehicle exhaust emissions.

BSi was extractable from both the unforested (UL2) and forested (FHb) cores but the distribution in the cores, relative to chronologies, suggested mobility of BSi indicating that ^{32}Si dating would not be appropriate for establishing peat chronologies.

Metal inventories were consistently higher for the unforested core (UH) than for the forested core (FH). Comparison of Pb deposition over defined time periods, between 1850 and the present day, revealed this to be a long term pattern rather than an influence of the temporary presence of the forest. Therefore the study confirmed peat cores can provide reliable records of temporal variations in deposition of anthropogenic contaminants. However, the significant difference in inventories of metals between the two coring sites highlights the limitations in using inventories from a single core as a basis for estimating regional deposition.

4.13 Suggestions for future work

The following are suggestions for potential future work which would further examine and expand on the findings of this project:

- Repeat of the Pb isotope analysis to determine if the results reported here are real or artefacts of analysis
- ^{14}C analysis for determination of longer term chronologies
- ^{241}Pu analysis for comparison with ^{241}Am chronologies
- Comparison with other contaminants of known historical variations in input e.g. persistent organic pollutants
- More detailed analysis of metal distributions and inventories with comparison between the forested and unforested sites.

REFERENCES

Appleby, P.G. 2001. Chronostratigraphic Techniques in Recent Sediments. Last, W.M. & Smol, J.P. (eds.), Tracking Environmental Change Using Lake Sediments. Volume 1: Basin Analysis, Coring and Chronological Techniques, Kluwer Academic Publishers, The Netherlands, 171-203.

Appleby, P.G. 2008. Three decades of dating recent sediments by fallout radionuclides: a review. The Holocene, **18(1)**, 83-93.

Asada, T. and Warner, B.G. 2005. Surface Peat Mass and Carbon Balance in a Hypermaritime Peatland. Soil Science Society of America Journal, **69,** 549-562.

Ascough, P., Cook, G. and Dugmore, A. 2005. Methodological approaches to determining the marine radiocarbon reservoir effect. Progress in Physical Geography, **29(4)**, 532-547.

Bao, K., Yu, X., Jia, L. and Wang, G. 2010. Recent Carbon Accumulation in Changbai Mountain Peatlands, Northeast China. Mountain Research and Development, **30(1)**, 33-41.

Bard, E., Rostek, F. and Ménot-Combes, G. 2004. Radiocarbon calibration beyond 20,000 ^{14}C yr B.P. by means of planktonic foraminifera of Iberian Margin. Quaternary Research, **61**, 204-214.

Berset, J.D., Kuehne, W. and Shotyk, W. 2001. Concentrations and distributions of some polychlorinated biphenyls (PCBs) and polycyclic aromatic hydrocarbons (PAHs) in an ombrotrophic peat bog profile of Switzerland. The Science of the Total Environment, **267**, 67-85.

Bindler, R., Klarqvist, M., Klaminder, J. and Förster, J. 2004. Does within-bog spatial variability of mercury and lead constrain reconstructions of absolute deposition rates from single peat records? The example of Sore Mosse, Sweden. Global Biogeochemical Cycles, **18**, 1-11.

Binford, M.W. 1990. Calculation and uncertainty analysis of ^{210}Pb dates for PIRLA project lake sediment cores. Journal of Paleolimnology, **3**, 253-267.

Bronk Ramsey, C. 2001. Development of the radiocarbon calibration program. Radiocarbon, **43**, 355-363.

Bronk Ramsey, C. 2008. Deposition models for chronological records. Quaternary Science Reviews, **27**, 42-60.

Browne, E. and Firestone, R.B. 1986. Table of Radioactive Isotopes. John Wiley & Sons, New York.

Burleigh, R. 1981. W.F.Libby and the development of radiocarbon dating. Antiquity, **LV**, 96-98.

Carter, M.W. and Moghissi, A. 1977. Three decades of nuclear testing. Health Physics, **33**, 55-71.

Choppin, G., Rydberg, J. and Liljenzin, J.O. 1995. Radiochemistry and Nuclear Chemistry. Butterworth-Heinemann Ltd, 693 pages.

Cloy, J.M., Farmer, J.G.,Graham, M.C., MacKenzie,A.B. and Cook, G.T. 2005. A comparison of antimony and lead profiles over the past 2500 years in Flanders Moss ombrotrophic peat bog, Scotland. RSC Journal of Environmental Monitoring, **7**, 1137-1145.

Cloy, J.M., Farmer, J.G., Graham, M.C., MacKenzie, A.B. and Cook, G.T. 2008. Historical records of atmospheric Pb deposition in four Scottish ombrotrophic peat bogs: An isotopic comparison with other records from western Europe and Greenland. Global Biogeochemical Cycles, **22**, 1-16.

Clymo, R.S. 1984. The Limits to Peat Bog Growth. Phil. Trans. R. Soc. Lond. B, **303**, 605-654.

Clymo, R.S. and Bryant, C.L. 2008. Diffusion and mass flow of dissolved carbon dioxide, methane, and dissolved organic carbon in a 7-m deep raised peat bog. Geochimica et Cosmochimica Acta, **72**, 2048-2066.

Conley, D.J. 1998. An interlaboratory comparison for the measurement of biogenic silica in sediments. Marine Chemistry, **63**, 39-48.

Dellapenna, T.M., Kuehl, S.A. and Schaffner, L.C. 1998. Sea-bed Mixing and Particle Residence Times in Biologically and Physically Dominated Estuarine Systems: a Comparison of Lower Chesapeake Bay and the York river Subestuary. Estuarine, Coastal and Shelf Science, **46**, 777-795.

DeMaster, D.J. 1980. The half-life of ^{32}Si determined from a varved Gulf of California sediment core. Earth and Planetary Science Letters, **48**, 209-217.

Dreyer, A., Radke, M., Turunen, J. and Blodau, C. 2005. Long-Term Change of Polycyclic Aromatic Hydrocarbon Deposition to Peatlands of Eastern Canada. Environmental Science & Technology, **39**, 3918-3924.

Eades, L.J., Farmer, J.G., MacKenzie, A.B., Kirika, A. and Bailey-Watts, A.E. 1998. High-resolution Profile of Radiocaesium Deposition in Loch Lomond Sediments. Journal of Environmental Radioactivity, **39 (2)**, 107-115.

Farmer, J.G., Eades, L.J., MacKenzie, A.B., Kirika, A. and Bailey-Watts, A.E. 1996. Stable lead isotope record of lead pollution in Loch Lomond sediments since 1630 A.D. Environmental Science & Technology, **30**, 3080-3083.

Farmer, J.G., Eades, L.J. and Graham, M.C. 1999. The lead content and isotopic composition of British coals and their implications for past and present releases of lead to the UK environment. Environmental Geochemistry and Health, **21**, 257-272.

Farmer, J.G., Eades, L.J., Graham, M.C. and Bacon, J.R. 2000. The changing nature of the ^{206}Pb/^{207}Pb isotopic ratio of lead in rainwater, atmospheric particulates, pine needles and leaded petrol in Scotland, 1982-1998. RSC Journal of Environmental Monitoring, **2**, 49-57.

Farmer, J.G., Eades, L.J., Atkins, H. and Chamberlain, D.F. 2002. Historical Trends in the Lead Isotopic Composition of Archival Sphagnum Mosses from Scotland (1838-2000). Environmental Science & Technology, **36**, 152-157.

Farmer, J.G., Graham, M.C., Bacon, J.R., Dunn, S.M., Vinogradoff, S. and MacKenzie, A.B. 2005. Isotopic characterisation of the historical lead deposition record at Glensaugh, an organic-rich, upland catchment in rural N.E. Scotland. Science of the Total Environment, **346**, 121-137.

Farmer, J.G., Graham, M.C., Yafa, C., Cloy, J.M., Freeman, A.J. and MacKenzie, A.B. 2006. Use of $^{206}Pb/^{207}Pb$ ratios to investigate the surface integrity of peat cores used to study the recent depositional history and geochemical behaviour of inorganic elements in peat bogs. Global and Planetary Change, **53**, 240-248.

Farmer, J.G., Anderson, P., Cloy, J.M., Graham, M.C., MacKenzie, A.B. and Cook, G.T. 2009. Historical accumulation rates of mercury in four Scottish ombrotrophic peat bogs over the past 2000 years. Science of the Total Environment, **407**, 5578-5588.

Fifield, K.L. and Morgenstern, U. 2009. Silicon-32 as a tool for dating the recent past. Quaternary Geochronology, **4**, 400-405.

Gleizon, P. and McDonald, P. 2010. Modelling radioactivity in the Irish Sea: From discharge to dose. Journal of Environmental Radioactivity, **101**, 403-413.

Goldberg, E.D. 1963. Geochronology with Lead-210. A Symposium on Radioactive Dating, International Atomic Energy Agency, Vienna, 121-131.

Gorham, E. 1991. Northern Peatlands: role in the carbon cycle and probable responses to climatic warming. Ecological Applications, **1(2)**, 182-195.

Goslar, T., van der Knaap, W.O., Hicks, S., Andrič, M., Czernik, J., Goslar, E., Räsänen, S. and Hyötylä, H. 2005. Radiocarbon dating of modern peat profiles: pre- and post-bomb ^{14}C variations in the construction of age-depth models. Radiocarbon, **47**, 115-134.

Grover, S.P.P., Baldock, J.A. and Jacobsen, G.E. 2012. Accumulation and attrition of peat soils in the Australian Alps: Isotopic dating evidence. Austral Ecology, **37**, 510-517.

Gunnarsson, U., Boresjö Bronge, L., Rydin, H. and Ohlson, M. 2008. Near-zero recent carbon accumulation in a bog with high nitrogen deposition in SW Sweden. 2008. Global Change Biology, **14**, 2152-2165.

Hyvarinen, A. 1990. Deposition on Forest Soils - Effect of Tree Canopy on Throughfall. Acidification in Finland, **1**, 199-213.

Ingram, H.A.P. 1978. Soil Layers in Mires: Function and Terminology. Journal of Soil Science, **29**, 224-227.

Katata, G., Ota, M., Terada, H., Masamichi, C. and Nagai, H. 2012. Atmospheric discharge and dispersion of radionuclides during Fukushima Dai-ichi Nuclear

Power Plant accident. Part I: Source term estimation and local-scale atmospheric dispersion in early phase of the accident. Journal of Environmental Radioactivity, **109**, 103-113.

Komárek, M., Ettler, V., Chrastný, V. and Mihaljevič, M. 2008. Lead isotopes in environmental sciences: A review. Environment International, **34**, 562-577.

Koning, E., Epping, E. and Van Raaphorst, W. 2002. Determining Biogenic Silica in Marine Samples by Tracking Silicate and Aluminium Concentrations in Alkaline Leaching Solutions. Aquatic Geochemistry, **8**, 37-67.

Lähteenoja, O., Ruokolainen, K., Schulman, L. and Alvarez, J. 2009. Amazonian floodplains harbour minerotrophic and ombrotrophic Peatlands. Catena, **79**, 140-145.

Lal, D., Goldberg, E.D. and Koide, M. 1960. Cosmic-Ray Produced Silicon-32 in Nature. Science, **131**, 332-337.

Lal, D., Nijampurkar, V.N., Somayajula, B.L.K., Koide, M. and Goldberg, E.D. 1976. Silicon-32 specific activities in coastal waters of the world oceans. Limnology and Oceanography, **21(2)**, 285-293.

Langdon, P.G. and Barber, K.E. 2005. The climate of Scotland over the last 5000 years inferred from multiproxy peatland records: inter-site correlations and regional variability. Journal of Quaternary Science, **20(6)**, 549-566.

Le Roux, G., Aubert, D., Stille, P., Krachler, M., Kober, B., Cheburkin, A., Bonani, G. and Shotyk, W. 2005. Recent atmospheric Pb deposition at a rural site in southern Germany assessed using a peat core and snowpack, and comparison with other archives. Atmospheric Environment, **39**, 6790-6801.

Libby, W.F. 1946. Atmospheric Helium Three and Radiocarbon from Cosmic Radiation. Physical Review, **LXIX**, 671-672.

Libby, W.F. 1970. Radiocarbon dating. Philosophical Transactions of the Royal Society, **269**, 1-10.

Lindner, M. 1953. New Nuclides Produced in Chlorine Spallation. Physical Review, **91(3)**, 642-644.

MacKenzie, A.B. 2000. Environmental radioactivity: experience from the 20th century - trends and issues for the 21st century. The Science of the Total Environment, **249**, 313-329.

MacKenzie, A.B. and Scott, R.D. 1993. Sellafield waste radionuclides in Irish Sea intertidal and salt marsh sediments. Environmental Geochemistry and Health, **15(2/3)**, 173-184.

MacKenzie, A.B. and Pulford, I.D. 2002. Investigation of contaminant metal dispersal from a disused mine site at Tyndrum, Scotland, using concentration gradients and stable Pb isotope ratios. Applied Geochemistry, **17**, 1093-1103.

MacKenzie, A.B., Farmer, J.G. and Sugden, C.L. 1997. Isotopic evidence of the relative retention and mobility of lead and radiocaesium in Scottish ombrotrophic peats. The Science of the Total Environment, **203**, 115-127.

MacKenzie, A.B., Logan, E.M., Cook, G.T. and Pulford, I.D. 1998(a). Distribution, inventories and isotopic composition of lead in ^{210}Pb-dated peat cores from contrasting biogeochemical environments: implications for lead mobility. Science of the Total Environment, **223**, 25-35.

MacKenzie, A.B., Logan, E.M., Cook, G.T. and Pulford, I.D. 1998(b). A historical record of atmospheric depositional fluxes of contaminants in west-central Scotland derived from an ombrotrophic peat core. The Science of the Total Environment, **222**, 157-166.

MacKenzie, A.B., Stewart, A., Cook, G.T., Mitchell, L., Ellet, D.J. and Griffiths, C.R. 2006. Manmade and natural radionuclides in north east Atlantic shelf and slope sediments: Implications for rates of sedimentary processes and for contaminant dispersion. Science of the Total Environment, **369**, 256-272.

MacKenzie, A.B., Hardie, S.M.L., Farmer, J.G., Eades, L.J. and Pulford, I.D. 2011. Analytical and sampling constraints in ^{210}Pb dating. Science of the Total Environment, **409**, 1298-1304.

Maguire, S., Pulford, I.D., Cook, G.T. and MacKenzie, A.B. 1992. Caesium sorption- desorption in clay-humic acid systems. Journal of Soil Science, **43**, 689-696.

Marquez, L. and Costa, N.L. 1955. The Formation of ^{32}P from Atmospheric Argon by Cosmic Rays. Il Nuovo Cimento, **II(5)** 1038-1041.

Martínez Cortizas, A., Peiteado Varela, E., Bindler, R., Biester, C. and Cheburkin, A. Reconstructing historical Pb and Hg pollution in NW Spain using multiple cores from the Chao de Lamoso bog (Xistral Mountains). 2012. Geochimica et Cosmochimica Acta, 82, 68-78.

McCall, P.L., Robbins, J.A. and Matisoff, G. 1984. ^{137}Cs and ^{210}Pb Transport and Geochronologies in Urbanized Reservoirs with Rapidly Increasing sedimentation Rates. Chemical Geology, **44**, 33-65.

McKinley, I.G., Baxter, M.S., Ellett, D.J. and Jack, W. 1981. Tracer Applications of Radiocaesium in the Sea of the Hebrides. Estuarine, Coastal and Shelf Science, **13**, 69-82.

Mitchell, P.I., Schell, W.R., McGarry, A., Ryan, T.P., Sanchez-Cabeza, J.A. and Vidal-Quadras, A. 1992. Studies of the vertical distribution of ^{134}Cs, ^{137}Cs, ^{238}Pu, ^{239,240}Pu, ^{241}Pu, ^{241}Am and ^{210}Pb in ombrogenous mires at mid- latitudes. Journal of Radioanalytical and Nuclear Chemistry, **156(2)**, 361-387.

Molto, J.E., Stewart, J.D. and Reimer, P.J. 1997. Problems in Radiocarbon Dating Human Remains from Arid Coastal Areas: An Example from the Cape Region of Baja California. American Antiquity, **62(3)**, 489-507.

Morgenstern, U., Gellermann, R., Hebert, D., Börner, I., Stolz, W., Vaikmäe, A., Rajamäe, R. and Putnik, H. 1995. ^{32}Si in limestone aquifers. Chemical Geology, **120**, 127-134.

Morgenstern, U., Geyh, M.A., Kudrass, H.R., Ditchburn, R.G. and Graham, I.J. 2001. ^{32}Si dating of marine sediments from Bangladesh. Radiocarbon, **43**, 909-916.

Nijampurkar, V.N., Rao, D.K., Oldfield, F. and Renberg I. 1998. The half-life of ^{32}Si: a new estimate based on varved lake sediments. Earth and Planetary Science Letters, **163**, 191-196.

Novák, M., Emmanuel, S., Vile, M.A., Erel, Y., Véron, A., Pačes, T., Weider, R.K., Vaněček, M., Štěpánová, M., Břízová, E. and Hovorka, J. 2003. Origin of Lead in Eight Central European Peat Bogs Determined from Isotope Ratios, Strengths, and Operation Times of Regional Pollution Sources. Environmental Science & Technology, **37(3)**, 437-445.

Novak, M., Brizova, E., Adamova, M., Erbanova, L. and Bottrell, S.H. 2008. Accumulation of organic carbon over the past 150 years in five freshwater peatlands in western and central Europe. Science of the Total Environment, **390**, 425-436.

Olid, C., Garcia-Orellana, J., Martínez-Cortizas, A., Masqué, P., Peiteado, E. and Sanchez-Cabeza, J.A. 2008. Role of Surface Vegetation in ^{210}Pb-Dating of Peat Cores. Environmental Science & Technology, **42**, 8858-8864.

Reimer, P.J. and Reimer, R.W. 2001. A Marine Reservoir Correction Database and On-line Interface. Radiocarbon, **43**, 461-463.

Reimer, P.J., Baillie, M.G.L., Bard, E., Bayliss, A., Beck, J.W., Blackwell, P.G., Bronk Ramsey, C., Buck, C.E., Burr, G.S., Edwards, R.L., Friedrich, M., Grootes, P.M., Guilderson, T.P., Hajdas, I., Heaton, T.J., Hogg, A.G., Hughen, K.A., Kaiser, K.F., Kromer, B., McCormac, F.G., Manning, S.W., Reimer, R.W., Richards, D.A., Southon, J.R., Talamo, S., Turney, van der Plicht, J. and Weyhenmeyer, C.E. 2009. IntCal09 and Marine09 radiocarbon age calibration curves, 0-50,000 years Cal BP. Radiocarbon, **51**, 1111-1150.

Robbins, J.A. 1978. Geochemical and geophysical applications of radioactive lead. Nriagu, J.O. (ed), The Biogeochemistry of Lead in the Environment, Elsevier Scientific, Amsterdam, 285-293.

Robbins, J.A. and Herche, L.R. 1993. Models and uncertainty in ^{210}Pb dating of sediments. Verh. Internat. Ver. Limnol, **25**, 217-222.

Russell, C.A. 2000. Chemistry, Society and Environment. The Royal Society of Chemistry, 47,209 & 217.

Sauer, D., Saccone, L., Conley, D.J., Herrmann, L. and Sommer, M. 2006. Review of methodologies for extracting plant-available and amorphous Si from soils and aquatic sediments. Biogeochemistry, **80**, 89-108.

Savel'eva, A.V., Yudina, N.V. and Inisheva, L.I. 2010. Composition of Humic Acids in Peats with Various Degrees of Humification. Solid Fuel Chemistry, **44(5)**, 305-309.

Shakhashiro, A., Tarjan, S., Ceccatelli, A., Kis-Benedek, G. and Betti, M. 2012. IAEA-447: A new certified reference material for environmental radioactivity measurements. Applied Radiation and Isotopes, **70**, 1632-1643.

Shand, C.A., Cheshire, M.V. and Smith, S. 1994. Distribution of Radiocaesium in Organic Soils. Journal of Environmental Radioactivity, **23**, 285-302.

Shotyk, W., Cheburkin, A.J., Appleby, P.G., Fankhauser, A. and Kramers, J.D. 1996. Two thousand years of atmospheric arsenic, antimony, and lead deposition recorded in an ombrotrophic peat bog profile, Jura Mountains, Switzerland. Earth and Planetary Science Letters, **145**, E1-E7.

Shotyk, W., Weiss, D., Heisterkamp, M., Cheburkin, A.K., Appleby, P.G. and Adams, F.C. 2002. New Peat Bog Record of Atmospheric Lead Pollution in Switzerland: Pb Concentrations, Enrichment Factors, Isotopic Composition, and Organolead Species. Environmental Science & Technology, **36**, 3893-3900.

Simpson, J.A. 1951(a). The Change of Cosmic-Ray Neutron Intensity Following Solar Disturbances. Physical Review, **81(4)**, 639-640.

Simpson, J.A. 1951(b). The Neutrons from the Nucleonic Component as an Indicator of Changes in Primary Intensities. Physical Review, **81(5)**, 895-896.

Simpson, J.A. 1951(c). Neutrons Produced in the Atmosphere by the Cosmic Radiations. Physical review, 83(6) 1175-1188.

Smith, J.N. 2001. Why should we believe ^{210}Pb sediment geochronologies? Journal of Environmental Radioactivity, **55**, 121-123.

Suess, H.E. 1958. The Radioactivity of the Atmosphere and Hydrosphere. Annu. Rev. Nucl. Sci. **8**, 243-256.

Sugden, C.L., Farmer, J.G. and MacKenzie, A.B. 1993. Isotopic ratios of lead in contemporary environmental materials from Scotland. Environmental Geochemistry and Health, **15**, 59-65.

Swan, D.S., Baxter, M.S., McKinley, I.G. and Jack, W. 1982. Radiocaesium and ^{210}Pb in Clyde Sea Loch Sediments. Estuarine, Coastal and Shelf Science, **15**, 515-536.

Thomson, J., Cook, G.T., Anderson, R., MacKenzie, A.B., Harkness, D.D. and McCave, I.N. 1995. Radiocarbon age offsets in different-sized carbonate components of deep-sea sediments. Radiocarbon, **37(2)**, 91-101.

Turetsky, M.R., Manning, S.W. and Wieder, R.K. 2004. Dating Recent Peat Deposits. Wetlands, **24(2)**, 324-356.

UNSCEAR. 1993. Sources and effects of ionizing radiation. Report to the General Assembly by the United Nations Scientific Committee on the effects of Atomic Radiation, Annex B. United Nations, New York.

UNSCEAR. 2000. Sources and effects of ionizing radiation. Report to the General Assembly by the United Nations Scientific Committee on the effects of Atomic Radiation, Volume 1, Annex C. United Nations, New York.

UNSCEAR. 2008. Sources and effects of ionizing radiation. Report to the General Assembly by the United Nations Scientific Committee on the effects of Atomic Radiation, Volume II, Annex C. United Nations, New York.

van der Linden, M., Barke, J., Vickery, E., Charman, D.J. and van Geel, B. 2008 (a). Late Holocene human impact and climate change recorded in a North Swedish peat deposit. Palaeogeography, Palaeoclimatology, Palaeoecology, **258**, 1-27.

van der Linden, M., Vickery, E., Charman, D.J. and van Geel, B. 2008 (b). Effects of human impact and climate change during the last 350 years recorded in a Swedish raised bog deposit. 2008. Palaeogeography, Palaeoclimatology, Palaeoecology, **262**, 1-31.

Vile, M.A., Wieder, R.K. and Novák, M. 2000. 200 Years of Pb Deposition throughout the Czech Republic: Patterns and Sources. Environmental Science & technology, **34(1)**, 12-21.

Waddington, J.M. and Roulet, N.T. 1996. Atmosphere-wetland carbon exchanges: Scale dependency of CO_2 and CH_4 exchange on the developmental topography of a peatland. Global Biogeochemical Cycles, **10(2)**, 233-245.

Wieder, R.K. 2001. Past, present, and future peatland carbon balance: an empirical model based on ^{210}Pb dated cores. Ecological Applications, **11(2)**, 327-342.

Wieder, R.K., Novák, M., Schell, W.R. and Rhodes, T. 1994. Rates of peat accumulation over the past 200 years in five Sphagnum-dominated peatlands in the United States. Journal of Paleolimnology, **12**, 35-47.

Zaccone, C., Cocozza, C., Cheburkin, A.K., Shotyk, W. and Miano, T.M. 2008. Distribution of As, Cr, Ni, Rb, Ti and Zr between peat and its humic fraction along an undisturbed ombrotrophic bog profile (NW Switzerland). Applied Geochemistry, **23**, 25-33.

Websites accessed

www.ctbto.org. Comprehensive Nuclear Test Ban Treaty Organisation, accessed 24/09/12.

www.folm-ek.org. Friends of Langlands Moss LNR, accessed 20/06/12.

www.humicsubstances.org. International Humic Substances Society, accessed 19/04/11.